Uncertainty Analysis of Reinforced Concrete Masonry Walls under Out-of-plane Loading

by

ZIEAD METWALLY

A thesis submitted in partial fulfillment of the requirements for the degree of

Master of Science

in

STRUCTURAL ENGINEERING

Department of Civil and Environmental Engineering
University of Alberta

ABSTRACT

Masonry, as a conventional construction material, is widely used due to its durability, strength, hygrothermal performance, and aesthetics. However, the behaviour of masonry structures is not fully comprehended, especially in the face of uncertainty. This lack of understating on the behaviour of masonry structures is usually compensated by imposing overly conservative design provisions. Inherent uncertainties in the material and geometric properties of masonry structures result in large scatter in the experimentally or analytically predicted behaviour. Thus, understanding the influence of these uncertainties on the structural behaviour of masonry structures is of paramount importance to lay down the basis for reliable structural design.

This thesis focuses on the uncertainty analysis of the out-of-plane behaviour of reinforced concrete masonry walls using mechanics-based finite element (FE) models and experimental testing data. Specifically, this thesis includes three main phases. In the first phase, the probabilistic behaviour of reinforced concrete masonry walls is investigated, employing mechanics-based macro FE models in conjunction with Monte Carlo simulations (MCS). The effect of the inherited uncertainties in the material and geometric properties on different response quantities (e.g., load capacity and deformation capacity) is also investigated through a variance-based global sensitivity analysis. Additionally, the model uncertainty in FE-predicted load capacity is quantified to characterize the model error, which is found to be influential compared to geometric and material uncertainties, though FE models are commonly used for numerical studies.

The second phase focuses on assessing the reliability of reinforced concrete masonry walls loaded out-of-plane with the limit state functions formulated employing the developed macro FE models. In this phase, the importance of model uncertainty on the reliability assessment is

revealed. The reliability assessment conducted considering different global and local failure criteria provides insights into their effect on the safety levels of walls. The reliability assessment is found to be sensitive to the adopted failure criteria. In addition, different factors are found to influence the reliability assessment of the walls designed according to the masonry design code; specifically, walls with different slenderness ratios and load eccentricities show inconsistent reliability levels.

The model errors associated with the out-of-plane load capacity provided in masonry design codes in North America (i.e., CSA S304-14 and TMS 402-16) are investigated in the third phase. FE-based and experimental data are used to quantify the model error associated with design code-based models. In addition, the sensitivity of the model error to the variations associated with different design parameters is investigated. It is found that CSA S304-14 is overly conservative for highly slender walls with low load eccentricities, while TMS 402-16 gives more reasonable capacity predictions for such walls. However, TMS 402-16 is found to overestimate the capacities of highly slender walls with relatively high reinforcement ratios and load eccentricities. The code-based models are employed in reliability assessment to investigate the influence of the accuracy of the behavioural model on the reliability of the masonry walls. It is found that using the code-based models in the reliability assessment without considering their model error results in significantly biased reliability results. This highlights the need and potential room for design code model improvement.

ACKNOWLDEGEMENTS

First, I would like to express my sincere gratitude to my friend and supervisor, Dr. Yong Li. His continuous support, help and patience were surprisingly generous and consistent throughout this program. Working with Dr. Li helped me be a passionate researcher, who is doing research to enjoy and grow.

During the last two years, I had the opportunity to work and interact with many brilliant students, from whom I have learned a lot. Our discussions, laughs and moments of joy were of great help throughout this exciting journey. Special thanks to Ahmed Mowafy, Ahmed Khaled, Saher Attia, Mahmoud Hossam, Bowen Zeng, Wanyan Liu and Miguelangel Bilotta.

Special thanks to Prof. Samer Adeeb; he was a great role model for me, professionally and personally. I would also like to thank Dr. Carlos Cruz-Noguez, who guided my first steps into the exciting world of masonry structures. Additionally, I would like to thank the Natural Sciences and Engineering Research Council for the financial support for this study.

Endless thanks to my family members. Everything I accomplished is because of you. Your unconditional love, support and protection made this possible. You are the most important thing in my life.

TABLE OF CONTENTS

LIST OF TABLES

LIST OF FIGURES

CHAPTER 1:Introduction

1.1 Background

Masonry is one of the ancient building materials used by humans to build magnificent structures that withstand a variety of loads for thousands of years. In the meantime, masonry is still widely used as a building material for its durability, strength, hygrothermal performance, and aesthetics. However, understanding the behaviour of masonry walls loaded out-of-plane is still considered to be a challenging task. Due to the complex behaviour of masonry attributed to the inherited heterogeneity and complex interaction between different components (i.e., unit, mortar, grout, and steel reinforcement). In addition, the behaviour of masonry walls is highly affected by the inherent uncertainties associated with their material and geometric properties. Such uncertainties are typically neglected, or at most implicitly considered, within the scope of deterministic analysis and design. Specifically, this problem is often addressed by adopting a conservative approach and increasing the safety margins in the design codes. In addition to the uncertainties in material and geometric properties, the simplified design code models and numerical models used to predict the behaviour of masonry structures are not accurate. In fact, every model is associated with a model error. However, this error is typically neglected without its importance quantified, although it can be relatively significant compared to other uncertainties. To this end, considering the different uncertainties in material and geometric properties as well as the model uncertainty is essential to comprehend the uncertain behaviour of masonry structures. Without rigorous quantification and incorporation of the aforementioned uncertainties, the decision-making in the design and analysis process of masonry structures can be misinformative.

1.2 Problem Statement and Motivation

Different numerical models and simplified analytical models (e.g., design code equations or procedures) were developed to predict the behaviour or load-bearing capacities of masonry structures. The error associated with the prediction model in addition to the uncertainties associated with the material and geometric properties should be considered to support the design and analysis process. As such, this thesis aims to understand the effect of the aforementioned uncertainties on the probabilistic behaviour and reliability assessment of masonry structures, emphasizing model uncertainty.

Inherent uncertainties in the material and geometric properties of masonry structures result in large scatter in the experimentally or analytically predicted behaviour. Thus, understanding the influence of these uncertainties on the structural behaviour of masonry structures is of paramount importance to lay down the basis for reliable structural design, instead of imposing unduly conservative provisions by the design codes. The aforementioned uncertainties can be incorporated into the behavioural model (e.g., finite element (FE) models) to perform probabilistic structural analysis or reliability assessment. However, the uncertainty associated with the predictions can affect the reliability of the aforementioned analyses. Accordingly, this necessitates the rigorous consideration of the model uncertainty in the uncertainty analysis framework (e.g., probabilistic structural analysis and reliability assessment).

1.3 Objectives, Methods, and Scope

This thesis aims to investigate the effect of different uncertainties on the probabilistic behaviour and reliability of reinforced concrete masonry walls under out-of-plane loading. To do so, the

following sub-objectives are identified. In addition, the scope and methods corresponding to each sub-objective are illustrated as follows.

- Investigating the probabilistic structural behaviour of reinforced concrete masonry walls loaded out-of-plane
    - A mechanics-based macro FE element model is developed to predict the global behaviour of the reinforced masonry walls.
    - The pertinent material and geometric uncertainties are incorporated into the FE models and propagated to different response quantities (e.g., load capacity and ductility) using Monte Carlo simulations (MCS).
    - The uncertainty associated with the FE models prediction of load capacity is quantified using an experimental database compiled from the literature. Hence, the effect of the model uncertainty on the probabilistic capacity is investigated.
    - The relative importance of the considered uncertainties with respect to the load capacity and ductility is quantified using variance-based global sensitivity analysis.
- Assessing the reliability of reinforced concrete masonry walls loaded out-of-plane
    - The developed macro FE models are used to formulate the limit-state function for the reliability problems for walls subjected to different out-of-plane loads (e.g., eccentric vertical loads and wind loads) considering slenderness effects.
    - The reliability assessment is conducted using the efficient subset simulations algorithm in conjunction with Polynomial-Chaos-Kriging (PCK) surrogate models.

    - The influence of the model error and the different failure criteria on the reliability assessment is investigated.
- Examining the model error associated with the masonry design codes
    - The error of the North American codes, CSA S304-14 and TMS 402-16, is quantified probabilistically using well-validated FE-based data.
    - The sensitivity of the model error to the variations of different design parameters (e.g., load eccentricity, slenderness ratio, masonry compressive strength and reinforcement ratio) is investigated.
    - The design codes are used to conduct reliability assessment to assess the influence of the accuracy of the behavioural model on the reliability of the masonry walls.

1.4 Organization of Thesis

The thesis includes six chapters, and these chapters are organized as follows:

- Chapter 1 introduces the research background, problem statement, research motivation, objectives, methods, and scope of this thesis work.
- Chapter 2 presents a comprehensive literature review, including existing experimental testing of concrete masonry walls, numerical models, uncertainty analysis, probabilistic structural analysis methods and applications to masonry walls, relevant aspects specified in masonry design codes, as well as structural reliability analysis methods and applications to masonry structures.
- Chapter 3 focuses on the probabilistic structural analysis of reinforced concrete masonry walls under out-of-plane loading based on FE models. Uncertainties considered include those in material and geometric properties, as well as the uncertainty associated with the

FE-prediction of load-bearing capacity of masonry walls, which is quantified using an experimental database compiled from the literature. Furthermore, variance-based global sensitivity analysis is also presented to show the relative importance of material and geometric properties, as well as the model uncertainty.

- Chapter 4 provides FE-based reliability analysis of reinforced concrete masonry walls considering slenderness effects. This shows the importance of model uncertainty on the reliability assessment and relative conservatism associated with different failure criteria that can be used in the design process.
- Chapter 5 examines the design code models and quantifies the error associated with these codes in a probabilistic manner. It is found that reliability assessment results can be significantly biased when assuming design code models are accurate without model error.
- Chapter 6 summarizes the findings of this thesis, conclusions, limitations, and recommendations for future work.

CHAPTER 2:Literature Review

2.1 Introduction

Considerable research efforts were devoted to investigate and comprehend the out-of-plane (OOP) behaviour of reinforced concrete masonry walls under eccentric vertical loads or lateral loads (e.g., wind). For instance, different experimental tests were conducted to investigate the behavioural characteristics of masonry walls, such as the second-order effects, the effect of boundary conditions, and the effective flexural rigidity (e.g., Yokel et al. 1970, Hatzinkolas et al. 1978, ACI-SEASC 1982, Suwalski 1986, Aridru 1997, Liu and Dawe 2001, Mohsin 2005). Among these tests, very few focused on highly slender walls (i.e., with height-to-thickness ratio, or slenderness ratio (h/t) >30). The lack of understanding of the behaviour of such walls due to the scarcity of experimental data is compensated, hopefully by overly conservative design code provision (Mohsin 2005). As complementary to the experimental studies, several researchers have worked on developing mechanics-based numerical models or empirical models to study or predict the behaviour of masonry structures. However, the accuracy of the aforementioned models is a key aspect of any subsequent analysis. In that sense, special attention is given in this study to the significance of model uncertainty for mechanics-based finite element (FE) models and design codes-based models, which are commonly used for the OOP behaviour and load capacity prediction. In the face of uncertainty, countable studies considered the uncertainties inherent in the material and geometric properties of masonry structures. Thus, this thesis will mainly focus on uncertainty analysis of masonry walls under OOP loading mainly including four types of problems. They are: (1) probabilistic structural behaviour analysis, (2) variance-based global sensitivity analysis, (3) model uncertainty quantification or statistical model error

assessment using experimental data, and (4) structural reliability analysis of masonry walls using FE models and design code modes.

This chapter provides a brief review of the relevant research on masonry walls, mainly in terms of experimental testing, numerical modelling, model error quantification, probabilistic structural analysis, structural reliability analysis, and the investigation of the relative conservatism associated with the design codes.

2.2 Experimental Studies

To understand the behaviour of masonry structures, several experimental programs were conducted to study reinforced concrete masonry walls under out-of-plane (OOP) loading such as (e.g., Yokel et al. 1970, Hatzinkolas et al. 1978, ACI-SEASC 1982, Suwalski 1986, Aridru 1997, Liu and Dawe 2001, Mohsin 2005). The aforementioned experimental programs were conducted with different aims such as understanding the behaviour of highly slender walls (e.g., Yokel et al. 1970, ACI-SEASC 1982), evaluating the effective flexural rigidity (e.g., Hatzinkolas et al. 1978, Aridru 1997, Liu and Dawe 2001), evaluating the effect of the load eccentricity on the load-bearing capacity and failure modes (e.g., Hatzinkolas et al. 1978, Suwalski 1986), and the effect of the support conditions (e.g., Mohsin 2005). The aforementioned experimental programs are further discussed in this section.

2.2.1 Yokel et al. (1970)

In this experimental program, a total of 60 concrete masonry walls were tested under vertical loads applied at different eccentricities. The tested walls had various slenderness ratios (h/t) ranging from 21 to 43 and the same boundary conditions which were designed to resemble a fixed-roller state. The findings of this study revealed that the failure mode was highly sensitive to

the slenderness ratio (*h/t*) because walls with lower slenderness ratios (e.g., *h/t* = 21) tended to fail due to masonry crushing under compression while highly slender walls (e.g., *h/t* = 43) were noticed to exhibit flexure failure with excessive deformation accompanied by stiffness degradation. It was found that the load capacity of the slender concrete masonry walls can be conservatively predicted by the moment magnifier method, which is a simplified approach to account for second-order effects.

2.2.2 Hatzinkolas et al. (1978)

A total of 68 concrete masonry walls were tested under vertical loads applied at different eccentricities. The slenderness ratio (*h/t*) of the tested walls ranged from 14 to 24. All of the walls were tested in pinned-roller conditions. The experimental program was designed to investigate the effect of different factors (e.g., load eccentricity (*e*), slenderness ratios) on the behaviour of masonry walls. It was found that the axial load capacity decreased with increasing eccentricity and/or slenderness ratios. This trend was attributed to the effect of the eccentricity and slenderness ratios on the effective flexural rigidity. Other factors were also reported to be influential regarding the effective flexural rigidity, such as stress distribution and intensity on the cross-section, and tensile bond strength between the mortar and the block. Incorporating the aforementioned factors in the moment magnifier method led to more realistic predictions when compared to the experimental results.

2.2.3 ACI-SEASC (1982)

To investigate the behaviour of highly slender reinforced masonry walls, a total of 30 walls were tested with slenderness ratios (*h/t*) varying from 30 to 51. All the walls were tested in pinned-roller boundary conditions. Loading-wise, an eccentric vertical load was applied to simulate the

gravity loads, followed by lateral loads slowly applied with increasing magnitude. The experimental load-deflection curves of the tested walls indicated the ability of highly slender masonry walls to efficiently withstand lateral loads in a ductile manner, even after steel bars yielding. Additionally, walls showed no evidence of lateral instability within the range of the applied vertical load (i.e., less than 10% of the axial load capacity). Intuitively, second-order effects were most pronounced in thinner walls. The findings of this study inspired the later design provisions in different aspects, such as the limitations on the minimum and maximum reinforcement ratios and the maximum permissible vertical loads.

2.2.4 Suwalski (1986)

A total of 14 concrete masonry walls were tested under vertical loading with various eccentricity ratios and pure bending. All the walls had a slenderness ratio (*h/t*) of 17 and were tested in pinned-roller conditions. The experimental findings indicated that the axial load capacity was affected by the load eccentricity and the slenderness of the walls, which conformed to the findings reported in (Hatzinkolas et al. 1978).

2.2.5 Aridru (1997)

Aiming to develop a rigorous approach for evaluating the effective flexural rigidity of masonry walls, a total of 73 concrete masonry walls were tested under vertical loading applied axially and at various eccentricities. The slenderness ratio (*h/t*) of the tested walls ranged from 7 to 9.5. The walls were all tested in pinned-roller conditions. Different aspects were investigated within the scope of this experimental program, such as the effect of load eccentricities, grouting and reinforcement configuration. Conforming to the findings of the aforementioned experimental programs, the load eccentricity was shown to affect the failure pattern substantially. The walls

associated with lower eccentricities failed mainly by crushing of the masonry units in compression. As eccentricity increased, the failure mode shifted from compression to flexural. However, in the case of partially grouted cores, the failure was attributed to diagonal splitting cracks. Finally, the effective flexural rigidity was reported to be influenced mainly by the non-linearities associated with the stress-strain behaviour of masonry for walls with lower load eccentricities. On the contrary, the flexural tensile cracking was most influential for the effective flexural rigidity of walls with higher load eccentricities.

2.2.6 Liu & Dawe (2001)

As an extension to the experimental work presented in (Adridu 1997), a total of 36 reinforced masonry walls were tested under different combinations of axial and lateral loads. In addition, this study focused on the effect of the pre-compression level on the flexural rigidity and out-of-plane load capacity. The experimental findings of this study revealed that the failure pattern was influenced by the axial pre-compression level. The walls loaded with lower pre-compression levels (i.e., less than 30% of the axial load capacity) were found to fail due to tensile cracking along the mid-height bed joints. However, for very high pre-compression levels (i.e., more than 60% of the axial load capacity), the failure pattern shifted to explosive crushing accompanied by web splitting. Most importantly, the experimental results revealed that the effective flexural rigidity was correlated to the pre-compression levels and the load eccentricity. Finally, the Canadian design provisions (CSA S304-94) were found to produce very conservative predictions for the effective flexural rigidity for walls loaded with relatively low load eccentricities (e.g., $^{e}/_{t} < 0.4$). On the contrary, slightly un-conservative predictions were associated with walls loaded with larger eccentricities (e.g., $^{e}/_{t} > 0.4$).

2.2.7 Mohsin (2005)

To investigate the behaviour of slender reinforced concrete masonry walls considering the rotational stiffness of the support conditions provided by the strip footings, a total of 8 walls were tested under eccentric vertical loads. The experimental findings showed that incorporating the rotational stiffness at the support substantially increased the out-of-plane load capacity. Additionally, walls with higher support rotational stiffness were less vulnerable to the slenderness effect as they were associated with higher effective flexural rigidity. Based on these observations, the study concluded that ignoring the support stiffness for highly slender walls (i.e., $h/t > 30$) was not justified. Furthermore, the study found that the Canadian design provisions (CSA S304-04) significantly underestimate the effective flexural rigidity for all the tested walls, even those tested without base support stiffness.

2.3 Numerical Studies

As complementary to experimental studies, various numerical modelling approaches have been developed to predict the behaviour of reinforced concrete masonry walls. The modelling approaches can be mainly categorized into two main families: micro and macro modelling. The micro modelling approach explicitly accounts for the material heterogeneity (i.e., unit, mortar, and/or unit-mortar interfaces) and the actual texture of masonry composites. Thus, this approach allows to capture local failure in mortar joints and provides detailed insight into the behaviour of masonry walls. On the contrary, the macro modelling approach ignores the inhomogeneity of masonry walls and offers a simpler and more efficient alternative to capture the global behaviour of masonry walls. The previous research on the aforementioned two modelling approaches is discussed in this section.

2.3.1 Micro models

One of the first implementations of the micro modelling approach was presented in (Page 1978). In this study, elastic plane-stress continuum elements were used to model the masonry units, whereas the mortar joints were defined using non-linear linkage elements. However, the model was not able to account for the non-linearities associated with the masonry units. In addition, the model was not able to predict the ultimate load capacity due to the absence of defined failure criteria for the masonry (e.g., compression cap for the units or the joints, shear strength). Afterwards, Ali et al. (1986) developed a non-linear micro FE model and incorporated different local failure criteria (e.g., bond failure), resulting in a relatively good match between the FE simulations with the experimental tests. After that, the micro modelling approach was used to predict complex failure mechanisms such as web-splitting, as reported in (Sayed-Ahmed and Shrive 1994). The well-known interface-based micro modelling approach was first introduced by Lotfi and Shing (1994). The mortar layers were modelled as zero-thickness interface elements, while the masonry units were modelled based on a smeared crack approach. The use of the interface elements was shown to be efficient in accounting for different local failure mechanisms. Afterwards, Lourenco and Rots (1997) extended the interface-based modelling approach by developing a multi-surface interface element. In that sense, all the non-linearities related to the mortar joints and bonding between mortar and units and the compressive failure of masonry were incorporated in the zero-thickness interface elements. The aforementioned multi-surface interface approach was later used to model the behaviour of partially grouted masonry walls, accompanied by a smeared crack model for masonry units (Shing and Cao 1997). However, the aforementioned developed models were more suited to walls subjected to in-plane (IP) loading (Mohsin 2005).

The interface-based micro modelling approach was introduced to model masonry walls under out-of-plane loadings in (Martini 1997). However, this study reported considerable discrepancies between the experimental tests and numerical simulations. These discrepancies were attributed to the lack of information on different modelling parameters and the negligence of the non-linear properties of the masonry units. The study also concluded that the proposed model was computationally intensive, and the same level of accuracy can be obtained using simpler and more efficient models. Recently, more accurate micro models were developed to model the out-of-plane behaviour of masonry walls. For instance, Kuang and Yuen (2013) accurately captured the non-linear behaviour and failure modes of masonry-infilled reinforced concrete frames under different combinations of IP and OOP loads. D'Altri et al. (2018) developed a detailed micro model that was employed to predict the behaviour of masonry walls subjected to IP and OOP loads. In this study, the mortar joints were modelled explicitly while the bonding between the mortar joints and the masonry units was modelled using a zero-thickness rigid-cohesive-frictional interface.

However, all the introduced micro models were not suited to applications that require numerous simulations (e.g., reliability analysis of masonry walls) due to their computational expense. In addition, they were more applicable to unreinforced masonry walls and more advanced modelling strategies are required for reinforced masonry walls (Koutromanos et al. 2011). Alternatively, the macro modelling approach can be efficiently employed to predict the behaviour of masonry structures, especially for cases when global behaviour is of interest.

2.3.2 Macro models

An early application of the macro modelling approach was introduced by Lourenco et al. (1995). In this model, the masonry units and joints were smeared out in a 2D anisotropic homogenous continuum based on the average stress/strain relationships of the composite material. In that sense, the model neglected the interactions between the different constitutes. However, the model was proved to be capable of capturing the global behaviour of sufficiently large unreinforced masonry walls. Similar work can be found in Lopez et al. (1999).

In the context of masonry walls under OOP loading, the beam-based approach was proved well-suited to sufficiently tall walls subjected to OOP loading with negligible edge effects (Ganduscio and Romao 1997). In that sense, the beam-based macro modelling approach was considered a viable alternative for modelling slender unreinforced masonry walls. For instance, Lu (2003) adopted this approach to predict the global behaviour of slender unreinforced masonry walls considering the material and geometric non-linearities. The beam-based macro modelling approach was proven to successfully reproduce the entire load-deflection curve for the considered experimental tests.

Similarly, the beam-based macro modelling approach provides a viable and efficient alternative for modelling reinforced slender masonry walls. For instance, Wang et al. (1997) developed a beam-based macro model to model the behaviour of slender masonry cavity walls under eccentric vertical loads. In this model, the modelling parameters of masonry were derived based on the corresponding prism tests. Afterwards, they were fed into a predefined concrete material model in Abaqus. The model was able to reproduce the experimental results in an accurate and computationally efficient way. Similarly, Liu (2002) developed beam-based macro models to

predict the OOP behaviour of reinforced masonry walls considering different parameters (e.g., eccentricity ratios and slenderness ratios). The developed models were validated against experimental simulations, and they were shown to be providing predictions with acceptable accuracy and sufficient efficiency. After that, the beam-based macro modelling approach was widely used by other researchers (e.g., Mohsin 2005, Pettit 2020, Bilotta and Cruz 2021) for reinforced masonry walls with different aims, such as evaluating the flexural rigidity and the effect of the different boundary conditions.

In this thesis, the beam-based macro modelling approach is employed to study the probabilistic behaviour and the reliability of reinforced concrete masonry walls subjected to OOP loading. This modelling approach is well-suited to the considered applications as it provides predictions with sufficient accuracy at relatively reasonable computational cost, which is of paramount importance for such computationally intensive applications.

Although many efforts were conducted to develop numerical models of masonry walls, the masonry wall behaviour is highly affected by different uncertainties (e.g., geometrical and material uncertainties) that remain outside of the capability of deterministic prediction models (D'Altri et al., 2019). The inherent uncertainty is typically treated in the design provisions conservatively by increasing the safety margin to a certain degree. Accordingly, to lay down the basis for a reliable structural design, rigorous evaluation of the uncertainty in the behaviour of masonry structures in a probabilistic manner is of paramount importance.

2.4 Probabilistic Structural Analysis

Different methods were developed to propagate the input uncertainties (e.g., uncertainties in material and geometric properties) into output uncertainties in response quantities (e.g., load

capacity of masonry walls). These methods include approximate methods such as first-order second-moment (FOSM) (Barbato et al. 2010), and stochastic sampling methods such as crude Monte Carlo simulation (MCS) (Metropolis and Ulam 1949, Dimov and Georgieva 2010, Barbato et al. 2014). FOSM is widely adopted in the literature due to its relative simplicity (Athmani et al. 2018). However, it is associated with several drawbacks that can emerge from the embedded assumptions, such as the linearization mapping between the response quantities and the input parameters and the inability to fully incorporate input parameters distributions information (Barbato et al. 2010). On the contrary, the stochastic sampling method (e.g., MCS) allows incorporating the non-linearities associated with complex systems in the probabilistic analysis and is considered more accurate than the approximate methods. More importantly, it is very easy to use, which often makes it the first choice of engineers.

Specific to applications to probabilistic analysis of masonry structures, several studies were conducted to investigate the effect of different uncertainties on the probabilistic behaviour of unreinforced masonry walls by employing MCS. For instance, (Li et al. 2014) investigated the probabilistic behaviour of unreinforced masonry walls loaded in vertical bending. In this study, probabilistic analysis was used to quantify the statistical characteristics of different behavioural characteristics (e.g., base cracking load, mid-height cracking load, and the peak load capacity). In addition, the effect of the unit-to-unit spatial variability of the flexural bond strength on the aforementioned behavioural characteristics was also considered. Afterwards, the same authors conducted a similar analysis on unreinforced masonry walls loaded in horizontal bending (Li et al. 2016). Similarly, Zhu et al. (2017) developed a stochastic micro FE model for hollow concrete masonry wallets loaded in compression. The uncertainties associated with different

material parameters were incorporated in the FE model, and thus the probabilistic compressive strength was obtained. More recently, Isfeld et al. (2021) developed a stochastic micro FE model for unreinforced walls of different heights subjected to OOP loading. The outcomes of this study revealed that the narrow unreinforced walls were more sensitive to the variations associated with material parameters and spatial variabilities.

To the best of the author's knowledge, no previous studies investigated the probabilistic behaviour of reinforced concrete masonry walls. The probabilistic structural analysis of reinforced masonry walls can be carried out by incorporating the inherited uncertainties in micro or macro FE models. However, the computational cost of the micro FE modelling approach constitutes a significant challenge for such an application, and the probabilistic characterization of the basic random variables (e.g., mechanical properties of the reinforcement-grout bond) in the micro FE model is rarely available. Alternatively, the macro FE modelling approach is more appropriate for such an application and thus will be used in this thesis.

In addition to the probabilistic structural analysis, variance-based global sensitivity analysis can be carried out to get a deeper insight into the effect of the variations of the uncertain parameters on the considered response quantities (e.g., load capacity).

2.5 Variance-based Global Sensitivity Analysis

Sensitivity analysis is categorized into two main categories: local and global. In the local sensitivity analysis, the effect of input parameters on the considered response is assessed on a one-factor-at-a-time basis employing gradient-based techniques or finite difference method by perturbation analysis. In contrast, global sensitivity analysis quantifies the output variance by simultaneously accounting for the uncertainty of all input parameters, which allows a global

assessment of their relative contribution, including interaction effects (Su et al. 2018, Sudret 2008). Although global sensitivity analysis provides more reliable measures for the relative influence of input parameters, it is often associated with a high computational expense (Dimov and Georgieva 2010). A common way to overcome this problem is to adopt a fast-to-evaluate surrogate model constructed from a feasible number of evaluations of the original computational model. Hence, the constructed surrogate model substitutes the original computational model, which is time-consuming, with enhanced computational performance (Su et al. 2017). To this end, different surrogate models have been developed, such as polynomial chaos expansion (PCE) (Sudret 2008), Gaussian process regression (kriging) (Su et al. 2017) and high dimensional model representation (HDMR) (Mukherjee et al. 2011). Surrogate model-based global sensitivity analysis has been employed in several past studies (Li et al. 2014, Li et al. 2016, Sudret 2008, Bastug et al. 2013).

In the context of masonry structures, previous studies attempted to employ the local sensitivity analysis technique. For instance, Lourenco (1998) assessed the influence of variations of different material parameters on the response of unreinforced masonry shear walls. Similarly, Bhosale et al. (2016) conducted a local sensitivity analysis to identify the most influential parameters with respect to the seismic performance of masonry infilled frames. However, the local sensitivity analysis approach adopted in these studies did not consider the interactions between different parameters. In addition, the variance attributed to the variabilities associated with the uncertain parameters cannot be rigorously quantified within its framework. These drawbacks can be avoided when the global sensitivity approach is adopted.

Different studies conducted a global sensitivity analysis to quantify the contribution of the different parameters to the variance associated with the behaviour of masonry structures. For instance, Mukherjee et al. (2011) conducted an HDMR-based global sensitivity analysis using a micro model of unreinforced masonry shear walls. The analysis revealed that the collapse load was most sensitive to the friction coefficient of mortar joints. Zhu et al. (2017) carried out a PCE-based global sensitivity analysis based on a micro FE model to identify the most influential parameters on the compressive strength of concrete masonry wallets. The analysis revealed that most of the variance (i.e., >75%) was attributed to the tensile strength of the blocks. Tubaldi et al. (2020) carried out a kriging-based global sensitivity analysis using a micro model of backfilled masonry arch bridge. Different uncertainties related to the backfill and the masonry properties were considered. In addition, the sensitivity of different responses (e.g., peak load capacity and secant stiffness) to the considered uncertainties was investigated. The analysis revealed that the peak capacity was mainly affected by the backfill properties, whereas the secant stiffness mainly depended on the block parameters.

However, to the best of the author's knowledge, no similar work is reported for reinforced masonry walls subjected to out-of-plane loading. This gives rise to the need for global sensitivity analysis to determine the influential parameters that dominate the behaviour of such walls. In that sense, different response quantities can be considered, such as peak load capacity and deformation capacity (e.g., ductility).

However, the reliability of the aforementioned analyses (e.g., probabilistic structural analysis and sensitivity analysis) relies significantly on the accuracy of the adopted numerical (FE) model. Accordingly, special attention should be devoted to the error associated with the numerical

model predictions. Although the aforementioned mechanics-based FE models are known to be more reliable compared to empirical models, they are not error-free. The error in the model predictions can arise from various sources such as model simplification, assumptions, or approximations used to represent the physical reality, as well as the variability of experimental conditions and random measurement error (Jiang et al. 2013). In that sense, the rigorous quantification of the model error is necessary to support the analysis and design process of masonry structures.

2.6 Model Error Quantification

The model error should resemble the observed disparity between the model predictions and experimental results. Typically, this error is quantified using a database of reference data (e.g., experimental test data or high-fidelity data) by comparing the experimental-based and model-based predictions. The systematic correlation between the model parameters and the model error is then investigated (Holický et al. 2016). If there is no systematic correlation between the model parameters and the model error, the model error is typically modelled as an independent random variable. Otherwise, the dependency between the model error and the model parameters can be modelled using stochastic regression models such as Gaussian process regression (GPR) (Jiang et al. 2013) and Bayesian linear regression (BLR) (Gardoni et al. 2002).

However, the previous studies on probabilistic analysis or global sensitivity analysis of masonry structures did not account for model uncertainty. Namely, they ignored the influence of the modelling error on the probabilistic behaviour and thus neglected the variance contribution attributed to model uncertainty with respect to the variance attributed to other material and geometrical parameters (Mukherjee et al. 2011, Li et al. 2014, Li et al. 2016, Zhu et al. 2017,

Tubaldi et al. 2020, and Isfeld et al. 2021). In the author's opinion, the effect of the model error on the probabilistic behaviour is worthy of investigation. In addition, incorporating the modelling error was proven to be of paramount importance to have a more confident assessment of reliability levels. This is based on the findings of different studies that investigated the reliability analysis of unreinforced masonry walls subjected to different loading conditions. For instance, Zhai et al. (2012) conducted a reliability analysis for unreinforced masonry walls loaded in shear. It was shown that the reliability indices were highly sensitive to the statistical properties of the model error parameters. Similar findings were reported in other studies (Stewart and Lawrence 2007, Mojsilović and Stewart 2015).

2.7 Reliability Analysis

The structural resistance (i.e., load capacity) of a structural member is essentially uncertain due to the variabilities inherent in the material and geometric properties. Likewise, the demand (i.e., load effects) is also uncertain due to the randomness in the loads applied to the structural member. Accordingly, the actual values of the resistance (i.e., load capacity) and the demand (i.e., load effects) can be different from their corresponding nominal or design values (Mirza 1996). In that sense, the probability that the demand exceeds the resistance (i.e., the probability of failure P_f.) is investigated through structural reliability analysis.

The simplest reliability analysis method is the Monte Carlo simulation (MCS). In this method, the limit state function (G) is evaluated numerous times until a converged probability of failure (P_f) is achieved. However, this approach is not practical for cases where the evaluation of the limit state function is computationally expensive. As such, different methods have been developed to assess the reliability of structures in a computationally efficient manner. These

methods can be categorized into two main categories: approximate analytical methods and advanced simulation-based methods (Jiang et al. 2013). Approximate analytical methods such as first- and second-order reliability methods (FORM and SORM) approximate the non-linear limit state function G at the most probable failure point, referred to as the design point, by a first- or a second-order Taylor expansion in the transformed probability space (standardized normal) of random variables (Hu et al. 2011). However, there are some limitations associated with the approximate analytical methods. For instance, they fail to predict an accurate probability of failure when the considered limit state function is highly nonlinear in the transformed probability space. Furthermore, FORM and SORM require the derivative information of the response quantities with respect to the input parameters, which is usually a challenge for reliability problems with implicit limit state functions (e.g., formulated based on FE models).

Alternatively, advanced simulation-based methods offer a middle ground between the MCS and the approximate analytical methods. In that sense, advanced simulation-based methods provide more accurate estimates of P_f in a relatively computationally efficient manner. Two well-acknowledged methods are Importance sampling (IS) (Melchers 1989) and Subset Simulations (SS) (Au et al. 2007). Although IS and SS significantly increase the computational efficiency, their applicability is still limited for certain applications in which obtaining a sufficient number of samples remains computationally expensive. To tackle this problem, methods based on surrogate models have been introduced.

As mentioned previously, a Surrogate model is a fast-to-evaluate model that mimics the original numerical model with enhanced computational efficiency. The surrogate model is constructed from a limited number of evaluations of the original numerical model, which are performed to

learn the functional relationship between input variables and the output response. Given that the mentioned relationship is established, the surrogate model can be used to define or approximate the limit stat function. Hence, the reliability of the considered structural system can be evaluated employing the aforementioned methods (e.g., FORM, SORM, MCS, IS and SS) in an extremely efficient manner (Su et al. 2017).

Previous studies (Turkstra and Ojinaga 1980, Ellingwood and Tallin 1985, Stewart and Lawrence 2007, Zhai and Stewart 2010, Zhai et al. 2012, Moosavi and Korany 2014) investigated the reliability of masonry structures subjected to different loading conditions (e.g., concentric compression, flexure, and shear). However, these studies were based on the empirical design codes models or simplified analytical models, which can be associated with significant model error. However, the reliability assessment can be susceptible to the accuracy of the adopted behavioural model (Holický et al. 2016). Thus, the negligence of the model error in the reliability assessment can lead to significantly biased results. In order to assess the effect of considering model uncertainty on the reliability assessment, the reliability assessment is conducted with and without considering model uncertainty in this thesis.

Furthermore, in design practice, different failure criteria (e.g., structural member failure, cross-section failure, and material fibre failure) can be used. Thus, the corresponding formulations of limit state function can be influential on the reliability assessment results (Frangopol et al. 1996, Milner et al. 2001). Reliability assessment of masonry walls loaded under eccentric compression and lateral loads is also conducted to reveal the relative conservatism associated with different failure criteria, when walls are designed according to the design codes.

2.8 Relevant Design Provisions of Masonry Walls Against OOP Loading

This section describes the code-based models of CSA S304-14 and TMS 402-16 for reinforced concrete masonry walls loaded out-of-plane. In addition, a brief side-by-side comparison between the two codes is provided. More detailed comparisons can be found in (Erdogmus et al. 2021, Sustersic et al. 2021). It should be noted that only provisions for reinforced concrete masonry walls are considered.

2.8.1 Comparison between CSA S304-14 and TMS 402-16

- Stress block parameters: Both codes adopt the widely known equivalent stress-block approach to account for the stress distribution along the cross-section. Additionally, both codes assume the depth of the compression block equals ($0.80c$), where c is the depth of the neutral axis. However, the uniform masonry stress along the depth of the stress block is taken as $0.85f'_m$ and $0.80f'_m$, where f'_m is the masonry characteristics compressive strength, for CSA S304-14 and TMS 402-16, respectively.
- Maximum usable compression strain (ε_{mu}): CSA S304-14 adopts a value of 0.003 for the maximum usable strain at the critical fibre, while a value of 0.0025 is adopted in the TMS 402-16.
- Modules of elasticity of masonry (E_m): CSA S304-14 relates the modulus of elasticity of masonry E_m to the characteristics masonry compressive strength f'_m with the following expression ($E_m = 850\ f'_m, E_m \leq 20\ GPa$), whereas TMS 402-16 proposes the expression ($E_m = 900\ f'_m$).
- Material resistance and strength reduction factors: CSA S304-14 imposes two different material resistance factors ($\phi_m = 0.60$ and ϕ_s =0.85) for masonry and steel

reinforcement bars, respectively. Conversely, TMS 402-16 imposes a strength reduction factor ($\phi = 0.90$) on the resistance of the structural member. However, this resistance factor is well-suited for tension-controlled sections only. Accordingly, other modifications are proposed for the planned 2022 edition. These modifications include different resistance factors for the compression-controlled and transition sections (Chrysler et al. 2021).

- Maximum permissible axial load: CSA S304-14 limits the maximum permissible axial load to $0.80(0.85\phi_m f'_m A_e)$. While TMS 402-16 adopts a gradual upper bound that depends on (h/r) where (h) is the wall height and (r) is the radius of gyration. Specifically, for walls with ($h/r \leq 99$), the axial load capacity is limited to $0.80[0.80 f'_m(A_n - A_{st}) + f_y A_{st}][1 - [\frac{h}{140\, r}]^2]$, where A_n is the net area of the cross-section, A_{st} is the reinforcement bars area and f_y is the yield strength of the reinforcement bars. While for walls with ($h/r > 99$) an upper bound of $0.80[0.80 f'_m(A_n - A_{st}) + f_y A_{st}][\frac{70r}{h}]^2]$ is applied.
- Cracked neutral axis: CSA S304-14 determines the location of the cracked neutral axis (c) based on an assumption of linear stress distribution along the cross-section while neglecting the effect of the applied axial loads. On the contrary, TMS 402-16 adopts a non-linear stress distribution and considers the effect of the axial load in such an application.
- Cracked moment of inertia (I_{cr}): a major difference between the two considered design codes is the inclusion of the axial load in the calculations of the cracked moment of inertia (I_{cr}). To illustrate, in CSA S304-14, I_{cr} depends only on the cross-sectional

properties, and the applied axial loads are neglected. This is not the case with TMS 402-16 as it considers the axial loads when calculating I_{cr} and cracking moment M_{cr} (Pettit et al. 2020). The considered codes (i.e., CSA S304-14 and TMS 402-16) determine the cracked moment of inertia I_{cr} as follows:

$$I_{cr}(CSA\ S304) = \frac{bc^3}{3} + nA_{st}(d-c)^2 \qquad (2-1)$$

$$I_{cr}(TMS\ 402) = \frac{bc^3}{3} + n\left(A_{st} + \frac{P}{f_y}\right)(d-c)^2 \qquad (2-2)$$

In the formulas above, b is the wall width, c is the cracked neutral axis depth, n is the modular ratio, A_{st} is the area of reinforcement bars, d is the reinforcement bar depth, and P is the axial load.

However, the second-order effects typically dominate the design of slender masonry walls. Accordingly, special care should be devoted to each code approach in determining the second-order effects. CSA S304-14 and TMS 402-16 account for the second-order effects through the P-delta or moment magnifier methods. In the context of this thesis, the widely used moment magnifier method is of interest. The moment magnifier method involves magnifying the maximum applied primary moment (M_p) on the structural member (e.g., concrete masonry wall) by a factor (ψ) to calculate the magnified moment (M_u) due to second-order effects. The following formulas introduce the moment magnifier method in its primal form. The moment magnifier factor is defined as follows:

$$\psi = \frac{C_m}{1 - \frac{P}{P_{cr}}} \quad \text{, in which } P_{cr} = \frac{\pi^2 E I_{eff}}{(kh)^2} \qquad (2-3)$$

Here, C_m is the moment diagram factor, P is the axial load acting on the wall, P_{cr} is Euler buckling load of the wall, EI_{eff} is the effective flexural rigidity, k is the effective length coefficient depending on the boundary conditions (e.g., k = 1.0 for simply supported), and h is the clear unsupported wall length.

However, various differences exist between the two codes in consideration of the second order-effect and the implementation of the moment magnifier method. These differences can be summarized as follows:

- Design for second-order effects: CSA S304-14 divides reinforced concrete masonry walls into three main categories; each of them has its distinct requirements. These categories are defined by the ratio $\left({}^{kh}/_{t}\right)$, where k is the effective length coefficient, h is the wall height and t is the thickness of the wall.
  - Walls with ${}^{kh}/_{t} < (10 - 3.5\ {}^{e_1}/_{e_2})$, where e_1 and e_2 are the end eccentricities, the second-order effects are ignored, and the walls are assumed to fail in crushing upon reaching a specified crushing strain for the extreme masonry compression fibre.
  - Walls with ${}^{kh}/_{t} > (10 - 3.5\ {}^{e_1}/_{e_2})$ and ${}^{kh}/_{t} < 30$, CSA S304-14 requires the consideration of the second-order effect using the aforementioned P-delta or moment magnifier methods.
  - Walls with ${}^{kh}/_{t} > 30$, CSA S304-14 imposes more restrictive requirements such as assuming pinned-pinned boundary conditions for all walls, limiting the

permissible axial stress to $0.06f'_m$ and limiting the flexural reinforcement ratio to ensure a ductile failure.

On the other hand, TMS 402-16 requires the consideration of second-order effects for all walls regardless of the slenderness ratio. However, TMS 402-16 also assumes pinned-pinned boundary conditions for the highly slender walls.

- Maximum permissible axial load: CSA S304-16 limits the axial load for highly slender walls (i.e., $^{kh}/_{t} > 30$) to ($0.1\phi_m f'_m A_e$), where A_e is the effective cross-setion area. On the other hand, TMS 402-16 adopts a limit of ($0.05f'_m A_g$) for the same walls, where A_g is the cross-sectional area.
- Effective flexural rigidity: In both provisions, the effective flexural rigidity (EI_{eff}) is highly influenced by the cracked moment of inertia (I_{cr}). The differences between the two provisions regarding (I_{cr}) is discussed earlier in this chapter. However, TMS 402-16 conservatively adopts the cracked inertia for the entire wall height when the applied moment (M_P) exceeds the cracking moment (M_{cr}). On the other hand, CSA S304-14 penalizes (EI_{eff}) with a stiffness reduction factor ($\phi_{er} = 0.75$) regardless of the applied moment.

The considered codes (i.e., CSA S304-14 and TMS 402-14) determine the effective flexural rigidity EI_{eff} as follows:

$$EI_{eff}(CSA\ S304) = E_m I_{cr} \leq E_m \left[0.25I_o - (0.25I_o - I_{cr})\left(\frac{e - e_k}{2e_k}\right)\right] \leq 0.25E_m I_o \quad (2-4)$$

$$EI_{eff}(TMS\ 402) = \begin{cases} 0.75E_m I_o & M_p < M_{cr} \\ E_m I_{cr} & M_p \geq M_{cr} \end{cases} \quad (2-5)$$

In the formulas above, E_m is the masonry modulus of elasticity, I_o is the gross moment of inertia, I_{cr} is the cracked moment of inertia, e is the eccentricity which is defined as the ratio between the primary moment (M_p) and the axial load (P), e_k is the kern eccentricity which is defined between the ratio between the section modulus (S_e) and the effective mortared area A_e, and M_{cr} is the cracking moment.

A summary of the differences between the considered codes (i.e., CSA S304-14 and TMS 402-16) is provided in Table 2-1.

Table 2-1 Summary of the comparison between CSA S304-14 and TMS 402-16

Parameter	***CSA S304-14***	***TMS 402-16***
ε_{mu}	0.003	0.0025
E_m	$850f'_m$ Upper bound: $20\ GPa$	$900f'_m$
Stress block uniform stress	$0.85f'_m$	$0.80f'_m$
Resistance factors	$\phi_m = 0.65$ $\phi_s = 0.85$ $\phi_{er} = 0.75$	$\phi = 0.9$
Maximum permissible axial load	$0.80(0.85\phi_m f'_m A_e)$	$0.8[0.8f'_m(A_n - A_{st}) + f_y A_{st}][1 - [\frac{h}{140\ r}]^2]$, $(h/r \leq 99)$ $0.8[0.8f'_m(A_n - A_{st}) + f_y A_{st}]\left[\frac{70r}{h}\right]^2]$ $(h/r > 99)$
I_{cr}	$\frac{bc^3}{3} + nA_{st}(d-c)^2$	$\frac{bc^3}{3} + n(A_{st} + \frac{P}{f_y})(d-c)^2$

Maximum permissible axial load for highly slender walls	$0.1\phi_m f'_m A_e$	$0.05 f'_m A_g$
EI_{eff}	$E_m[0.25I_o - (0.25I_o - I_{cr})(\frac{e - e_k}{2e_k})]$ Lower bound: $E_m I_{cr}$ Upper bound: $0.25E_m I_o$	$0.75E_m I_o$, $(M_p < M_{cr})$ $E_m I_{cr}$, $(M_p \geq M_{cr})$

2.8.2 Investigation of the design codes

The inaccuracy in the considered design codes (i.e., CSA S304, TMS 402) has been examined by other researchers (Liu and Dawe 2003, Mohsin 2005, Isfeld et al. 2019, Pettit et al. 2021, Bilotta and Cruz 2021). The findings of the mentioned studies indicated that the design codes are associated with systematic errors. For instance, CSA S304-14 can be overly conservative for highly slender walls loaded with low load eccentricities. For instance, Isfeld et al. (2019) investigated the provisions of using a broad set of available experimental data for unreinforced and reinforced masonry walls. It was found that CSA S304 provides a very conservative design for highly slender walls. Similar observations were reported in Mohsin (2005). On the other hand, TMS 402-16 is shown to produce significantly unconservative results for walls with low compressive strength (f_m) and high reinforcement ratio (ρ_s).

However, none of these studies investigated the modelling error of the design provisions in a probabilistic manner. Instead, they emphasized specific aspects, and the conclusions drawn were based on a limited number of experimental simulations or simple parametric studies. In this study, the model error associated with design code-based models is quantified probabilistically using a combination of numerical and experimental simulations. After that, the original design code-based models are corrected and employed in reliability assessment.

2.9 References

Athmani A., Khemis A., Hacene-Chaouche A., Tee K.F., Ferreira T.M., Vicente R. (2019). Buckling uncertainty analysis for steel pipelines buried in elastic soil using FOSM and MCS methods. International Journal of Steel Structures, 19 (2) 381–397.

ACI-SEASC Task Committee on Slender Walls. (1982). Test report on slender walls. Los Angeles, California.

Ali,S., Page A.W. and Kleeman P.W. (1986). Non-Linear Finite Element Model for Concrete Masonry with Particular Reference to Concentrated Loads. 4th Canadian Masonry Symposium-1986, New Brunswick, Canada.

Aridru, G.G. 1997. Effective flexural rigidity of plain and reinforced concrete masonry walls. Ph.D. thesis, Department of Civil Engineering, University of New Brunswick, Fredericton, N.B.

Au, S. K., Ching, J., & Beck, J. L. (2007). Application of subset simulation methods to reliability benchmark problems. Structural Safety, 29(3), 183-193. doi:10.1016/j.strusafe.2006.07.008

Bastug, E., Menafoglio, A., & Okhulkova, T. (2013). "Polynomial chaos expansion for an efficient uncertainty and sensitivity analysis of complex numerical models." European safety and reliability, Amsterdam, Netherlands.

Barbato, M., Gu, Q., & Conte, J. P. (2010). Probabilistic push-over analysis of structural and soil-structure systems. Journal of Structural Engineering, *136*(11), 1330-1341. doi:10.1061/(ASCE)ST.1943-541X.0000231

Barbato, M., Zona, A., & Conte, J. P. (2014). Probabilistic nonlinear response analysis of steel-concrete composite beams. Journal of Structural Engineering, *140*(1), 4013034. doi:10.1061/(ASCE)ST.1943-541X.0000803

Bilotta, M. and Cruz, Y. (2021). Evaliation of Second-order Effects in Slender Reinforced Masonry Walls. Proc., 14th Canadian Masonry Symposium, Montreal, QC, Canada.

Chen, W. F., & Atsuta, T. (1973). Strength of eccentrically loaded walls. *International Journal of Solids and Structures, 9*(10), 1283-1300. doi:10.1016/0020-7683(73)90115-7

Chrysler J, Bannett M.R., Peterson R, Dalrymple A., Pierson D., Samblanet P.J. (2021). A Preview of Expected Changes to TMS 402/602, with a Look at the 6-year Revisions Cycle. 14th Canadian Masonry Symposium, Montreal, QC, Canada.

CSA S304. (2014). Design of Masonry Structures. Canadian Standards Association, Mississauga, Canada.

D'Altri AM, Sarhosis V, Milani G, Rots J, Cattari S, Lagomarsino S, Sacco E, Tralli A, Castellazzi C, & de Miranda S. "A review of numerical models for masonry structures." Numerical modeling of masonry and historical structures. Woodhead Publishing; 2019. p. 3–53.

D'Altri, A. M., de Miranda, S., Castellazzi, G., & Sarhosis, V. (2018). A 3D detailed micro-model for the in-plane and out-of-plane numerical analysis of masonry panels. Computers & Structures, *206*, 18-30. doi:10.1016/j.compstruc.2018.06.007

Dawe, J. L., & Liu, Y. (2003). Analytical modeling of masonry load-bearing walls. Canadian Journal of Civil Engineering, *30*(5), 795-806. doi:10.1139/l03-036

Dimov, I., & Georgieva, R. (2010). Monte carlo algorithms for evaluating sobol' sensitivity indices. Mathematics and Computers in Simulation, 81(3), 506-514. doi:10.1016/j.matcom.2009.09.005

Drysdale, R. G. and Hamid, A. A. (2005). *Masonry Structures Behaviour and Design*, Canada Masonry Design Centre, Mississauga, ON, Canada

Ellingwood B, Galambos TV, MacGregor JG, Cornell CA (1980). Development of a probability based load criterion for American national standard A58, National Bureau of Standards Special Publication 577, U.S. Government Printing Office, Washington, DC.

Ellingwood, B.M. & Tallin, A.A. 1(985). Limit States Criteria for Masonry Construction, Journal of Structural Engineering, 111: 108

Erdogmus E, Dutrisac H, Thompson J, Bennett B.(2021). Comparison of Selected CSA S304-14 AND TMS 402-16 Reinforced Masonry Design Provisions and Material Properties. 14th Canadian Masonry Symposium, Montreal, QC, Canada.

Frangopol, D. M., Ide, Y., Spacone, E., & Iwaki, I. (1996). A new look at reliability of reinforced concrete columns. Structural Safety, 18(2), 123-150. doi:10.1016/0167-4730(96)00015-X

Ganduscio S, Romano F. (1997). FEM and analytical solutions for buckling of nonlinear masonry members. Journal of Structural Engineering,123(1):104–11.

Gardoni, P., Der Kiureghian, A., & Mosalam, K. M. (2002). Probabilistic capacity models and fragility estimates for reinforced concrete columns based on experimental observations. Journal

of Engineering Mechanics, 128(10), 1024-1038. doi:10.1061/(ASCE)0733-9399(2002)128:10(1024)

Jiang, Z., Chen, W., Fu, Y., & Yang, R. (2013). Reliability-based design optimization with model bias and data uncertainty. SAE International Journal of Materials and Manufacturing, 6(3), 502-516. doi:10.4271/2013-01-1384

Hatzinikolas, M., Longworth, J., and Warwaruk, J. (1978). Concrete Masonry Walls. University of Alberta - Structural Engineering Report No. 70. Department of Civil and Environmental Engineering, University of Alberta. Edmonton, AB.

Holický, M., Retief, J. V., & Sýkora, M. (2016). Assessment of model uncertainties for structural resistance. Probabilistic Engineering Mechanics, 45, 188-197.

Hu, C., & Youn, B. (2011). Adaptive-sparse polynomial chaos expansion for reliability analysis and design of complex engineering systems. Structural and Multidisciplinary Optimization, 43(3), 419-442. doi:10.1007/s00158-010-0568-9

Isfeld, A. C., Müller, A. L., Hagel, M., & Shrive, N. G. (2019). Analysis of safety of slender concrete masonry walls in relation to CSA S304-14. Canadian Journal of Civil Engineering, 46(5), 424-438. doi:10.1139/cjce-2018-0210

Isfeld, A. C., Stewart, M. G., & Masia, M. J. (2021). Stochastic finite element model assessing length effect for unreinforced masonry walls subjected to one-way vertical bending under out-of-plane loading. Engineering Structures, 236, 112115. doi:https://doi.org/10.1016/j.engstruct.2021.112115

Koutromanos, I., Stavridis, A., Shing, P. B., & Willam, K. (2011). Numerical modeling of masonry-infilled RC frames subjected to seismic loads. Computers & Structures, 89(11), 1026-1037. doi:https://doi.org/10.1016/j.compstruc.2011.01.006

Kuang JS, Yuen Y. Simulations of masonry-infilled reinforced concrete frame failure. Proc Inst Civ Eng – Eng Comput Mech 2013;166(4):179.

Li, J., Masia, M. J., Stewart, M. G., & Lawrence, S. J. (2014). Spatial variability and stochastic strength prediction of unreinforced masonry walls in vertical bending. *Engineering Structures, 59*, 787-797. doi:10.1016/j.engstruct.2013.11.031

Li, J., Stewart, M. G., Masia, M. J., & Lawrence, S. J. (2016). Spatial correlation of material properties and structural strength of masonry in horizontal bending. *Journal of Structural Engineering, 142*(11), 4016112. doi:10.1061/(ASCE)ST.1943-541X.0001488

Liu, Y., and Dawe, J.L. (2001). Experimental determination of masonry beam–column behaviour. Canadian Journal of Civil Engineering, 28(5): 794–803.

Lourenco PB & Rots JG. (1997). A multi-surface interface model for the analysis of masonry structures. Journal of Engineering Mechanics 1997: 123(7): 660–668

Lourenco PB, Rots JG, Blaauwendraad J. (1995). Two approaches for the analysis of masonry structures: micro and macro-modeling. Heron, 1950;40(4):313–40.

Lopez, J. Oiler, S., Onate, E. and Lubliner J. (1999) A homogeneous Constitutive Model for Masonry. International Journal for Numerical Methods in Engineering, Vol. 46, pp. 1651-1671,1999.

Lu, M. 2003. Stability of Unreinforced Masonry Members Under Simultaneous Vertical & Out-of-Plane Lateral Loads. Ph.D., University of Minnesota, Minnesota.

Martini, K. 1997. Finite Element Studies in the Out-of-Plane Failure of Unreinforced Masonry. In Proc., 7th Int. Conf. on Computing in Civil & Building Engineering, Vol. 1, pp. 179-184.

Melchers, R. E. (1989). Importance sampling in structural systems. Structural Safety, 6(1), 3-10. doi:10.1016/0167-4730(89)90003-9

Metropolis, N., & Ulam, S. (1949). The monte carlo method. Journal of the American Statistical Association, 44(247), 335-341. doi:10.1080/01621459.1949.10483310

Metwally, Z. and Li, Y. (2021). Finite Element-based Probabilistic Behavior Analysis of Slender Reinforcement Masonry Walls Under Out-of-plane Loading. Proc., 14th Canadian Masonry Symposium, Montreal, QC, Canada.

Milner, J., David M, Spacone, E., & Frangopol, D. M. (2001). New light on performance of short and slender reinforced concrete columns under random loads. Engineering Structures, 23(2), 147-157. doi:10.1016/S0141-0296(00)00036-5

Mirza, S. A. (1996). Reliability-based design of reinforced concrete columns. Structural Safety, 18(2), 179-194. doi:10.1016/0167-4730(96)00010-0

Mohsin, E. (2005). Support stiffness effect on tall load bearing masonry walls. PhD Thesis, University of Alberta, Edmonton.

Mojsilović, N., & Stewart, M. G. (2015). Probability and structural reliability assessment of mortar joint thickness in load-bearing masonry walls. Structural Safety, 52, 209-218. doi:https://doi.org/10.1016/j.strusafe.2014.02.005

Moosavi H.. (2017). Structural reliability of non-slender loadbearing concrete masonry members under concentric and eccentric loads. PhD thesis, Department of Civil and Environmental Engineering, University of Alberta, Edmonton, AB.

Moosavi, H., & Korany, Y. (2014). Assessment of the structural reliability of loadbearing concrete masonry designed to the canadian standard S304.1. Canadian Journal of Civil Engineering*, 41*(12),

MSJC. 2016. Building Requirements and Specifications for Masonry Structures. Standard TMS 402/602- 16, The Masonry Society, Longmont, CO.1046-1053. doi:10.1139/cjce-2013-0498

Mukherjee, D., Rao, B. N., & Meher Prasad, A. (2011). Global sensitivity analysis of unreinforced masonry structure using high dimensional model representation. Engineering Structures, 33(4), 1316-1325. doi:https://doi.org/10.1016/j.engstruct.2011.01.008

Ozbakkaloglu, T., & Saatcioglu, M. (2004). Rectangular stress block for high-strength concrete. ACI Structural Journal, 101(4) doi:10.14359/13333

Page, A.W. (1978). Finite Element Model for Masonry. Journal of Structural Division, ASCE, Vol. 104, No. ST, August 1978, pp. 1267-1285.

Pettit, C. 2020. Effect of Rotational Base Stiffness on the Behaviour of Loadbearing Masonry Walls. M.Sc. thesis, Department of Civil and Environmental Engineering, University of Alberta, Edmonton, AB.

Pettit, C. E. J., Mohsin, E., Cruz-Noguez, C., & Elwi, A. E. (2021). Experimental testing of slender load-bearing masonry walls with realistic support conditions. Canadian Journal of Civil Engineering, doi:10.1139/cjce-2020-0297

Sayed-Ahmed, E.Y. and Shrive, N.G. (1996) "Nonlinear Finite Element Model of Hollow Masonry" Journal of Structural Engineering,Vol.l22, No.6 June 1996, pp. 683-1587.

Shing PB, Cao L. (1997) Analysis of partially grouted masonry shear walls. Gaitherburg (MD): US Department of Commerce. National Institute of Standards and Technology. NISTIR GCR 97-710.

Stewart MG, Lawrence SJ. (2007). Model error, structure reliability and partial safety factors for structural masonry in compression. Masonry International, 20(3):107–16.

Su, G., Peng, L., & Hu, L. (2017). A Gaussian process-based dynamic surrogate model for complex engineering structural reliability analysis. Structural Safety, 68, 97-109. doi:10.1016/j.strusafe.2017.06.003

Su, L., Wan, H., Li, Y. Y., & Ling, X. (2018). Soil-pile-quay wall system with liquefaction-induced lateral spreading: Experimental investigation, numerical simulation, and global sensitivity analysis. American Society of Civil Engineers (ASCE). doi:10.1061/(asce)gt.1943-5606.0001977

Sundararajan, C. (1995). Probabilistic structural mechanics handbook. Houston, Texas: Springer Science+ Business Media Dordrecht.

Sudret, B. (2008). Global sensitivity analysis using polynomial chaos expansions. Reliability Engineering & System Safety, 93(7), 964-979. doi:10.1016/j.ress.2007.04.002

Sustersic H, Stubbs D, Peterson R, Bannett R., Pettit C., Flisak B., Erdogmus E., Thompson J., Bennett B., Cruz C. (2021). Parametric Studies on Reinforced Masonry Walls Resisting Out-of-plane Loads: A Comparison of CSA S304-14 and TMS 402-16. 14th Canadian Masonry Symposium, Montreal, QC, Canada.

Suwalski, P.D. (1986). Capacity of eccentrically loaded slender concrete block walls. M.Sc. thesis, Department of Civil Engineering, MCMaster University, Hamilton, Ont.

Tubaldi E, Macorini L, Izzuddin BA. (2020). Identification of critical mechanical parameters for advanced analysis of masonry arch bridges. Structure and Infrastructure Engineering, 16(2):328–45.

Turkstra, C. & Ojinaga, J. (1980). Towards a Canadian Limit States Masonry Design Code. In Proceedings of the 2nd Canadian Masonry Symposium, Carleton University, Ottawa, Ontario, Canada.

Priestley, M. J. N., and Elder, D. M. (1983). Stress–strain curves for unconfined and confined concrete masonry. ACI J., 80-3, 192–201

Wang, R., Elwi, A. E., and Hatzinikolas, M. A. (1997). Numerical Study of Tall Masonry Cavity Walls Subjected to Eccentric Loads. Journal of Structural Engineering, Vol. 123, No. 10, pp.1287-1294

Yokel, F.Y., Mathey, R.G., and Dikkers, R.D. 1970. Compressive strength of slender concrete masonry walls. Building Science Series 33, U.S. National Bureau of Standards, Washington, D.C.

Zhai, X., and Stewart, M. G. (2010). Structural reliability analysis of reinforced grouted concrete block masonry walls in compression. Engineering Structures, 32(1), 106–114.

Zhai, X., Zhong, Z., & Stewart, M. G. (2012). Model error and structural reliability for reinforced concrete block masonry walls in shear. Advances in Structural Engineering, 15(3), 389-398. doi:10.1260/1369-4332.15.3.389

Zhu, F., Zhou, Q., Wang, F., & Yang, X. (2017). Spatial variability and sensitivity analysis on the compressive strength of hollow concrete block masonry wallettes. Construction & Building Materials*, 140*, 129-138. doi:10.1016/j.conbuildmat.2017.02.099

CHAPTER 3: Probabilistic Behaviour and Variance-based Sensitivity Analysis of Reinforced Concrete Masonry Walls under Out-of-plane Loading

Inherent uncertainties associated with masonry structures result in large scatter in the experimentally or analytically predicted behaviour. Rigorous investigation of the uncertainties in the structural behaviour of masonry structures is of paramount importance to lay down the basis for reliable structural design. In this study, the probabilistic behaviour of reinforced masonry walls under out-of-plane (OOP) loading is investigated. Uncertainties in material and geometric properties are incorporated in finite element (FE) models for probabilistic structural analysis. The individual and combined effect of different uncertain input parameters on the overall probabilistic behaviour is evaluated. Furthermore, the relative importance of uncertain variables to the load and deformation capacities is assessed using variance-based sensitivity analysis. The model uncertainty in FE-predicted load capacity is also quantified to characterize the model error, which is found to be non-negligible compared to geometric and material uncertainties.

3.1 Introduction

Masonry provides a competitive alternative compared to other construction materials for its durability, strength, hygrothermal performance, and aesthetics. However, masonry walls exhibit complex structural behaviour with relatively large scatter due to the inherited heterogeneity and complex interaction between different components (i.e., unit, mortar, grout, and steel reinforcement). To understand the complex behaviour, several experimental programs were conducted to study reinforced concrete masonry walls under out-of-plane (OOP) loading with different testing objectives (e.g., Yokel et al. 1970, Hatzinkolas et al. 1978, ACI-SEASC 1982, Mohsin 2005). In spite of these great efforts, experimental data generated for reinforced concrete

masonry walls under OOP loading remains limited to understand the wall behaviour from a probabilistic perspective considering inherent uncertainties associated.

As complementary to experimental studies, various analytical and numerical models have been developed to predict the load capacity or overall structural behaviour of reinforced masonry walls. Specifically, the behaviour of masonry walls under OOP loading can be predicted to various degrees of accuracy using the micro finite element (FE) modelling approach (Abdulla et al. 2017, Bui et al. 2017, D'Altri et al. 2018), macro FE modelling approach (Pluijm 1999), and simplified analytical procedures (e.g., Dawe and Liu 2003). The micro-FE modelling approach explicitly accounts for the material heterogeneity (i.e., unit, mortar, and/or unit-mortar interface). Thus, this approach allows to capture local failure in mortar joints and provides detailed insight into the behaviour of masonry walls. However, it is computationally expensive (Minga et al. 2019), and its prediction accuracy heavily depends on the calibration of various parameters in advanced three-dimensional constitutive models, which are used to describe the materials and interfaces. Alternatively, the macro FE modelling approach ignores the inhomogeneity of masonry walls and offers a simpler and more efficient solution to capture the global behaviour of masonry walls. For example, the nonlinear fibre-section-based beam approach is widely used to model the OOP behaviour of walls with negligible effect of lateral edge restraints, by considering the masonry material (unit plus mortar) as a homogenized continuum (Chen and Atsuta 1973, Ganduscio and Romano 1997). Compared with other simplified analytical methods and design code methods, nonlinear fibre-section-based beam approach considers the geometrical nonlinearity rigorously, instead of using the moment magnifier method (CSA 2014),

which has been widely used in the masonry literature for its efficiency and accuracy (Liu and Dawe 2003, Mohsin 2005, Bilotta and Cruz 2021).

However, due to model assumptions as well as geometric and material uncertainties that can dominate the behaviour of masonry walls (D'Altri et al. 2019), the development of a reliable behaviour prediction model remains a challenging task. To address this problem in engineering practice, a conservative approach is typically taken to increase the safety margin in design. However, to lay down the basis for reliable structural design as implied by the limit-state design philosophy, rigorous evaluation of the uncertainty in the behaviour of masonry walls is of paramount importance.

In recent years, researchers (Li et al. 2014, Li et al. 2016, Zhu et al. 2017) started to investigate the effect of uncertainties on unreinforced masonry walls by incorporating the randomness in material and geometric properties to assess the effect of spatial variability within a wall using micro FE models. Nevertheless, the micro FE modelling approach for probabilistic analysis is considered to be computationally challenging, and probabilistic characterization of spatial variability and uncertainty in variables of the micro FE model is rarely available. In contrast, the mechanics-based macro FE models (e.g., nonlinear fibre-section-based beam models) of masonry walls are more appropriate for probabilistic structural analysis and probabilistic characterization of the important material and geometric parameters can be readily found (Moosavi 2017). Thus, the pertinent material and geometric uncertainties can be incorporated into macro FE models and propagated to the load capacity and ductility of masonry walls, by stochastic sampling methods such as Monte Carlo simulation (MCS).

MCS is an accurate and robust technique to perform probabilistic structural analysis without intervening the FE simulation (Buonopane 2008, Barbato et al. 2010, Barbato et al. 2014, Grubišić et al. 2019). The simulated samples stochastically generated from MCS also allow conducting the variance-based sensitivity analysis, in which the variance in the FE model output is decomposed into contributions from individual parameters or parameter groups (Su et al. 2018). Eventually, this leads to further insight into the relative importance of different uncertain variables on a response of interest (e.g., load capacity, deformation capacity). Note that previous work on variance-based sensitivity analysis typically neglected modelling error, while in this study, the analysis of the variance in the load capacity prediction will be conducted with and without model uncertainty to reveal the importance of model uncertainty.

To summarize, this paper aims to study the probabilistic behaviour of reinforced masonry walls by integrating macro FE models with MCS to (1) perform probabilistic behaviour analysis and (2) variance-based sensitivity analysis with and without model uncertainty. To evaluate the accuracy of the macro FE models in predicting the load capacity, experimental data of masonry walls tests under OOP loading available from the literature is collected and used to quantify the model prediction accuracy by comparing FE predictions with the corresponding experimental data. The probabilistic behaviour considering the individual and combined effect of uncertain input parameters is investigated using MCS. A confidence envelope (5^{th} percentile and 95^{th} percentile) of the load-displacement curves is obtained, in addition to the probability distribution of load and deformation capacities. Additionally, variance-based global sensitivity analysis is performed to quantify the contribution from each uncertain variable to the variance of load and deformation capacities of reinforced concrete masonry walls under OOP loading.

3.2 FE models of Reinforced Concrete Masonry Walls

3.2.1 Masonry walls

The reinforced concrete masonry walls studied in this paper were tested in 1982, aiming to investigate the behaviour of slender masonry walls when subjected to eccentric axial and lateral loads (ACI-SEASC 1982). These walls are of the same size, 7300 mm in height (h) and 1200 mm in width (b), and were tested with pinned-roller boundary conditions. The walls are categorized into three groups according to the nominal thickness (t) and the corresponding slenderness ratio, defined as the height-to-thickness ratio *(h/t)*. Among the nine concrete masonry walls tested in this experimental program, three walls with different slenderness ratios are considered here, including wall#2 with h/t = 30 in group 1, wall #5 with h/t = 38 in group 2, and wall #9 with h/t = 51 in group 3, respectively (see Table 3-1). All walls were reinforced with five #4 bars of grade 60, which were designed to be located at half wall thickness (i.e., d_n =0.5t). Loading-wise, the walls were loaded first by axial compression (P) at an eccentricity e, equal to 7.62 cm plus half of the wall thickness (t) and then by uniform lateral pressure (q) using air-bag. The lateral pressure was monotonically increased until the walls deformed excessively with extensive stiffness degradation during the tests (ACI-SEASC 1982). The wall configuration is shown in Figure 3-1(a). Readers of interest for more details are referred to the experimental program report (ACI-SEASC 1982).

Table 3-1 Summary of reinforced concrete masonry walls studied

GP #	*Walls*	*Wall thickness* *t, in (cm)*	*Slenderness ratio* *h/t*	*Masonry compressive strength* f_m , *MPa*	*Young's modulus* E_0, *MPa*	*Axial load* *P, N*	*Steel yield strength* f_y , *MPa*	*Steel modulus* *E, MPa*
1	#2	10 (25.4)	30	17.0	14962	15250	482	197000
2	#5	8 (20.3)	38	17.9	11859	15250	482	197000
3	#9	6 (15.2)	51	22.0	10963	5670	482	197000

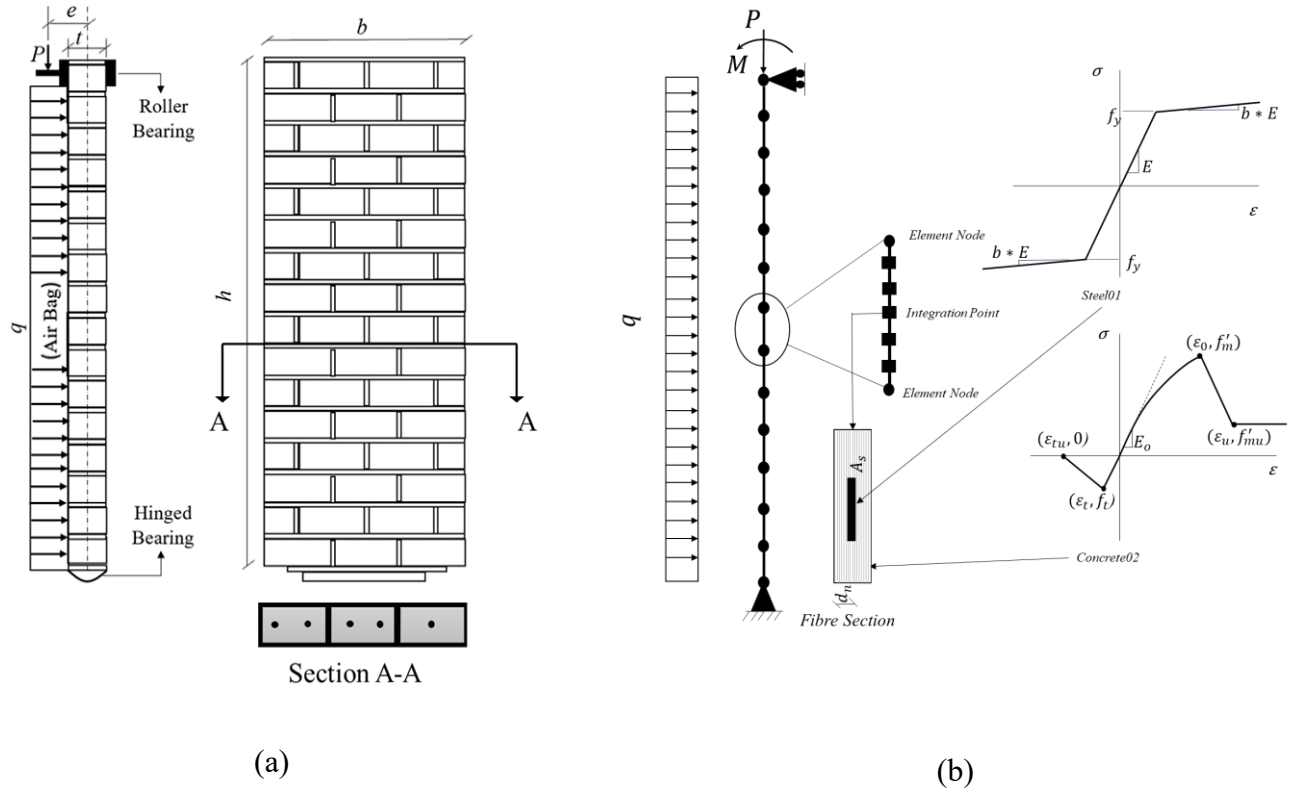

Figure 3-1 Reinforced concrete masonry walls studied: (a) test specimen, and (b) schematic view of the FE model

3.2.2 FE model development and validation

The reinforced concrete masonry walls considered are modelled using displacement-based fibre beam-column elements in an open-source FE software framework *OpenSees* (Mckenna et al.

2010). The schematic view of the FE model is shown in 3-1(b). According to a mesh convergence study, the wall is discretized into 14 displacement-based beam elements, and each element has five Gaussian-Legendre integration points with fibre sections to represent the cross-sectional behaviour. The cross-section is discretized into 20 masonry layers and 5 steel fibres, for which realistic uniaxial nonlinear material models are assigned to represent the stress-strain relationship for the corresponding material. Specifically, masonry fibres are represented by a uniaxial concrete material model (i.e., *Concrete02*), which has a linear elastic pre-cracking behaviour in tension before the peak tensile strength (f_t), followed by a linear tension softening branch until the maximum tensile strain (ε_{tu}) (Pluijm 1999). In compression, it has a parabolic pre-peak behaviour with the initial elasticity modulus (E_0), the peak compressive strength (f_m) with the corresponding strain $(\varepsilon_0 = 2f_m/E_o)$, followed by a linear softening branch up to the ultimate crushing strain (ε_u) with a residual compressive strength (f_{mu}). Steel bars are modelled using the bilinear steel material model (i.e., *Steel01*) with kinematic hardening. It remains elastic with Young's modulus (E) until reaching the yield strength (f_y), followed by a linear strain-hardening branch characterized by the post-yield strain-hardening ratio (b = 0.1 according to test results).

Among the abovementioned model parameters, f_m, ε_0, f_y and E are determined based on the tested values listed in Table 3-1. In contrast, other parameters, such as f_{mu}, ε_u, are defined based on literature findings due to the lack of information in this experimental program (ACI-SEASC 1982). Specifically, f_{mu} $(= 0.2\ f_m)$ and ε_u are determined according to the models proposed in (Priestley and Elder 1983) for homogenous masonry in the same way as used in existing studies (e.g. Liu and Dawe 2003, Moosavi 2017. Pettit 2020, Bilotta and Cruz 2021). On the other hand,

the peak tensile strength (f_t) is taken as 0.5 MPa (Drysdale and Hamid 2005, Mohsin 2005) and the maximum tensile strain (ε_{tu}) is taken as 0.004 (Wang et al. 1997).

Loading-wise, the axial compression (P) with the eccentricity (e) is modelled by means of equivalent axial compression and moment combination (P, $M = P \times e$) as shown in Figure 3-1(b). While the lateral pressure induced by the air-bag is modelled as a uniform lateral load along the length of walls. Figure 3-2 shows the comparison of the FE-predicted and experimental load-displacement curves for the masonry walls considered. The results show that the FE models achieve reasonable accuracy in predicting the overall load-displacement behaviour (e.g., elastic behaviour, cracking capacity, post-cracking stiffness, peak load capacity). The modelling accuracy for these walls is considered acceptable in view of the variability of experimental conditions and random measurement errors. Instead of improving the model accuracy (e.g., peak load capacity) further through calibration by adjusting unknown model parameters, the FE models developed here are considered validated with sufficient credibility for their subsequent use in uncertainty analysis. The model error for predicting the peak load capacities will be further quantified later in this paper.

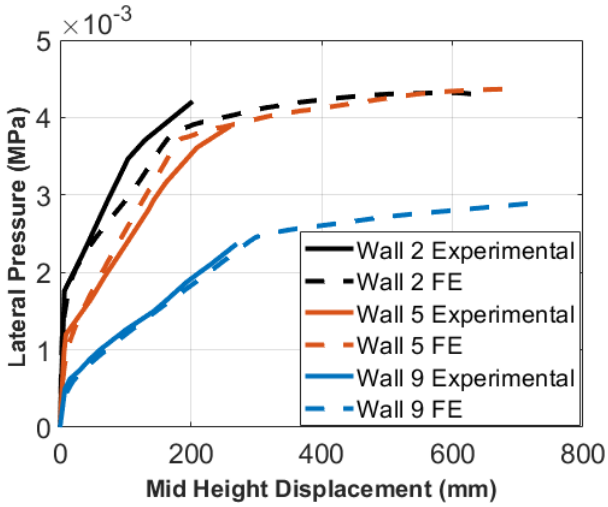

Figure 3-2 Comparison of the FE-predicted and experimental load-displacement curves for: wall #2, wall #5 and wall #9

3.3 Probabilistic Structural Behaviour Analysis

The macro FE model strategy validated above is used in conjunction with MCS for probabilistic structural analysis, aiming to study the effects of random properties on the behaviour of reinforced concrete masonry walls. To this end, both material and geometric uncertainties are propagated through the FE model to load-displacement curves, which reflect the uncertain structural behaviour, including load capacity, deformation capacity, etc. Specifically, this section considers three nominal walls, referred to as 10-inch wall, 8-inch wall, and 6-inch wall corresponding to wall #2, #5 and #9. It is worth noting that the specified masonry compressive strength f'_m is taken as 13.5 MPa, five steel bars are of grade 60 with the characteristic yield strength f_{yn} = 414 MPa (60 ksi) and located at half wall thickness (i.e., the nominal steel bar location d_n = 0.5t). To consider the natural variation of relevant properties, their statistical description is provided in the following section.

3.3.1 Statistical description of random variables

The following important properties of the reinforced concrete masonry walls are modelled as random variables: masonry compressive strength (f_m) and the corresponding strain (ε_o), masonry tensile strength (f_t), yield strength of steel reinforcement (f_y), Young's modulus of steel reinforcement (E), and steel bar location (d). Their statistical descriptors, including the mean value, coefficient of variations (COV), and probability distribution type, are provided in Table 3-2. Note that these random variables are assumed statistically independent as a common assumption used in the literature (Zhu et al. 2017).

Table 3-2 Statistical characterization of random variables considered

Random variable	***Mean (μ)***	***Coefficient of variation***	***Probability distribution***	***Reference***
f_m	1.6 f'_m	0.24	Gumbel	Moosavi and Korany 2014, Moosavi 2017
ε_o	0.002	0.20*	Normal*	Drysdale et al. 2005
f_t	0.69 MPa	0.4	Normal	Melander 1993, Hatzinkolas et al. 1978
f_y	1.14 f_{yn}	0.07	Normal	Moosavi 2017
E	200 GPa	0.033	Normal	Mirza, 1998
D	d_n	$4.0\ mm/d_n$	Normal	Moosavi 2017

*Assumed due to lack of information.

3.3.2 Probabilistic FE analysis

Note that the robustness and computational efficiency of the macro FE models developed allows probabilistic structural analysis using MCS, as summarized in Figure 3-3. In MCS-based probabilistic structural analysis of masonry walls, model parameter set samples, $\boldsymbol{x}^{(j)} = \{x_1^{(j)}, x_2^{(j)}, \ldots, x_i^{(j)}, \ldots, x_n^{(j)}\}$ (j = 1, 2, …, N) are firstly randomly generated in Step I according to the

probability models of basic random variable set $\mathbf{X} = \{X_1, X_2, \ldots, X_n\}$, where n is the number of basic random variables considered and N is the number of samples. Feeding each parameter set into the macro FE model of masonry walls (Step II), nonlinear FE analyses are performed in Step III, resulting in an ensemble of load-displacement curves. They can be used to reveal the overall probabilistic behaviour, as well as uncertainty in the histogram of a response quantity of interest (e.g., lateral load capacity) in Step IV and the fitted probabilistic density function (PDF) in step V. This procedure will be used first by considering a single random variable at a time (referred to as case 1, $n = 1$), aiming at studying the effect of each input variable uncertainty to provide insights into its individual role. Then the probabilistic behaviour of masonry walls is examined by considering all the above-mentioned random variables simultaneously (referred to as case 2, $n = 6$).

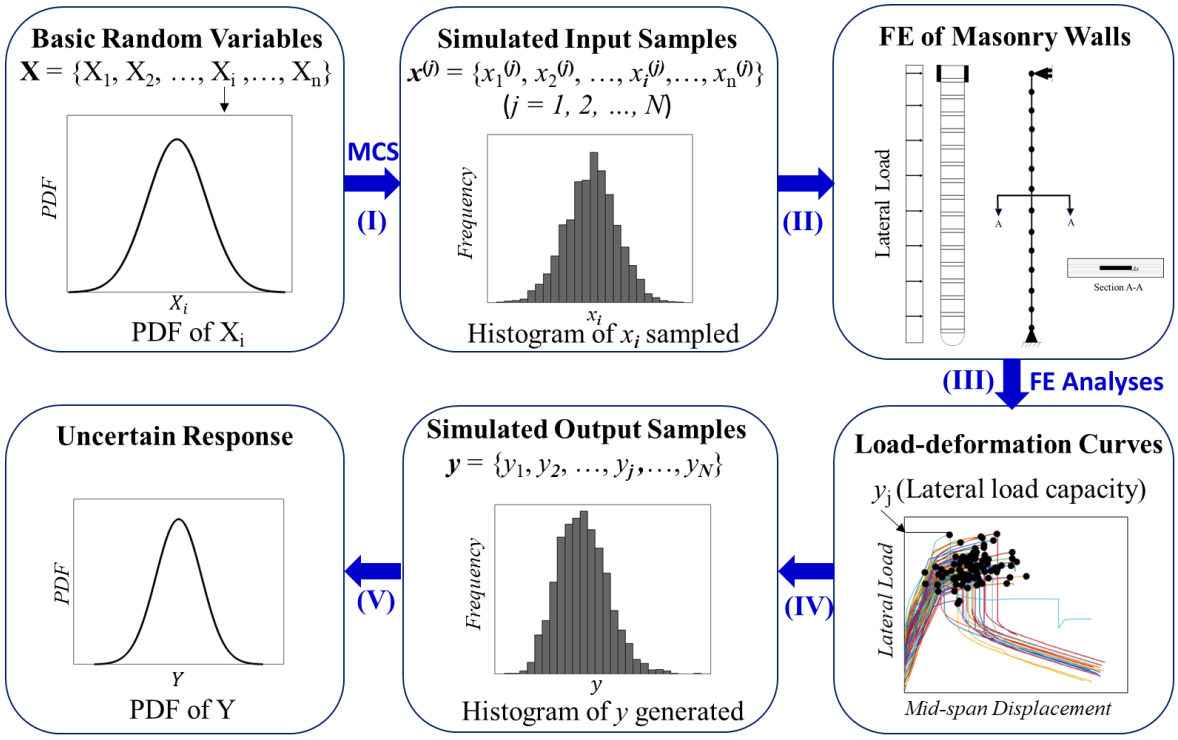

Figure 3-3 Probabilistic structural analysis procedure for reinforced concrete masonry walls

3.3.2.1 Case 1: considering a single random variable at a time

This section investigates the effect of the uncertainty in each individual variable on the global behaviour of reinforced concrete masonry walls considered. For this purpose, each time, only one of the six random variables considered is randomly generated with a large number (i.e., 2000 samples) according to its probabilistic distribution, while all the other variables are kept at their mean values. The analysis results for the 6-inch wall only are presented here, as similar observations can be made for the other two walls. Figure 3-4 presents the cluster of simulated load-displacement curves of the 6-inch reinforced concrete masonry walls, together with mean, 5th and 95th percentiles.

As observed in Figure 3-4, the uncertainty of each individual variable plays different roles on the wall behaviour. It is noticed that the pre-cracking behaviour is least affected, only by the randomness in tensile strength f_t. In contrast, the post-cracking (pre-yielding) behaviour is affected by the uncertainty in all variables except the yield strength of steel f_y. The uncertainty in the lateral load capacity and the post-peak behaviour of the masonry wall is significantly influenced by the randomness in the bar location d, the yield strength of steel f_y, and the masonry compressive strength f_m. It is worth noting that the randomness in the bar location d, which is mainly related to the construction quality control, significantly contributes to the scatter of the probabilistic behaviour. On the other hand, the deformation capacity is shown to be mainly affected by the masonry compressive strength f_m, as indicated by the 5th and 95th percentiles curves in Figure 3-4(a).

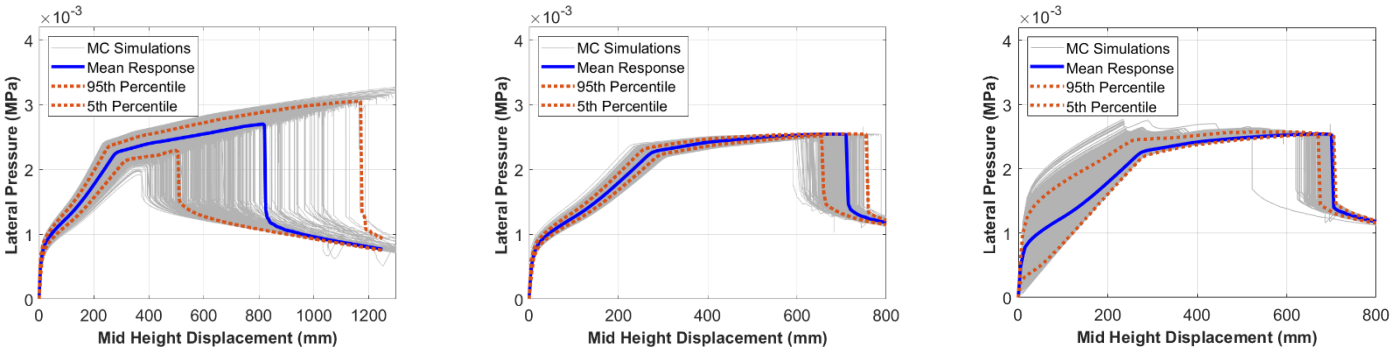

(a) (b) (c)

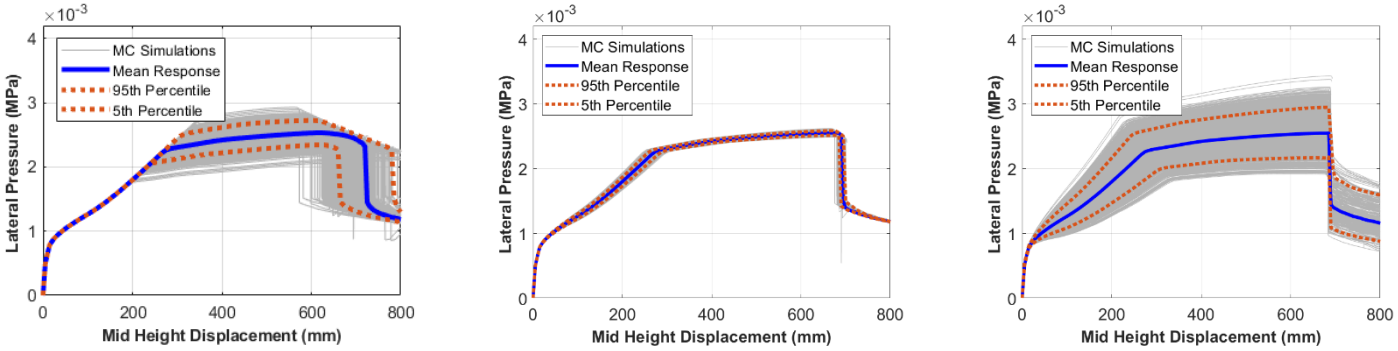

(d) (e) (f)

Figure 3-4 Probabilistic behaviour of the 6-inch wall when considering a single random variable: (a) f_m, (b) ε_0, (c) f_t, (d) f_y, (e) E, and (f) d

3.3.2.2 Case 2: considering all random variables simultaneously

This section aims to examine the uncertain behaviour of masonry walls after considering the aforementioned uncertainties in all six basic random variables. A similar approach to the earlier section is taken, but all random variables are simulated accordingly. Figure 3-5(a), (b), and (c) show the probabilistic structural analysis results for the three masonry walls considered, respectively, including the cluster of randomly simulated load-displacement curves together with mean, 5th and 95th percentiles. Additionally, the histograms and fitted probability distributions of the load capacity and deformation capacity are presented, together with the mean (μ) and coefficient of variation (COV). Note that the deformation capacity is measured by ductility, which is defined as the ratio between the maximum displacement without strength degradation of more than 20% and the corresponding displacement at the onset of steel yield. A large scatter in the cluster of load-displacement curves, which are associated with the behaviour of masonry walls, is observed as shown by the 5th and 95th percentiles. Additionally, the scatter is larger for the 6-inch wall that has a higher slenderness ratio (h/t = 51). Specifically, the COV of the load

capacity increases from 0.11 for the 10-inch wall to 0.13 for the 6-inch wall when the slenderness ratio (*h/t*) increases from 30 to 51.

In contrast, the ductility is shown to decrease with increasing slenderness. Specifically, the 10-inch wall has a mean ductility of 4.07, while the 6-inch wall is associated with a noticeably less ductile behaviour with a mean of 2.33. This reveals the importance of considering pertinent uncertainties to comprehend the probabilistic behaviour of reinforced concrete masonry walls. Note that the experimental curves for the masonry walls with the same nominal properties are also included in Figure 3-5, and a few of the randomly simulated load-displacement curves (as indicated by the pink curves) behave close to the experimental ones.

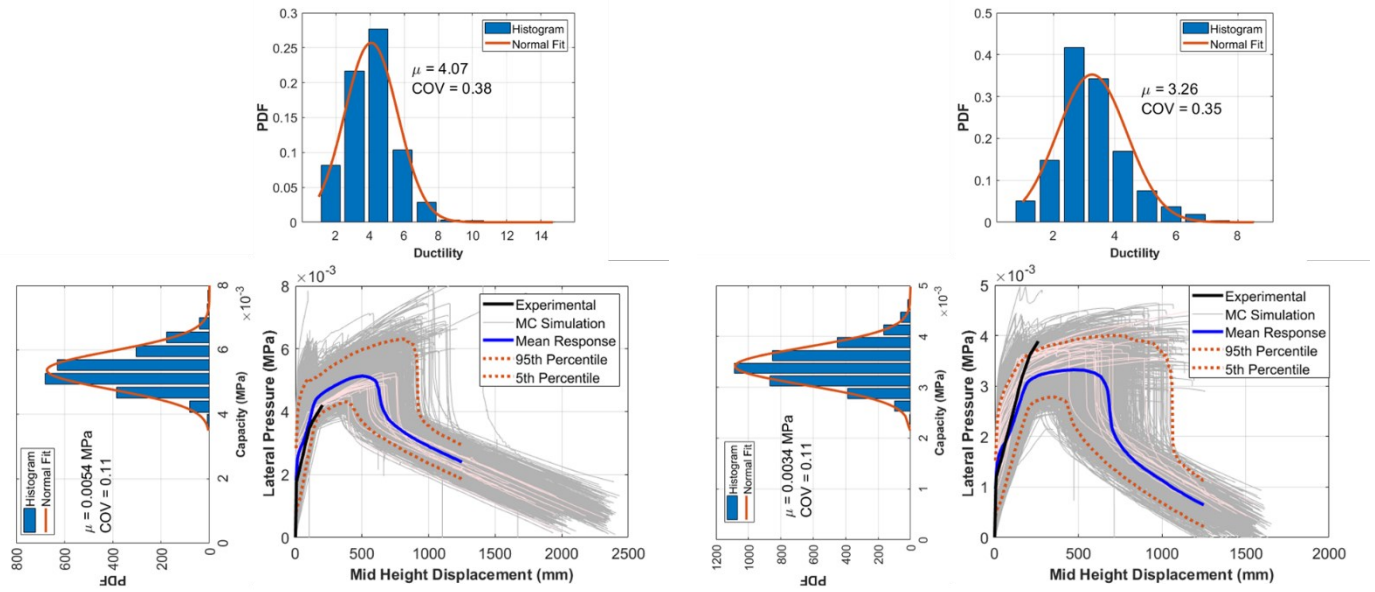

(a) (b)

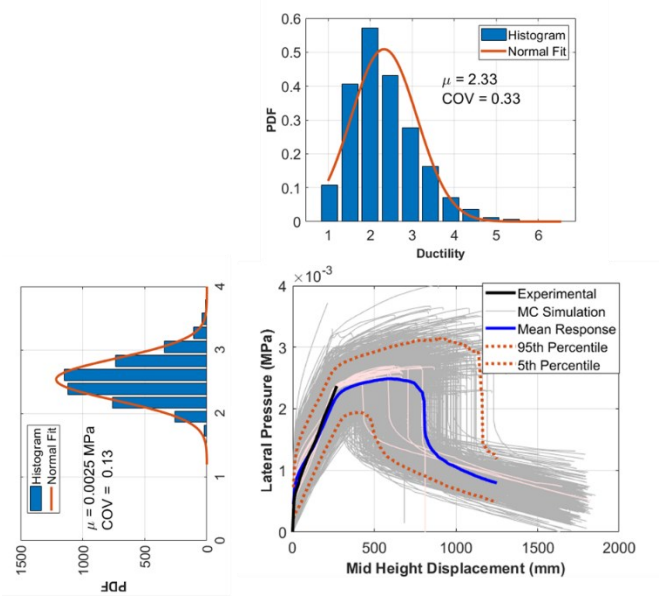

(c)

Figure 3-5 Probabilistic behaviour of masonry walls when considering all random variables: (a) 10-inch wall, (b) 8-inch wall, and (c) 6-inch wall

3.4 Model Uncertainty Quantification for Load Capacity Prediction

In addition to the model parameter uncertainty considered above, model error is another form of important uncertainty, arising from various sources such as simplification, assumptions, or approximations used to represent the physical reality, as well as the variability of experimental conditions and random measurement errors (Jiang et al. 2013). Mechanics-based FE models, though believed to be more reliable than empirical models or simplified design code-based models, are no exception. Nevertheless, the model error in FE models is typically neglected without quantifying the model error or assessing its relative importance compared to model parameter uncertainty. To address this issue for the macro FE model of reinforced concrete masonry walls under OOP loading, the FE model uncertainty for predicting the load capacity is quantified by evaluating the FE-predictions against the experimental test results. It is noteworthy that only the model uncertainty in determining peak capacity is considered in this study because

the experimental deformation capacities are unavailable for those walls tested under load control protocols.

In this study, an experimental database for reinforced concrete masonry walls tested under OOP loading (i.e., eccentric axial compression and lateral loading) is compiled from five testing programs in the literature (Yokel et al. 1970, Hatzinkolas et al. 1978, ACI-SEASC 1982, Suwalski 1986, Mohsin 2005). A total of 69 walls are included (Table 3-3), after eliminating the first two reinforced concrete masonry walls tested in (Mohsin 2005) due to their premature local failures. This dataset covers a wide range of slenderness ratios, with *h/t* ranging from 14 to 51, and eccentricity-to-thickness ratio with *e/t* ranging from 0.17 to 1.03 for walls subjected to eccentric axial loading. Among these walls, the pin-roller boundary condition was used for all walls considered, except that fixed-roller was used for the walls in (Yokel et al. 1970) and partially-fixed-roller was used for the walls in (Mohsin 2005). These walls are modelled using the aforementioned macro FE approach, while the boundary conditions are adjusted accordingly. Specifically, the partially-fixed condition for walls in (Mohsin 2005) is represented by explicitly modelling the boundary beam used in the test.

Table 3-3 Experimental database of reinforced concrete masonry walls under OOP loading

Experimental program (Reference)	***No. of walls***	***OOP Loading***	***Slenderness ratio h/t***	***Eccentricity ratio e/t***
Yokel et al. 1970	18	Eccentric axial	[21, 43]	[0.17, 0.33]
Hatzinkolas et al. 1978	28	Eccentric axial	[14, 24]	[0.17, 0.46]
ACI-SEASC 1982	9	Eccentric axial & lateral	[30, 51]	[0.8, 1.03]
Suwalski 1986 – R Series	6	Eccentric axial	17	[0.17, 0.75]
Suwalski 1986 – S Series	2	Lateral	17	-
Mohsin 2005	6	Eccentric axial	[29, 34]	0.33

The comparison between the experimental and FE-predicted capacities is shown in Figure 3-6. Note that the capacities are measured by the maximum axial load for eccentrically axially loaded walls and the maximum lateral load pressure (normalized by the wall area with a scale factor of 10 for plotting) for laterally loaded walls, respectively. The comparison shows that the FE models achieve reasonable accuracy with the trend line almost coinciding with the unit line (i.e., without severe bias). Thus, the commonly used test-to-prediction ratio (Holický et al. 2016) is evaluated for all 69 walls considered and used to quantify the model error (ME) probabilistically.

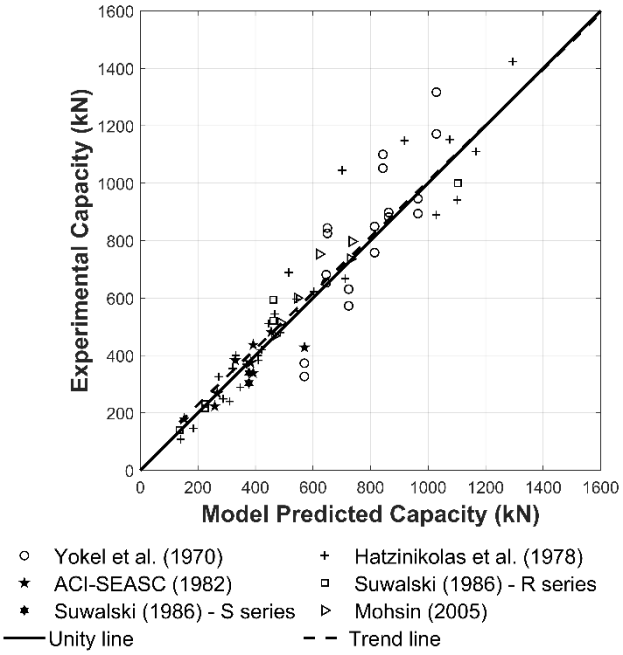

Figure 3-6 Comparison of the experimental and FE-predicted capacities for reinforced concrete masonry walls considered

To estimate the statistical parameters of ME, the cumulative distribution function (CDF) is fitted to the histogram. To this end, a normal distribution with a mean of $\mu_{ME} = 1.02$ and coefficient of variation $COV_{ME} = 0.17$ is found to be the best fit to represent the statistical nature of the model error, as shown in Figure 3-7. This reveals that the FE model slightly under-predicts the load capacity with a bias factor of 1.02 for the mean prediction.

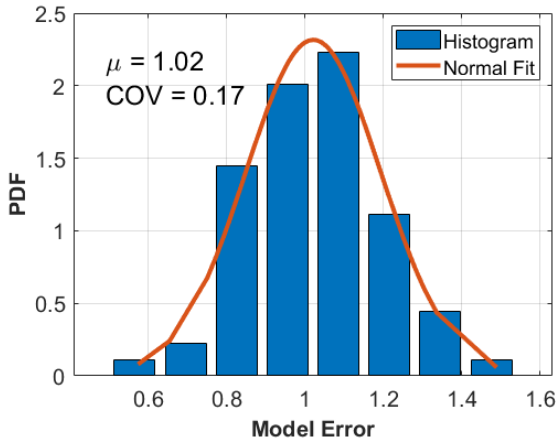

Figure 3-7 Histogram and fitted probability density function (PDF) for the model error distribution

When the model uncertainty is considered, the probabilistic load capacities can be obtained by applying a random multiplier ME to the load capacities obtained earlier from the FE model with uncertain model parameters only. Figure 3-8 shows the comparison between the load capacities obtained for 10-inch, 8-inch and 6-inch walls with and without considering model error. It is shown that incorporating model error leads to a slightly shifted mean and significantly higher variance in load capacities. Specifically, the COVs of the load capacity for 10-inch, 8-inch and 6-inch walls almost doubled due to additional uncertainty arising from ME. The relative contribution of ME to the uncertainty in the load capacity will be assessed rigorously with comparison to the contributions from other uncertain parameters in the next section.

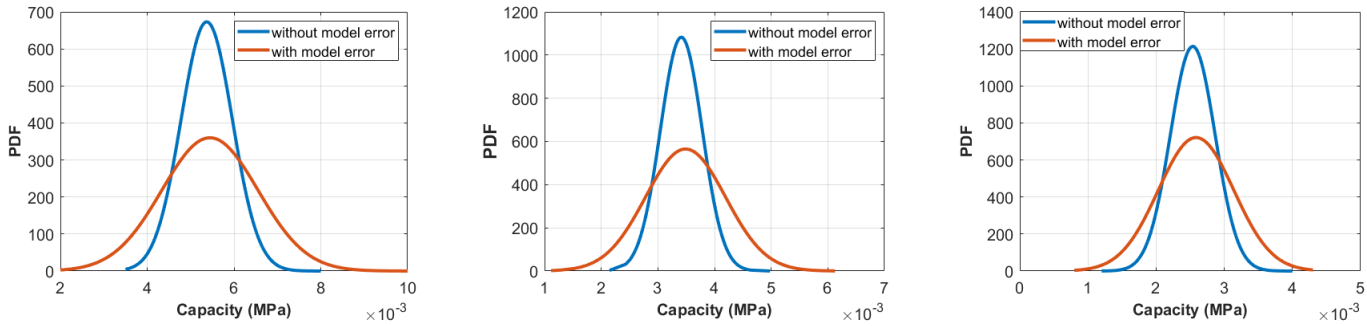

(a) (b) (c)

Figure 3-8 Comparison of probabilistic load capacities with and without considering model uncertainty: (a) 10-inch wall, (b) 8-inch wall, and (c) 6-inch wall

3.5 Variance-based Sensitivity Analysis

As revealed from the stochastic simulation results, the variance in the global behaviour of the masonry walls arises from the uncertainties in the basic (e.g., material, geometric) random variables. It is essential to quantify the relative importance of uncertain input variables based on their contributions to the variance of the response of interest, such as the lateral load capacity and the ductility, through variance-based global sensitivity analysis. In particular, it is imperative to examine the relative importance of model uncertainty (ME) compared to parameter uncertainties reflected in basic random variables. As such, variance-based global sensitivity analysis is conducted in this section for the FE-predicted load capacity with and without considering model uncertainty. To this end, this section adopts the polynomial Chaos expansion (PCE)-based Sobol' indices (Sudret 2008), which has been previously employed as sensitivity measures in different fields such as geotechnical earthquake engineering (Abbiati et al. 2021) and structural dynamics (Ardebili et al. 2021).

3.5.1 PCE-based Sobol' index approach

The basic idea behind Sobol' indices is to expend a function $Y = f(X_1, X_2, \dots, X_n)$, e.g., FE model in this paper, into a summation of functions of increasing dimension.

$$Y = f_o + \sum_{1 \le i \le n} f_i(X_i) + \sum_{1 \le i < j \le n} f_{ij}(X_i, X_j) + \cdots + f_{1,2,\dots,n}(X_1, X_2, \dots, X_n) \quad (3-1)$$

in which,

$$f_o = \mathbb{E}(y)$$

$$f_i(x_i) = \mathbb{E}(y|x_i) - \mathbb{E}(Y)$$

$$f_{ij}(x_i, x_j) = \mathbb{E}(Y|x_i, x_j) - f_i - f_j - \mathbb{E}(y) \qquad (3-2)$$

For the case with statistically independent variables $X_i(1,2,\dots,n)$, the variance of the output response $Y, \mathbb{V}(Y) = D$, can be written as

$$D = \sum_{1\le i\le n} D_i + \sum_{1\le i<j\le n} D_{i,j} + \sum_{1\le i<j<k\le n} D_{i,j,k} + \dots + D_{1,2,\dots,n} \qquad (3-3)$$

where

$$D_i = \mathbb{V}(\mathbb{E}(Y|X_i))$$

$$D_{i,j} = \mathbb{V}\left(\mathbb{E}(Y|\mathrm{X}_i, \mathrm{X}_j)\right) - D_i - D_j$$

$$D_{i,j,k} = \mathbb{V}\left(\mathbb{E}(y|\mathrm{X}_i, \mathrm{X}_j, \mathrm{X}_k)\right) - D_{i,j} - D_{i,k} - D_{j,k} - D_i - D_j - D_k$$

$$\dots \qquad (3-4)$$

where $\mathbb{V}(.)$ and $\mathbb{E}(.)$ denote the variance and expectations operators, respectively.

To this end, the total output variance $\mathbb{V}(Y) = D$ is decomposed into contributions of the individual parameters and their interactions of various orders. Consequently, their fractional contributions can be measured by the ratios between the partial variance and the total variance, leading to Sobol' sensitivity indices given by:

$$S_i = \frac{D_i}{D}, S_{i,j} = \frac{D_{i,j}}{D}, \dots, S_{1,2,\dots,n} = \frac{D_{1,2,\dots,n}}{D} \qquad (3-5)$$

Among the terms in Eq. (3-5), the first-order index S_i evaluates the amount of partial variance attributed to one variable alone (e.g., X_i). In contrast, the higher-order indices ($S_{i,j}, S_{i,j,k}$) account for the partial variance due to the interaction of one variable (e.g., X_i) with the others.

To this end, the derived Sobol' indices can indicate the relative importance of different input variables in predicting the output response (y). In this study, up to second-order indices are used to consider the effect of the latent interaction between different input variables. Sobol' indices are traditionally determined by Monte Carlo simulations, but the required number of samples can be extremely large and thus impractical for the FE model of masonry walls. As such, a fast-to-evaluate surrogate model based on PCE is adopted in this study since it allows the analytical derivation of Sobol' indices (Sudret 2008).

3.5.2 Results for load capacity prediction with & without model uncertainty

The variance associated with the load capacity of masonry walls due to the uncertainties associated with input parameters is firstly examined in this section. To this end, the 2000 samples used in the probabilistic structural analysis with and without considering model uncertainty are used. The sensitivity analysis results are shown in Figure 3-9 and Figure 3-10 for the cases without and with model error considered.

Figure 3-9 shows that the variance of the lateral load capacity is mainly attributed to the uncertainties associated with the three important parameters d, f_y, and f_m. It is shown that the first-order indices from these three important parameters contribute to a significant amount of the total variance of load capacity (i.e., 88%, 93% and 99% for 10-inch, 8-inch and 6-inch walls, respectively). Similar observations can be made based on the probabilistic structural analysis

results when considering a single random variable at a time (see Section 3.3.2). In contrast, the interactive effect among the input parameters, indicated by higher Sobol' indices, is found to be negligible for all the considered walls. Comparing the sensitivity results for the three walls, the effect of the parameter d increases with the decreasing wall thicknesses. It turns to be the most influential parameter for 8-inch wall and 6-inch wall.

Figure 3-10 shows that model uncertainty in FE prediction has a substantial effect on the total variance of the lateral load capacity, when ME is considered. The first-order sensitivity indices for ME show that ME contributes to 71%, 70%, and 63% of the total variance for 10-inch, 8-inch, and 6-inch wall, respectively. This implies the significant role of model uncertainty (ME), compared with other parameter uncertainties (e.g., material and geometric variables) that are commonly considered for FE-based probabilistic analysis.

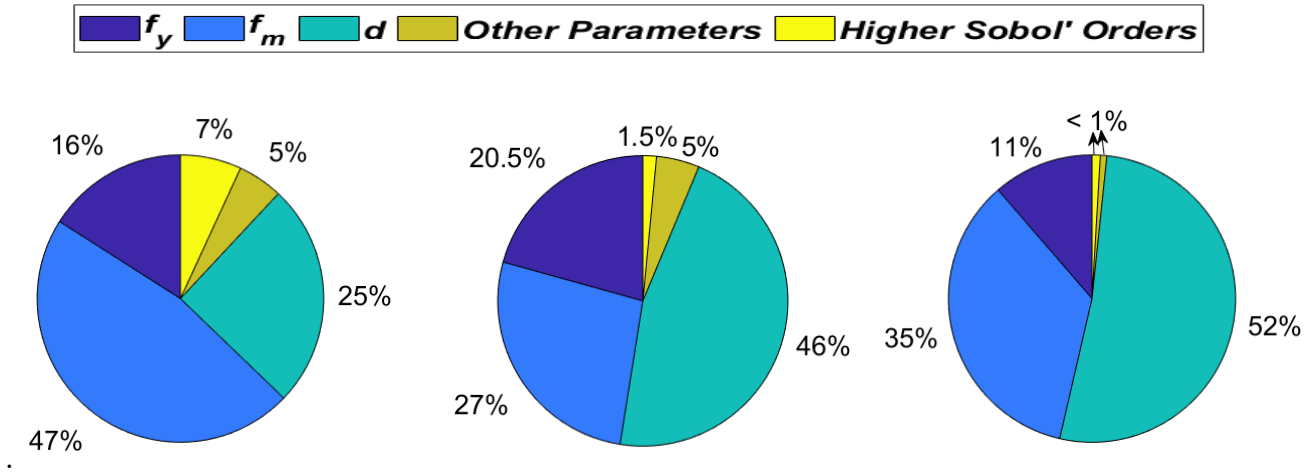

(a) (b) (c)

Figure 3-9 Variance decomposition for load capacity when no model error is considered: (a) 10-inch wall, (b) 8-inch wall, and (c) 6-inch wall

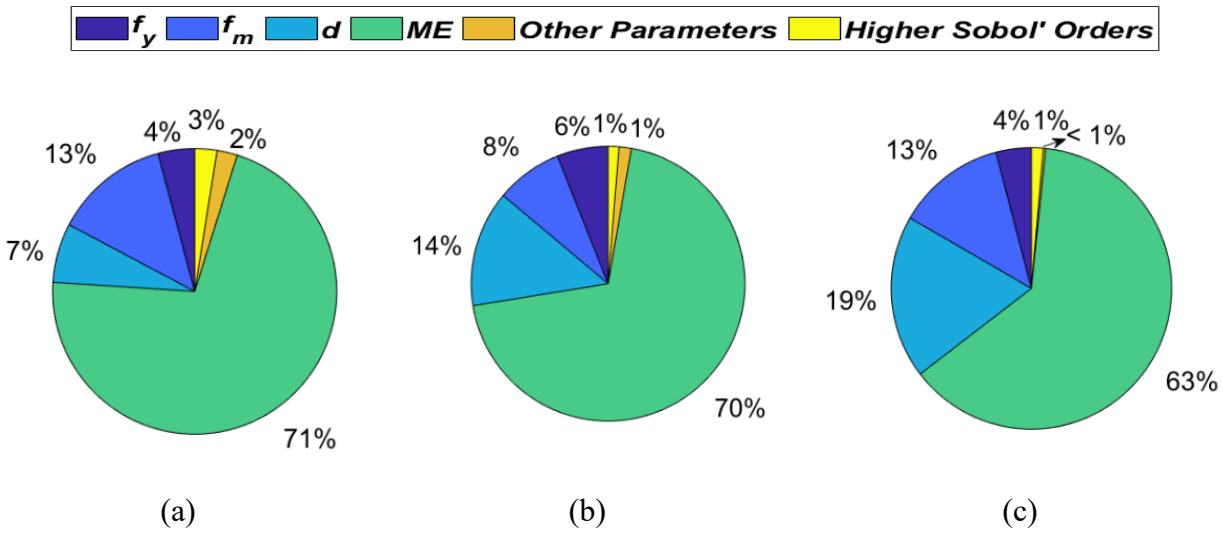

(a) (b) (c)

Figure 3-10 Variance decomposition for load capacity when model error is considered: (a) 10-inch wall, (b) 8-inch wall, and (c) 6-inch wall

3.5.3 Results for ductility prediction without model uncertainty

Similar sensitivity analysis is performed for the deformation capacity (i.e., ductility) of the three masonry walls considered. The sensitivity results are shown in Figure 3-11. It is found that the uncertainties in masonry compressive strength f_m and masonry tensile strength f_t contribute most to the ductility variance. The contribution of f_m increases with increasing slenderness, while the contribution of f_t decreases with increasing slenderness. It is worth mentioning that the interactive effects among the input parameters possess a considerable contribution to the variance of ductility, which is contrary to the observation made for the lateral load capacity.

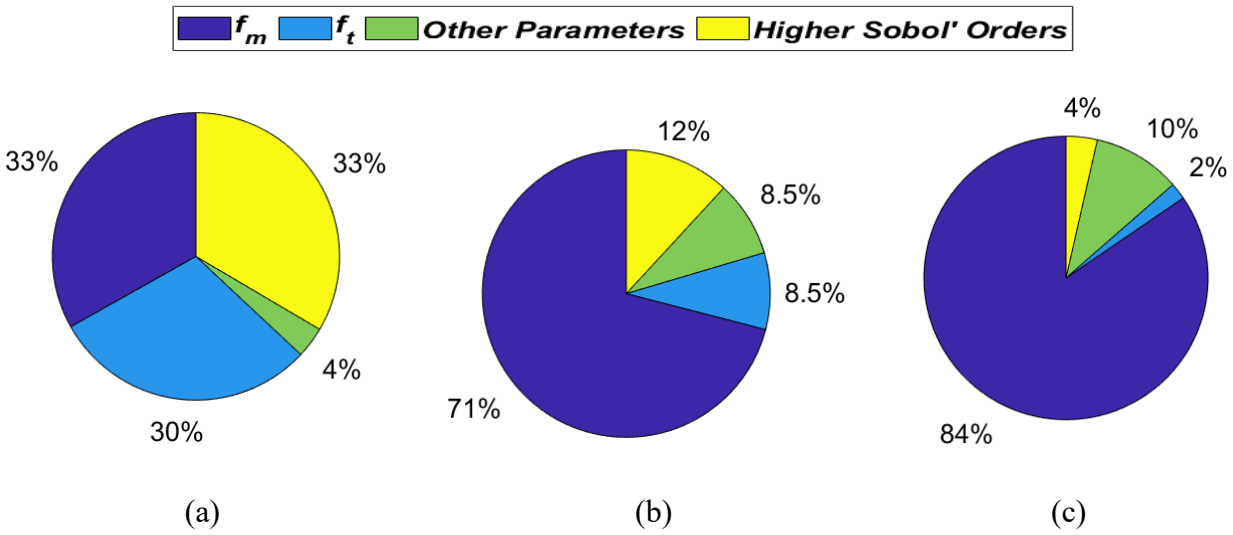

Figure 3-11 Variance-based sensitivity analysis results for ductility: (a) 10-inch wall, (b) 8-inch wall, and (c) 6-inch wall

3.6 Conclusions

In this study, macro finite element (FE) models were developed and validated for three reinforced concrete masonry walls under out-of-plane (OOP) loading. Based on the developed macro FE models, probabilistic structural analysis was conducted by propagating material and geometric uncertainties to the load-displacement curves of masonry walls. It revealed the influence of the random material and geometric parameters on the overall structural behaviour, as well as the specific responses of interest such as load capacity and deformation capacity. Among the three walls considered, the behaviour of the highly slender wall was found to be associated with larger scatter. Based on the experimental database compiled, the model error (ME) for FE-predicted load capacity was quantified, and it was found that incorporating ME led to a substantial increase in the variance of load capacity. To quantify the contribution of different random variables to the variance in the load and deformation capacities, variance-based global sensitivity analyses were conducted for walls with different slenderness or thicknesses. When the model error was ignored, the load capacity variance was mostly attributed to the uncertainty

associated with the masonry compressive strength f_m, the yield strength of steel f_y, and steel bar location d. In contrast, the deformation capacity variance is mostly attributed to the uncertainty associated with the masonry compressive strength f_m, and the masonry tensile strength f_t. When the model error was considered, a significant portion of the load capacity variance was contributed by the uncertainty associated with model error. This highlights the importance of considering model error for probabilistic structural analysis, particularly in FE-based reliability analysis.

3.7 References

Abbiati, G., Marelli, S., Tsokanas, N., Sudret, B., & Stojadinović, B. (2021). A global sensitivity analysis framework for hybrid simulation. Mechanical Systems and Signal Processing, 146, 106997. doi:https://doi.org/10.1016/j.ymssp.2020.106997

Abdulla, K. F., Cunningham, L. S., & Gillie, M. (2017). Simulating masonry wall behaviour using a simplified micro-model approach. Engineering Structures, *151*, 349-365. doi:10.1016/j.engstruct.2017.08.021

ACI-SEASC Task Committee on Slender Walls. (1982). *Test report on slender walls.* Los Angeles, California.

Barbato, M., Gu, Q., & Conte, J. P. (2010). Probabilistic push-over analysis of structural and soil-structure systems. Journal of Structural Engineering, *136*(11), 1330-1341. doi:10.1061/(ASCE)ST.1943-541X.0000231

Barbato, M., Zona, A., & Conte, J. P. (2014). Probabilistic nonlinear response analysis of steel-concrete composite beams. Journal of Structural Engineering, *140*(1), 4013034. doi:10.1061/(ASCE)ST.1943-541X.0000803

Bilotta, M. and Cruz, Y. (2021). Evaluation of Second-order Effects in Slender Reinforced Masonry Walls. Proc., 14th Canadian Masonry Symposium, Montreal, QC, Canada.

Bui, T. T., Limam, A., Sarhosis, V., & Hjiaj, M. (2017). Discrete element modelling of the in-plane and out-of-plane behaviour of dry-joint masonry wall constructions. Engineering Structures, *136*, 277-294. doi:10.1016/j.engstruct.2017.01.020

Buonopane, S. G. (2008). Strength and reliability of steel frames with random properties. Journal of Structural Engineering, *134*(2), 337-344. doi:10.1061/(ASCE)0733-9445(2008)134:2(337)

Chen, W. F., & Atsuta, T. (1973). Strength of eccentrically loaded walls. International Journal of Solids and Structures, *9*(10), 1283-1300. doi:10.1016/0020-7683(73)90115-7

CSA S304 (2014) Design of Masonry Structures. Canadian Standards Association, Mississauga, Canada.

D'Altri AM, Sarhosis V, Milani G, Rots J, Cattari S, Lagomarsino S, Sacco E, Tralli A, Castellazzi C, & de Miranda S. A review of numerical models for masonry structures. Numerical modeling of masonry and historical structures. Woodhead Publishing; 2019. p. 3–53.

D'Altri, A. M., de Miranda, S., Castellazzi, G., & Sarhosis, V. (2018). A 3D detailed micro-model for the in-plane and out-of-plane numerical analysis of masonry panels. Computers & Structures, *206*, 18-30. doi:10.1016/j.compstruc.2018.06.007

Dawe, J. L., & Liu, Y. (2003). Analytical modeling of masonry load-bearing walls. *Canadian Journal of Civil Engineering, 30*(5), 795-806. doi:10.1139/l03-036

Minga, E., Macorini, L., Izzuddin, B. A., & Calio', I. (2019). Chapter 8 - macromodeling. In B. Ghiassi, & G. Milani (Eds.), Numerical modeling of masonry and historical structures (pp. 263-294) Woodhead Publishing. doi:https://doi.org/10.1016/B978-0-08-102439-3.00008-7

Drysdale, R. G. and Hamid, A. A. (2005). Masonry Structures Behaviour and Design, Canada Masonry Design Centre, Mississauga, ON, Canada.

Ganduscio S, Romano F. (1997). FEM and analytical solutions for buckling of nonlinear masonry members. Journal of Structural Engineering,123(1):104–11.

Grubišić, M., Ivošević, J., & Grubišić, A. (2019). Reliability analysis of reinforced concrete frame by finite element method with implicit limit state functions. Buildings (Basel), *9*(5), 119. doi:10.3390/buildings9050119

Jiang, Z., Chen, W., Fu, Y., & Yang, R. (2013). Reliability-based design optimization with model bias and data uncertainty. SAE International Journal of Materials and Manufacturing, 6(3), 502-516. doi:10.4271/2013-01-1384

Hariri-Ardebili, M. A., Mahdavi, G., Abdollahi, A., & Amini, A. (2021). An RF-PCE Hybrid Surrogate Model for Sensitivity Analysis of Dams. Water, 13(3), 302.

Hatzinikolas, M., Longworth, J., and Warwaruk, J. 1978a. Concrete Masonry Walls. University of Alberta - Structural Engineering Report No. 70. Department of Civil and Environmental Engineering, University of Alberta. Edmonton, AB.

Holický, M., Retief, J. V., & Sýkora, M. (2016). Assessment of model uncertainties for structural resistance. Probabilistic Engineering Mechanics, 45, 188-197.

Li, J., Masia, M. J., Stewart, M. G., & Lawrence, S. J. (2014). Spatial variability and stochastic strength prediction of unreinforced masonry walls in vertical bending. Engineering Structures*, 59*, 787-797. doi:10.1016/j.engstruct.2013.11.031

Li, J., Stewart, M. G., Masia, M. J., & Lawrence, S. J. (2016). Spatial correlation of material properties and structural strength of masonry in horizontal bending. *Journal of Structural Engineering, 142*(11), 4016112. doi:10.1061/(ASCE)ST.1943-541X.0001488

Melander, J. M., & Lauersdorf, L. R. (1993). Masonry: design and construction, problems and repair. ASTM.

Mathews, G. M., & Vial, J. (2017). Overcoming model simplifications when quantifying predictive uncertainty. arXiv preprint arXiv:1703.07198.

Mckenna, F., Scott, M. H., & Fenves, G. L. (2010). Nonlinear finite-element analysis software architecture using object composition doi:10.1061/ASCÊCP.1943-5487.0000002

Mirza, S. A. (1998). Monte carlo simulation of dispersions in composite steel-concrete conumn strength interaction. Engineering Structures*, 20*(1), 97-104. doi:10.1016/S0141-0296(97)00049-7

Mohsin, E. 2005. Support Stiffness Effect on Tall Load Bearing Masonry Walls. Ph.D. thesis, Department of Civil and Environmental Engineering, University of Alberta, Edmonton, AB.

Moosavi H.. (2017). *S*tructural reliability of non-slender loadbearing concrete masonry members under concentric and eccentric loads. PhD thesis, Department of Civil and Environmental Engineering, University of Alberta, Edmonton, AB.

Moosavi, H., & Korany, Y. (2014). Assessment of the structural reliability of loadbearing concrete masonry designed to the canadian standard S304.1. *Canadian Journal of Civil Engineering, 41*(12), 1046-1053. doi:10.1139/cjce-2013-0498

Pettit, C. (2020). Effect of Rotational Base Stiffness on the Behaviour of Loadbearing Masonry Walls. M.Sc. thesis, Department of Civil and Environmental Engineering, University of Alberta, Edmonton, AB.

Pluijm, van der, R. (1999). Out-of-plane bending of masonry : behaviour and strength. Eindhoven: Technische Universiteit Eindhoven. https://doi.org/10.6100/IR528212

Sarhosis, V., & Lemos, J. V. (2018). A detailed micro-modelling approach for the structural analysis of masonry assemblages. *Computers & Structures, 206*, 66-81. doi:10.1016/j.compstruc.2018.06.003

Sobol′, I. M. (2001). Global sensitivity indices for nonlinear mathematical models and their monte carlo estimates. *Mathematics and Computers in Simulation, 55*(1-3), 271-280. doi:10.1016/s0378-4754(00)00270-6

Su, L., Wan, H., Li, Y. Y., & Ling, X. (2018). Soil-pile-quay wall system with liquefaction-induced lateral spreading: Experimental investigation, numerical simulation, and global

sensitivity analysis. American Society of Civil Engineers (ASCE). doi:10.1061/(asce)gt.1943-5606.0001977

Sudret, B. (2008). Global sensitivity analysis using polynomial chaos expansions. Reliability Engineering & System Safety, 93(7), 964-979. doi:10.1016/j.ress.2007.04.002

Suwalski, P.D. (1986). Capacity of eccentrically loaded slender concrete block

walls. M.Sc. thesis, Department of Civil Engineering, McMaster University,

Hamilton, Ont.

Priestley, M. J. N., and Elder, D. M. (1983). Stress–strain curves for unconfined and confined concrete masonry. ACI J., 80-3, 192–201

Wang, R., Elwi, A. E., and Hatzinikolas, M. A. (1997). Numerical Study of Tall Masonry Cavity Walls Subjected to Eccentric Loads. Journal of Structural Engineering, Vol. 123, No. 10, pp.1287-1294

Yokel, F.Y., Mathey, R.G., and Dikkers, R.D. (1970). Compressive strength of slender concrete masonry walls. Building Science Series 33, U.S. National Bureau of Standards, Washington, D.C.

Zhu, F., Zhou, Q., Wang, F., & Yang, X. (2017). Spatial variability and sensitivity analysis on the compressive strength of hollow concrete block masonry wallettes. Construction & Building Materials*, 140*, 129-138. doi:10.1016/j.conbuildmat.2017.02.099

CHAPTER 4: Finite Element-based Reliability Analysis of Reinforced Concrete Masonry Walls under Out-of-Plane Loading Considering Slenderness Effects

This paper presents finite element (FE)-based reliability analysis of reinforced concrete masonry walls under out-of-plane (OOP) loading considering slenderness effect. The main purpose is to (1) examine the importance of model uncertainty and (2) investigate the effect of different failure criteria on the reliability assessment of masonry walls. To achieve this goal, two representative walls with different slenderness ratios are selected for the reliability analysis. Finite element models of masonry walls are used to formulate the limit-state function for the reliability problems considered. Subset simulation algorithm in conjunction with Polynomial-Chaos-Kriging (PCK)-based surrogate models is used to address the computational cost involved in FE-based reliability analysis. It is found that the reliability assessment results are highly dependent on the model error. In addition, it is found that the local failure criteria are not always more conservative compared to global (wall) failure criteria due to the stability failure, particularly for slender walls or walls designed with vertical loads at low eccentricities. Furthermore, it is found that other factors are found to influence the reliability assessment, such as the slenderness ratios, which leads to reliability-inconsistent designs according to the current design codes.

4.1 Introduction

The structural resistance (i.e., load capacity) of the reinforced concrete masonry walls is essentially uncertain due to the variabilities inherent in the material and geometric properties. Likewise, the demand (i.e., load effects) is also uncertain due to the randomness in the loads applied to masonry walls. Accordingly, the actual values of the resistance (i.e., load capacity) and the demand (i.e., load effects) can be different from their corresponding nominal or design values, which can be computed in accordance with relevant design code (Mirza 1996). The structural reliability analysis can be performed to investigate the probability that the actual value of the load effect exceeds the resistance according to a certain failure criterion, namely, the probability of failure P_f. Structural design codes aim to ensure that the designed structures satisfy a target reliability level (i.e., to serve their intended function within a predetermined acceptable probability of failure).

Previous studies (Turkstra and Ojinaga 1980, Ellingwood and Tallin 1985, Stewart and Lawrence 2007, Zhai and Stewart 2010, Zhai et al. 2012, Moosavi and Korany 2014) investigated the reliability of masonry structures subjected to different loading conditions (e.g., concentric compression, flexure, and in-plane shear). However, these studies were based on the empirical design codes models or simplified analytical models, which can be associated with significant model error. Accordingly, Zhai and Stewart (2010) developed probabilistic models to incorporate the model error in the reliability assessment of masonry walls under in-plane shear loading by comparing the predictions of the adopted strength models with the available experimental results and selecting the best fit probability distribution. It was found that the reliability assessment is very sensitive to the model error.

As an alternative to reliability assessment using the design code models for the capacity or demand calculations, reliability assessment can be conducted using more accurate mechanics-based finite element (FE) models. This approach was previously used for other structures, such as reinforced concrete structures and steel structures (Grubišić et al. 2019, Yan et al. 2020). Nevertheless, in these studies, the model error associated with the FE models was neglected in the reliability assessment. Although the mechanics-based FE models are believed to be more reliable than simplified design code-based models, they are also associated with prediction error. In that sense, it is essential to incorporate the model uncertainty of the FE models in the reliability assessment and assess the importance of considering modelling uncertainty in reliability evaluation.

Generally, the reliability of a given structure is measured by the probability that this structure can fulfill its design purpose in the face of inherent uncertainties. For reliability analysis, the failure criteria can be defined mathematically through a limit state function (G), such that $G <= 0$ indicates a state in which the structure does not satisfy its design function (Grubišić et al. 2019, Zhai and Stewart 2010, Moosavi 2017). Emphasizing on the ultimate limit state for safety concerns, the structure is considered to fail if the applied load effects (i.e., demand) exceed its load capacity (i.e., load resistance). In that sense, global (i.e., wall) or local (i.e., section or material) failure criteria can be used to define the ultimate limit state depending on the engineering acceptance criteria. The adopted failure criteria can have a substantial effect on the reliability assessment (Frangopol et al. 1996, Milner et al. 2001). As indicated by other researchers (Moosavi and Korany 2014, Moosavi 2017), the transformation of CSA S304 from working stress to limit state design approach was not supported by comprehensive structural

reliability analysis. Therefore, Moosavi (2017) indicated the need for a comprehensive reliability analysis to support the limit-state-based provisions introduced in CSA S304 and thus performed a reliability assessment of non-slender reinforced masonry walls under OOP loading. In the mentioned study, the reliability assessment was performed for a limit state function formulated based on section check using simplified analytical models, which is assumed error-free.

To facilitate better reliability assessment of reinforced concrete masonry walls under OOP loading, slenderness effect is considered. To this end, finite element (FE) models that rigorously consider geometrical and material nonlinearities, together with model uncertainty, are used for limit state function formulation in reliability assessment. Without performing a comprehensive reliability-based code evaluation, this study focuses on FE-based reliability analysis, mainly to (1) examine the importance of model uncertainty and (2) investigate the effect of different failure criteria on the reliability assessment of masonry walls when considering the slenderness effect. However, FE-based reliability analysis can be computationally expensive, especially for cases when a large number of simulations is required to capture low probabilities of failure. To tackle this problem, this study employs surrogate models (i.e., Polynomial-Chaos-Kriging (PCK) (Schobi et al. 2015)) in conjunction with subset simulation (SS) (Au et al. 2007) for their efficiency and accuracy (Zuev et al. 2015).

4.2 Masonry Walls and Slenderness Effects

Masonry structures are becoming more competitive with other construction materials due to their strength, durability and ease of construction with the improvement of the relevant design codes (Isfeld et al. 2019). However, this is not the case for the relatively high (i.e., slender) walls as the design of such walls is still facing challenges due to the stringent design requirements imposed

by the design codes (e.g., CSA S304). The stringent requirements are attributed to the high vulnerability of highly slender walls to second-order effects, which is considered a critical and highly uncertain behavioural aspect (Pettit 2020). However, the design codes adopt the approximate moment magnifier method to account for second-order effects, which can be overly conservative (Bilotta and Cruz 2021). In that sense, it is important to rigorously consider the second-order effects (e.g., using mechanics-based FE models) in the reliability analysis. To this end, two reinforced fully grouted concrete masonry walls with different slenderness ratios (h/t) are considered in this paper, namely wall S with h/t = 16, and wall H with h/t = 42. The nominal material and geometric properties of the considered walls are summarized in Table 4-1. The walls configuration is shown in Figure 4-1(a). Note that the steel bars are designed to be located at mid-thickness of the walls, with reinforcement ratio (ρ_s) of 0.0019 representing a mid-range value between the minimum permissible reinforcement ratio (0.0013) by CSA S304-14 and the balanced reinforcement ratio (0.0025) (i.e., the steel ratio in which the yielding of the bars occurs simultaneously with the critical fibre in the cross-section reaches the crushing strain) for pure-bending case (Moosavi, 2017). It should be noted that higher reinforcement ratios (e.g., ρ_s > 0.0025) are prevented for walls with h/t > 30 because only ductile failure mode is permissible according to CSA S304-14 Therefore, only lightly reinforced walls are considered for comparison.

Table 4-1 Nominal properties of the walls considered

Wall	*Height* *(h)* *(mm)*	*Thickness* *(t)* *(mm)*	*Slenderness ratio* *(h/t)*	*Masonry nominal compressive strength* f'_m	*Reinforcement ratio* ρ_s	*Reinforcement bars yield strength* $f_{y,nominal}$	*Reinforcement bars location* d *(mm)*

				(MPa)		*(MPa)*	
Wall S	3000	190	16	10	0.0019	400	95
Wall H	8000	190	42	10	0.0019	400	95

Due to natural variation of material and geometric properties, their values for reinforced concrete masonry walls are uncertain and can be modelled as resistance random variables. The relevant statistical information is listed in Table 4-2, including the mean, coefficient of variation (COV), and probability distribution types for the most important and uncertain variables such as masonry compressive strength (f_m) and the corresponding strain (ε_o), masonry tensile strength (f_t), yield strength of steel reinforcement (f_y), Young's modulus of steel reinforcement (E), and steel bar location (d). Note that these random variables are assumed statistically independent as a common assumption used in the literature due to lack of information (Zhu et al. 2017).

Table 4-2 Statistical characterization of random variables considered

Random variable	***Mean (μ)***	***Coefficient of variation***	***Probability distribution***	***Reference***
f_m	1.6 f'_m	0.24	Gumbel	Moosavi and Korany 2014, Moosavi 2017
ε_o	0.002	0.20	Lognormal	Drysdale et al. 2005, Barbato et al. 2014 Mirza et al. 1979
f_t	0.69 MPa	0.4	Normal	Melander 1993, Hatzinkolas et al. 1978
f_y	1.14 $f_{y,nominal}$	0.07	Normal	Moosavi 2017
E	200 GPa	0.033	Normal	Mirza, 1998
D	d_n	$4.0\ mm/d_n$	Normal	Moosavi 2017

In order to study the structural behaviour considering slenderness effect, the macro FE modelling approach using fibre-based beam element in *OpenSees* is adopted. In this model, geometric nonlinearity is taken into account effectively through corotational transformation. The wall is modelled as a number of displacement-based fibre beam elements (e.g., 16 for wall S and 40 for wall H) with 5 Gaussian Legendre integration points. Each integration point is assigned with a generalized fibre section consisting of masonry and steel fibres and discretized from the cross-section of masonry walls. Each fibre is modelled by a material constitutive law to represent the uniaxial stress-strain behaviour of masonry or steel. Accordingly, the nonlinear behaviour of the reinforced masonry section can be integrated from the adopted nonlinear constitutive law of each fibre. In this study, *Concrete02* and *Steel01 in OpenSees* are adopted for modelling the masonry and steel fibres, respectively. In the material model adopted for masonry (i.e., *Concrete02*), $f_m, \varepsilon_0 \; and \; f_t$ are the masonry compressive strength, the corresponding strain and the masonry tensile strength, respectively, determined based on their random characteristics as provided in Table 4-2. While $f_{mu}, \varepsilon_u and \; \varepsilon_{tu}$, which represent the residual compressive strength, the corresponding strain and the ultimate tensile strain, respectively, are deterministic quantities deduced based on literature findings. Specifically, f_{mu}, ε_u are determine based on the models proposed in (Priestley and Elder 1983) for homogenous masonry, wheras ε_{tu} is taken as 0.004 (Wang et al. 1997). On the other hand, the parameters of the material model *Steel01* such as f_y and *E*, which represent the yield strength of steel reinforcement and corresponding Young's modulus, respectively, are defined based on their random characteristics provided in Table 4-2, whereas *b,* which is the strain hardening ratio, is taken as 0.01 (Wong et al. 2013). The configuration of the walls and the schematic view of the FE model used for walls loaded in eccentric compression are shown in Figure 4-1. In the model, the eccentric loading is applied

through a rigid beam with a length equals to the load eccentricity (e_n). Note that such a modelling approach is commonly validated and used to efficiently predict the loading behaviour of reinforced concrete masonry walls by the authors in (Metwally and Li 2021) and other researchers (e.g., Bilotta and Cruz 2021). However, it should be noted that the adopted modelling approach does not consider the effect of creep in the resistance calculations, which can affect the long-term resistance of masonry walls.

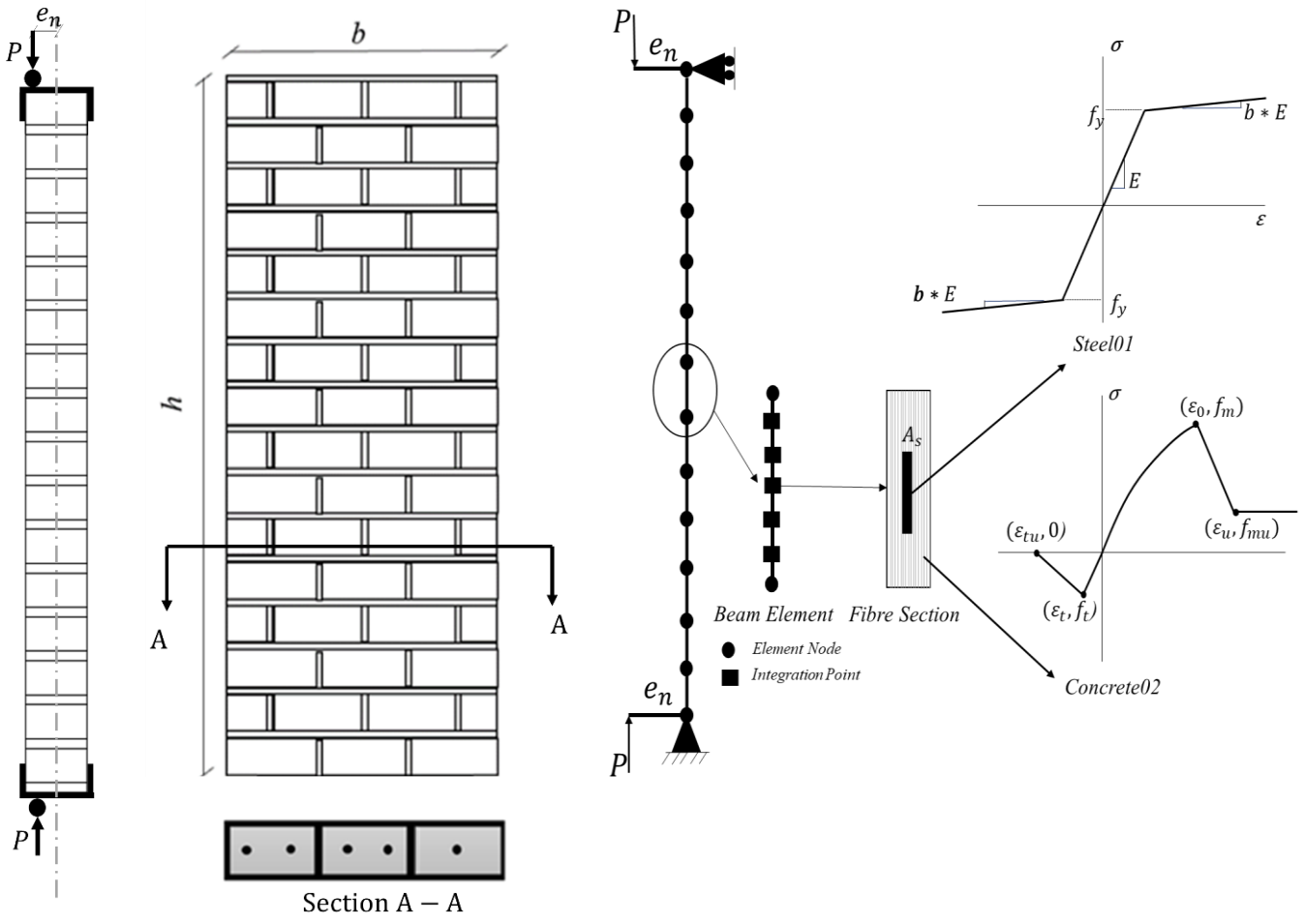

(a) (b)

Figure 4-1 Reinforced concrete masonry walls studied: (a) test specimen, and (b) schematic view of the FE model

As mentioned previously, the slenderness effects (i.e., geometric non-linearities) are considered within the developed FE model. It is found that the slenderness effects have a substantial effect on the global behaviour of the reinforced concrete masonry walls, especially those with high slender ratios (e.g., Wall H) in terms of load capacity (Figure 4-2). Note that this phenomenon is exemplified by the two walls with the load eccentricity-to-thickness ratio ($^{e_n}/_{t} = 0.1$), and a similar trend is observed for higher eccentricity-to-thickness ratios though the effect can eventually diminish when $^{e_n}/_{t}$ increases. In that sense, it is essential to consider the slenderness effect to get a realistic perspective into the behaviour and the reliability of reinforced concrete masonry walls.

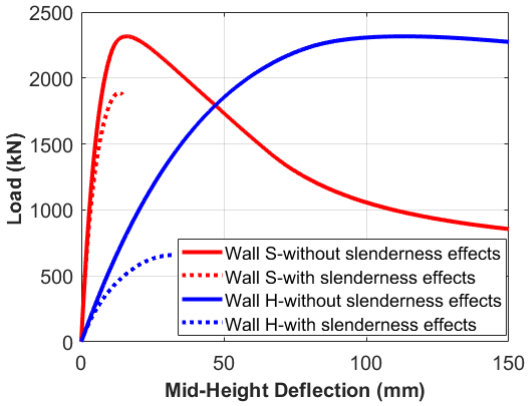

Figure 4-2 FE-based load-deflection curves for Walls S and H with $^{e_n}/_{t} = 0.1$

4.3 Uncertainty in Load Capacity

The load capacity P_c can be predicted using the aforementioned FE models, by extracting the peak axial load when the masonry wall is subjected to eccentric axial loading. Naturally, when the load applied to the wall is larger than the capacity, the wall would fail due to insufficient load

capacity. However, the FE model is by no means free of model error when compared with the experiments, and thus FE-predicted load capacity is inherent with model uncertainty. As such, the prediction-to-test ratio is introduced as a correction factor, to consider the model error (ME), and it is quantified using an experimental database consisting of 69 reinforced concrete masonry walls loaded under out-of-plane (i.e., eccentric axial compression and lateral loading) compiled from the literature (Yokel et al. 1970, Hatzinkolas et al. 1978, ACI-SEASC 1982, Suwalski 1986, Mohsin 2005).

Based on the comparison between the experimental and FE-predicted capacities, the statistical parameters of ME are quantified. It is found that ME follows a normal distribution with a mean of $\mu_{ME} = 1.02$ and coefficient of variation $COV_{ME} = 0.17$. The histogram, fitted distribution, mean (μ) and mean $\pm$ standard deviation ($\mu \pm \sigma$) are shown in Figure 4-3.

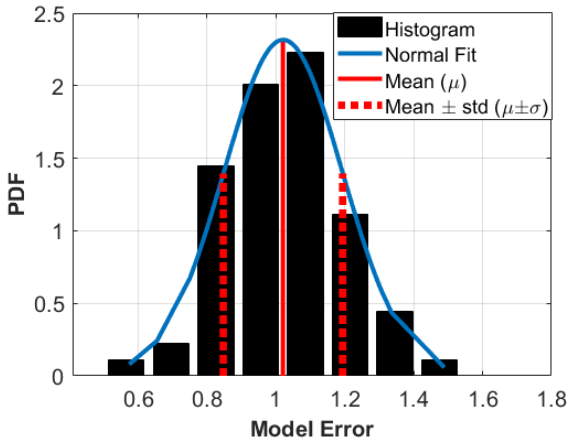

Figure 4-3 Histogram and fitted probability density function (PDF) for the model error distribution

ME accounts for the uncertainties that emerge from model simplification and embedded assumptions. In that sense, incorporating ME in quantifying the probabilistic behaviour and the reliability analysis can be essential. It is found that considering the model error in the

probabilistic capacity result in a significantly higher variance (i.e., more scattered capacity range) as indicated by the comparison of the empirical probability distribution functions (PDFs) of the probabilistic capacity of the considered walls (i.e., wall S and wall H) when loaded with $^{e_n}/_t = 0.1, 2.0$ with and without considering model error as shown in Figure 4-4.

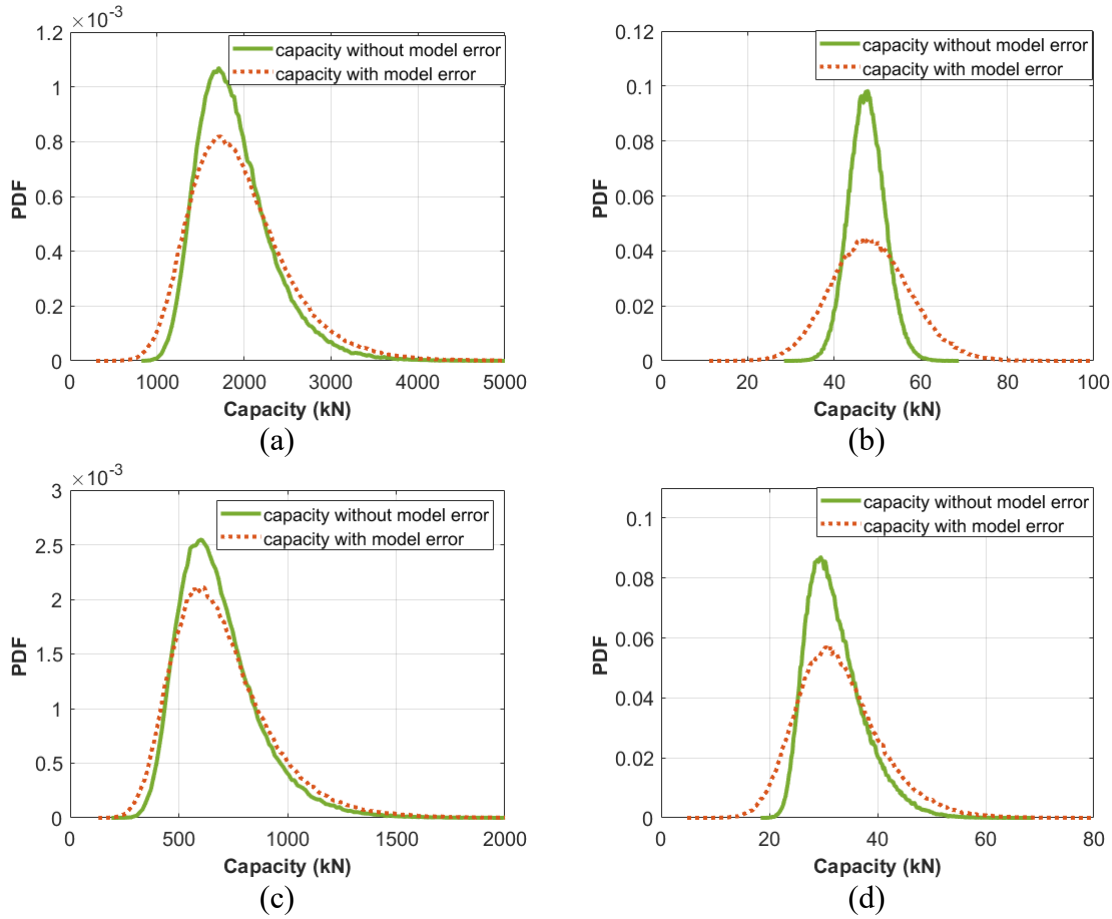

Figure 4-4 Comparison of load capacity PDFs with and without considering model error: (a) Wall S $^{e_n}/_t = 0.1$, (b) Wall S $^{e_n}/_t = 2.0$, (c) Wall H $^{e_n}/_t = 0.1$, and (d) Wall H $^{e_n}/_t = 2.0$

4.4 Uncertainty in Load Effects

In addition to the aforementioned uncertainties in the wall properties and thus the capacities, the loads (e.g., dead load, live load, snow load) applied directly or indirectly to the walls are also

uncertain. The corresponding statistical characteristics of the loading random variables are provided in Table 4-3, according to Bartlett et al. (2003). In Table 4-3, DL_n, LL_n, SL_n are the nominal dead load, live load and snow load, respectively. It should be noted that when the live or snow loads are principal loads, the statistics corresponding to 50-year maximum load are used in the reliability assessment. On the other hand, the point-in-time statistics are used for companion loads. In addition, the transformation to load effects statistics are introduced to account for modelling (e.g., uncertainties with an idealization of the actual load to equivalent uniformly distributed load) and analysis factors (e.g., uncertainties with calculating the straining actions induced by the loads) (Barlett et al. 2003).

Table 4-3 Statistical characterization for loads

Load Type		***Mean (μ)***	***Coefficient of variation***	***Distribution***
Dead		$1.05DL_n$	0.10	Normal
Live	50-year maximum load	$0.90LL_n$	0.17	Gumbel
	Point-in-time load	$0.27LL_n$	0.68	Weibull
	Transformation to load effects	1.00	0.21	Normal
Snow	50-year maximum load	$1.10SL_n$	0.20	Gumbel
	Point-in-time load	$0.20SL_n$	0.89	Weibull
	Transformation to load effects	0.60	0.42	Lognormal

Assuming the two walls were designed satisfying the CSA S304-14, the nominal load effects or loads that the walls were supposed to resist, can be back-calculated based on the limit state design criterion used. Namely, at the limit, the factored resistance should be equal to the factored load effect. As such, the nominal properties of the wall considered are used together with resistance factors to calculate its design resistance, represented by the column P-M interaction

diagram as derived from the section P-M interaction diagram using moment magnifier method with CSA S304-14). For a given eccentricity *e*, the nominal load effects can be traced back based on the corresponding load factors, depending on the load combinations considered in this paper. In this section, the three load combinations involving dead load, live load, snow load considered are: load combination#1 $1.4\,DL_n$ with dead load only; load combination #2 $1.25\,DL_n + 1.5\,LL_n + 0.5\,SL_n$ with the live load and snow load as the principal and companion load, respectively; and load combination #3 $1.25\,DL_n + 0.5\,LL_n + 1.5\,SL_n$ with the snow load and live load as the principal and companion load, respectively.

Specifically, for the load combination with dead load only, the design resistance of the cross-section is denoted by designed axial force resistance $P_{r,design}$ and the corresponding designed moment resistance $M_{r,design}$. denoted by point a $(P_{r,design}, M_{r,design})$ in Figure 4-5. This design moment resistance corresponds to the magnified primary moment by moment magnifier method; thus, the primary moment M_{Pn} can be deduced by reducing the designed moment resistance, denoted by point b $(P_{r,design}, M_{Pn})$ in Figure 4-5. Subsequently, the nominal dead load can be expressed as $P_{Dn} = \frac{P_{r,design}}{1.4}$ as indicated by point c (P_{Dn}, M_{Dn}). Subsequntally, the random properties of P_D can be obtained by the available statistical information for the dead load.

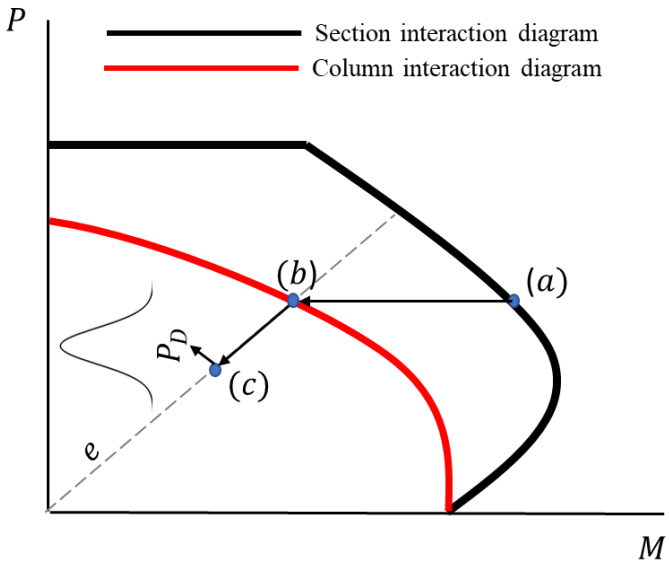

Figure 4-5 Typical interaction diagrams for walls loaded under dead load only

Consider load combinations that involve more loads in addition to dead load, e.g., load combination #2, the nominal axial load (P_{rn}) and moment (M_{rn}) resistances can be expressed as follows according to CSA S304-14:

$$P_{r,design} = 1.25P_{Dn} + 1.5P_{Ln} + 0.5P_{Sn} \qquad (4-1)$$

$$M_{r,design} = 1.25M_{Dn} + 1.5M_{Ln} + 0.5M_{Sn} \qquad (4-2)$$

where P_{Dn}, P_{Ln} and P_{Sn} are nominal axial load due to dead, live and snow loads, and M_{Dn}, M_{Ln} and M_{Sn} are the corresponding moments due to eccentricity. According to (Ellingwood et al. 1980), the typical load-ratios between the nominal values of live load P_{Ln} (or snow load P_{SL}) and the dead load P_{Dn} for masonry structures, α_{PL} (or α_{PS}), range from 0.25 to 2.0. Thus α_{PL} (or α_{PS}) = 0.25, 0.5, 1.0, and 2.0, are considered in this study. α_{PL} (or α_{PS}) are used to back-calculate the nominal values of the axial loads and the corresponding moments from the designed

values of resistances. Note that the moment ratios (i.e., α_{ML} and α_{MS}) are taken equal to the corresponding axial load ratios for a given eccentricity considered in this study.

Subsequently, P_{Dn} and M_{Dn}, can be determined based on $P_{r,\ design}$ and $M_{r,design}$, as follows:

$$P_{Dn} = \frac{P_{r,design}}{(1.25 + 1.5\ \alpha_{PL} + 0.5\alpha_{PS})} \qquad (4-3)$$

$$M_{Dn} = \frac{M_{r,design}}{(1.25 + 1.5\ \alpha_{PL} + 0.5\alpha_{PS})} \qquad (4-4)$$

Similar to load combination #2, P_{Dn} and M_{Dn}, can be determined based on $P_{r,\ desin}$ and $M_{r,design}$ for load combination #3 as follows:

$$P_{Dn} = \frac{P_{r,design}}{(1.25 + 0.5\ \alpha_{PL} + 1.5\alpha_{PS})} \qquad (4-5)$$

$$M_{Dn} = \frac{M_{r,design}}{(1.25 + 0.5\ \alpha_{PL} + 1.5\alpha_{PS})} \qquad (4-6)$$

For the load combinations considered above, masonry walls are subjected to eccentric axial loads only. In that sense, the applied axial loads (i.e., load effects) can be compared with the axial load capacity for the corresponding eccentricity. The probabilistic axial load capacity P_c, with and without considering model error, against the probabilistic load effects, for the walls considered with eccentricity to thickness ratio ($^{e_n}/_{t} = 0.1$) is presented in Figure 4-6.

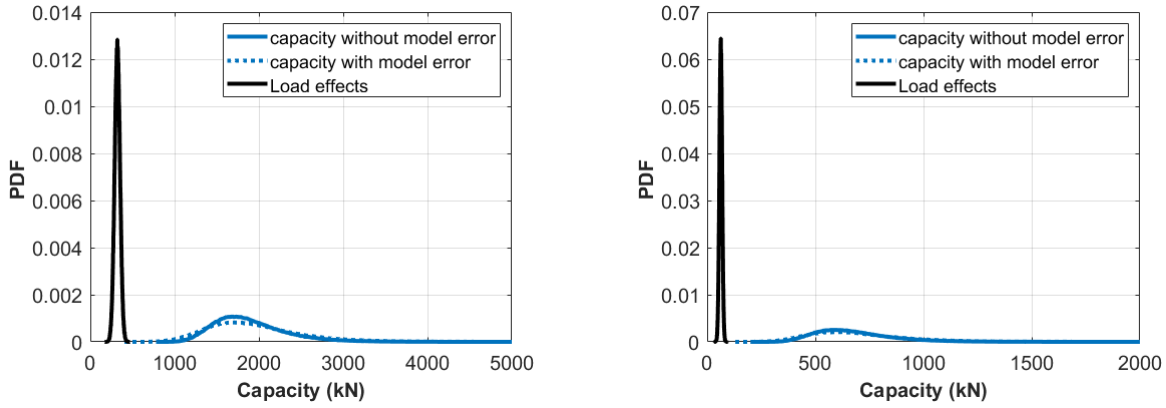

(a) (b)

Figure 4-6 Comparison between load capacity with and without model error and the load effects: (a) Wall S, and (b) Wall H

4.5 Reliability Analysis for Global Failure of Walls

4.5.1 Global failure-based limit state function

For the three load combinations involving eccentric axial loads only, load resistance R and load effect S are described by the axial load capacity P_c and the applied load, $P = P_D$ in the case of load combination #1 and $P = (P_D + P_L + P_S)$ in the cases of load combination #2 and #3. Hence, the limit state function can be defined as follows:

$$G = R(f_m, \varepsilon_0, f_t, f_y, E, d) - S(P_D, P_L, P_S) \qquad (4-7)$$

where R and S are random variables representing the structural resistance and the load effects (i.e., demand), respectively.

As found in Jiang et al. (2020), the nominal load eccentricity (e_n) significantly affects wall behaviour and thus the reliability analysis outcomes. Accordingly, the reliability of the considered walls is analyzed under a wide range of eccentricities. Specifically, $^{e_n}/_t$ = 0.1, 0.5, and 2.0, are considered in this study. In addition, the reliability assessment is conducted

considering two scenarios: with and without considering the model error, to demonstrate the importance of considering model error for accurate reliability assessment of the masonry walls.

4.5.2 Reliability analysis methods

As mentioned previously, structural reliability aims at investigating the probability that the actual value of the load effect exceeds the resistance considering a certain failure criterion. This probability is referred to as the probability of failure P_f. However, the analytical determination of the probability of failure (P_f.) is not feasible in several practical cases which involve complex numerical systems or implicit limit state functions. Alternatively, Monte Carlo (MCS) is the most commonly used method to calculate the probability of failure (P_f) as any form of the limit state functions (e.g., implicit functions) can be incorporated within its framework (Su et al. 2017).

Although MCS provides a robust and accurate tool for reliability analysis, it is associated with a low convergence rate. This limits MCS application for cases in which the evaluation of the limit state function is computationally expensive (Dubourg et al. 2013). To tackle this problem, other simulation-based methods were developed. Among these methods is Subset Simulation (SS), an adaptive stochastic simulation technique that aims to capture rare failure events and compute small failure probabilities. In SS, the target probability of failure is expressed as a product of larger conditional probabilities of adaptive intermediate failure events. To this end, computing small probabilities of failure becomes feasible by performing a sequence of problems involving more frequent events (Au et al. 2007, Tee et al. 2014).

To further resolve the computational cost using (SS) for FE-based reliability analysis, the original expensive FE model can be replaced with a fast-to-evaluate surrogate model. Among different surrogate models, polynomial chaos expansion (PCE) (Ghanem and Spanos 1991) and kriging (Schöbi et al. 2017) are the most widely used techniques in uncertainty quantification and reliability analysis (Yu et al. 2020, Bhattacharyya 2021). However, each of them is associated with certain drawbacks. For instance, PCE sometimes fails to accurately represent the tails of the model response distribution, which limits its applicability for reliability-related applications (Marelli and Sudret 2018). On the other hand, kriging relies significantly on the information provided by the training sample. Accordingly, kriging surrogating quality can be compromised if only a limited number of samples are available (Ling et al. 2020).

To overcome the aforementioned drawbacks, a new unified surrogate modelling technique, polynomial chaos kriging (PCK), was firstly introduced by (Schobi et al. 2015) to combine the advantages of both models. To do so, PCK employs PCE to approximate the main trend of the original computational model and kriging to account for the local variations. Intuitively, PCK was shown to be more accurate compared to PCE and kriging separately (Schobi et al. 2015). Thereafter, PC-Kriging was widely used in different applications, including reliability analysis (Das et al., 2020, Leifsson et al. 2020, Schöbi et al. 2017, Yu et al. 2020).

In this study, the PCK surrogate model is trained over (N=300) stochastic generated based on the *Latin hypercube sampling strategy* (*LHS*). The comparison between the empirical different surrogate models (e.g., PCK-100, PCK-300 and PCK-2000) developed to reproduce the peak capacity (i.e., resistance) for two extreme cases (i.e., Wall S with e_n/t=0.1 and wall H with e_n/t=2.0) is shown in Figure 4-7. Based on the comparison, it is found out that 300 FE

simulations are sufficient to construct the surrogate model with the same level of accuracy obtained with much larger number (e.g., 2000 FE simulations).

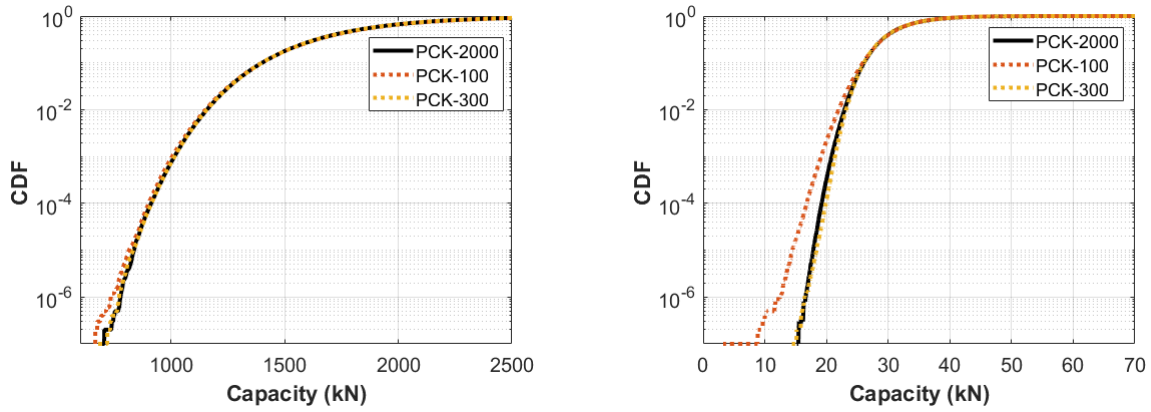

Figure 4-7 Comparison of the capacity CDFs based on different surrogate models: (a) Wall S, and (b) Wall H

4.5.3 Results and discussion

In this section, the reliability assessment results are shown for the three load combinations involving dead load, live load, snow load (i.e., Combination #1, Combination #2, Combination #3). For combination #2 and combination #3, different load ratios (i.e., α_{PL} and α_{PS}) are considered. Each combination of (combination #, α_{PL}, α_{PS}) resemble a unique case in the reliability assessment. Table 4-4 provides a summary of the considered cases.

Table 4-4 Cases considered in the reliability assessment

Case#	*Combination #*	α_{PL}, α_{ML}	α_{PS}, α_{MS}
1	1	-	-
2	2	0.25	0.25
3	3	0.25	0.25
4	2	0.5	0.5
5	3	0.5	0.5
6	2	1	1
7	3	1	1

8	2	2	2
9	3	2	2
10	2	1	0.25
11	2	1	0.5
12	2	1	2
13	3	0.25	1
14	3	0.5	1
15	3	2	1

It is found that the reliability assessment can be significantly influenced by the model error. Figure 4-8 shows the reliability indices (β) for the considered walls (i.e., Wall S and Wall H) loaded with design eccentricity to thickness ratio of with ($^{e_n}/_t$=0.1, 2.0) with and without considering model error. It is shown that incorporating ME results in noticeably lower reliability indices (β) (i.e., higher probabilities of failure) for the majority of the cases. This indicates that the negligence of ME in the reliability assessment is on the non-conservative side, even if mechanics-based FE models are adopted for the reliability analysis.

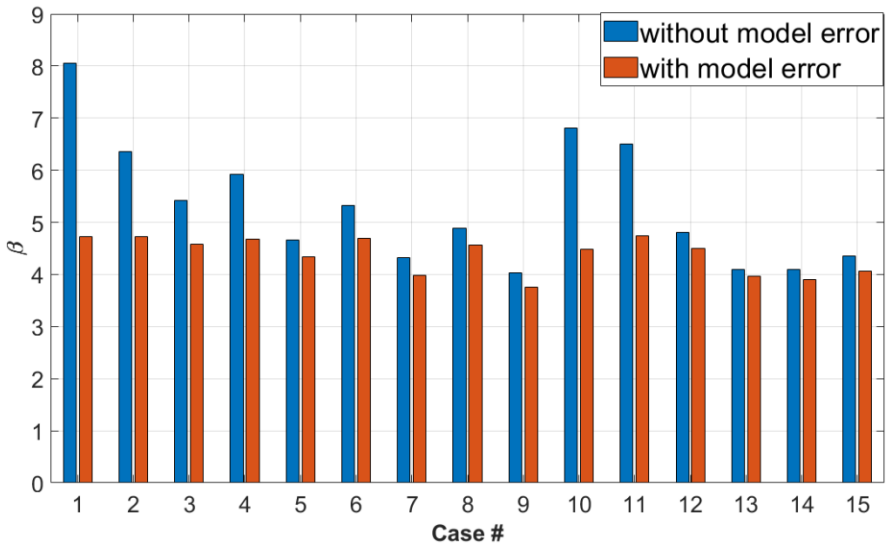

(a)

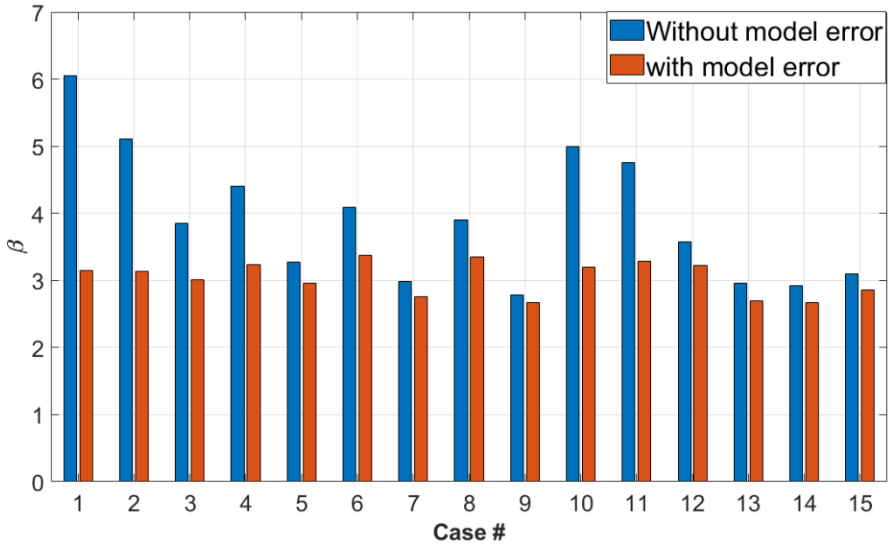
Without model error
with model error
β
Case #

(b)

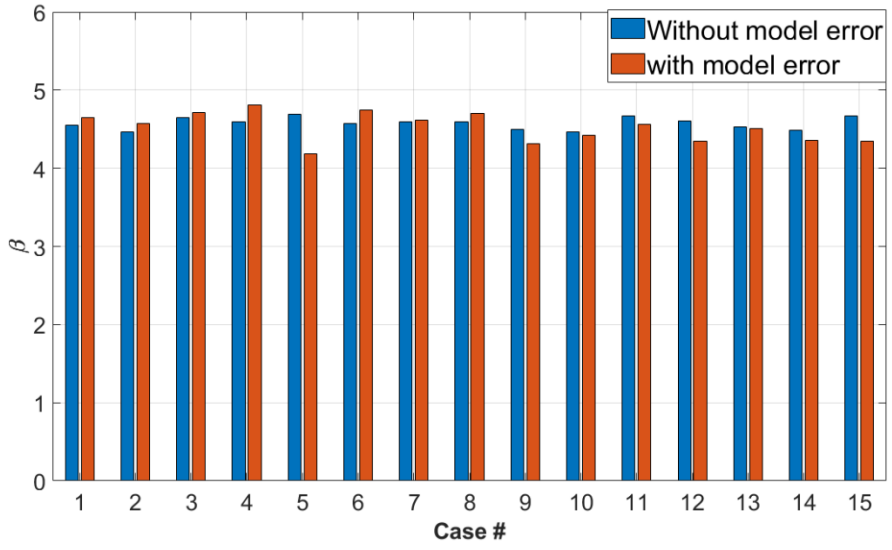
Without model error
with model error
β
Case #

(c)

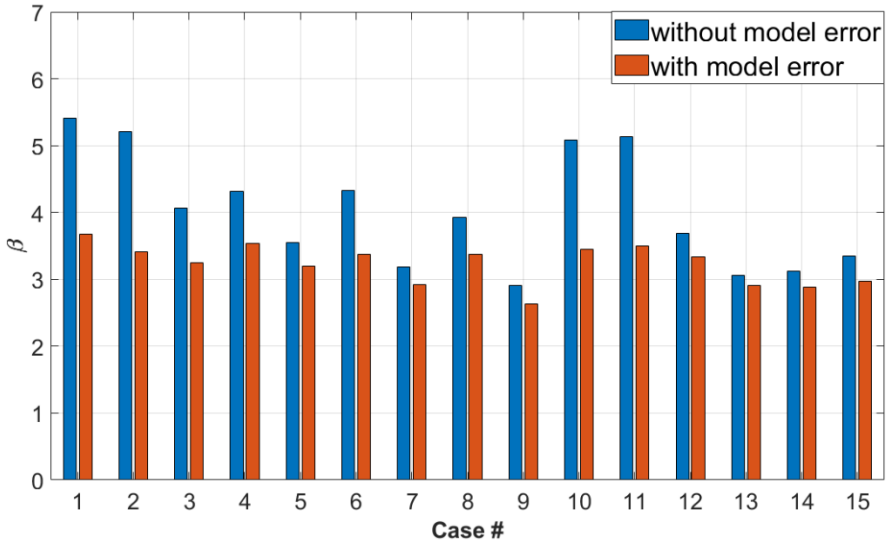

(d)

Figure 4-8 Comparison between the reliability indices (β) with and without considering model error: (a) Wall S ($^{e_n}/_t$=0.1), (b) Wall S ($^{e_n}/_t$=2.0), (c) Wall H ($^{e_n}/_t$=0.1), and (d) Wall H ($^{e_n}/_t$=2.0)

It is also found that the reliability indices (β) are sensitive to the design eccentricity to thickness ratio ($^{e_n}/_t$). Figure 4-9 shows a comparison for the reliability indices associated with the considered walls (i.e., Wall S and Wall H) at different design eccentricity to thickness ratios (e.g., $^{e_n}/_t = 0.1, 0.5, 2.0$). Note that the results shown here are with considering the model error. It is shown that the reliability indices corresponding to ($^{e_n}/_t = 0.1$) are significantly higher compared to the other ratios (e.g., $^{e_n}/_t = 0.5$, 2.0). This trend is observed for both of the considered walls. This conforms to the findings reported in (Liu and Dawe 2003), which indicated that CSA S304 is overly conservative for walls loaded with smaller design eccentricity to thickness ratios (e.g., $^{e_n}/_t$ =0.1). On the contrary, walls loaded with ($^{e_n}/_t$ =0.5) are found to be associated with the lowest reliability indices (β), which is most pronounced for wall H.

This conforms to the findings reported in (Isfeld et al. 2019, Liu and Dawe 2003), which indicated that the design code (i.e., CSA S304) underestimates the second-order effects for walls loaded with such eccentricity range.

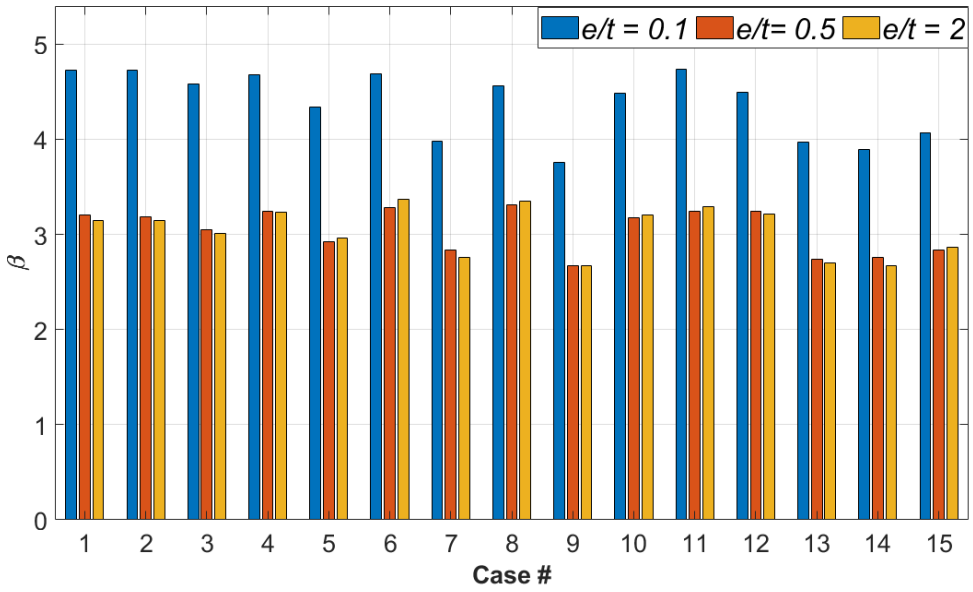

(a)

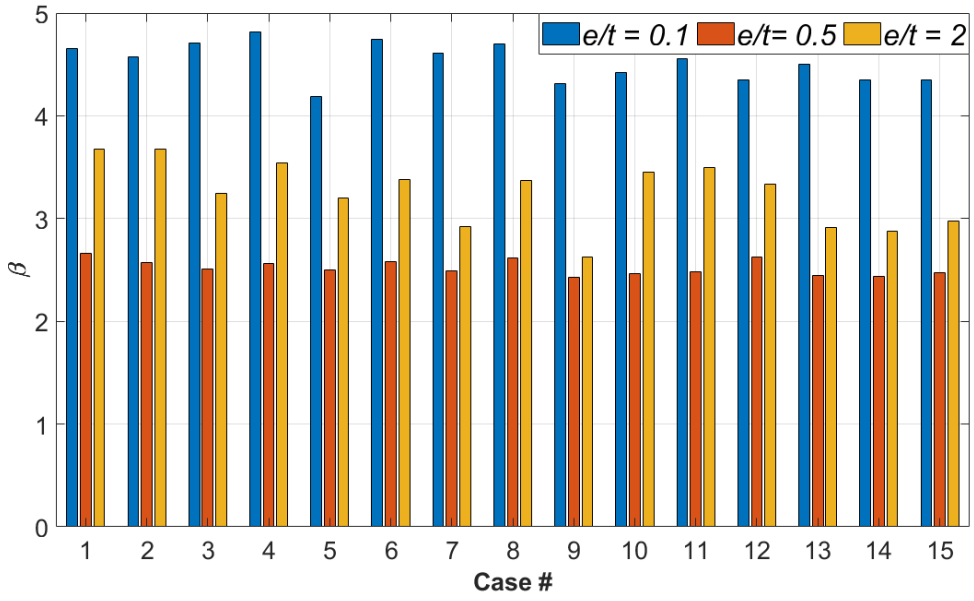

(b)

Figure 4-9 Comparison between the reliability indices (β) with different $^{e_n}/_t$ (a) Wall S, and (b) Wall H

In order to investigate the effect of the slenderness ratio on the reliability of the walls, the reliability indices (β) of the considered two walls (i.e., wall S and wall H) are compared for each considered load eccentricity to thickness ratio ($^{e_n}/_t = 0.1, 0.5, 2.0$), as shown in Figure 4-10. Note that the results shown are with considering model error. It is found that the reliability assessment for both walls yields similar reliability indices (β) throughout the considered 15 cases for ($^{e_n}/_t = 0.1, 2.0$). However, this was not the case for ($^{e_n}/_t = 0.5$) as the highly slender (i.e., wall H) is associated with noticeably lower reliability indices (β) compared to walls S. Another observation is that the reliability indices (β) for the considered walls for ($^{e_n}/_t = 0.5, 2.0$) are below 3.5, which is the target reliability indices recommended by (CSA S408,2011) for normal importance buildings with a gradual (ductile) failure mode.

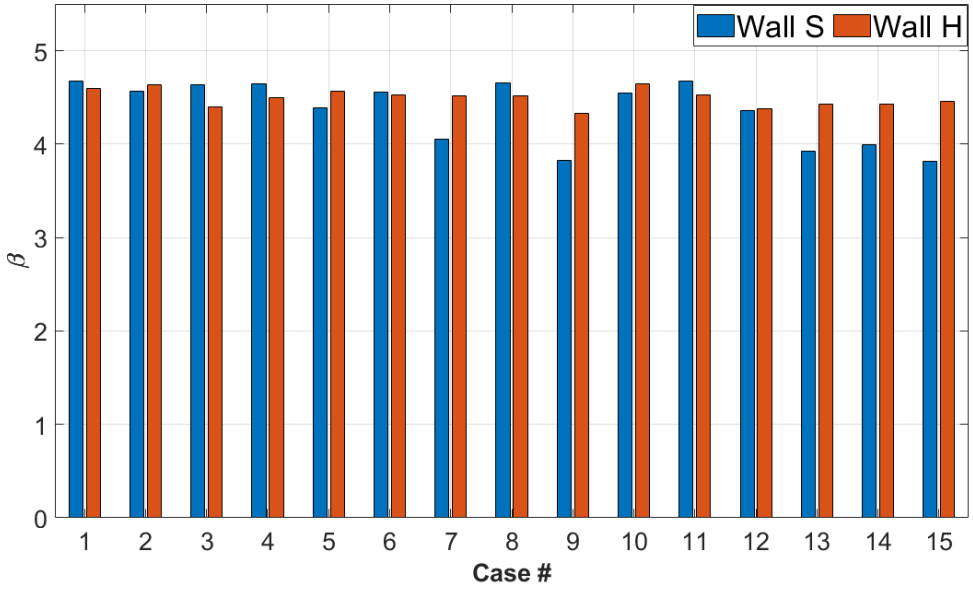

(a)

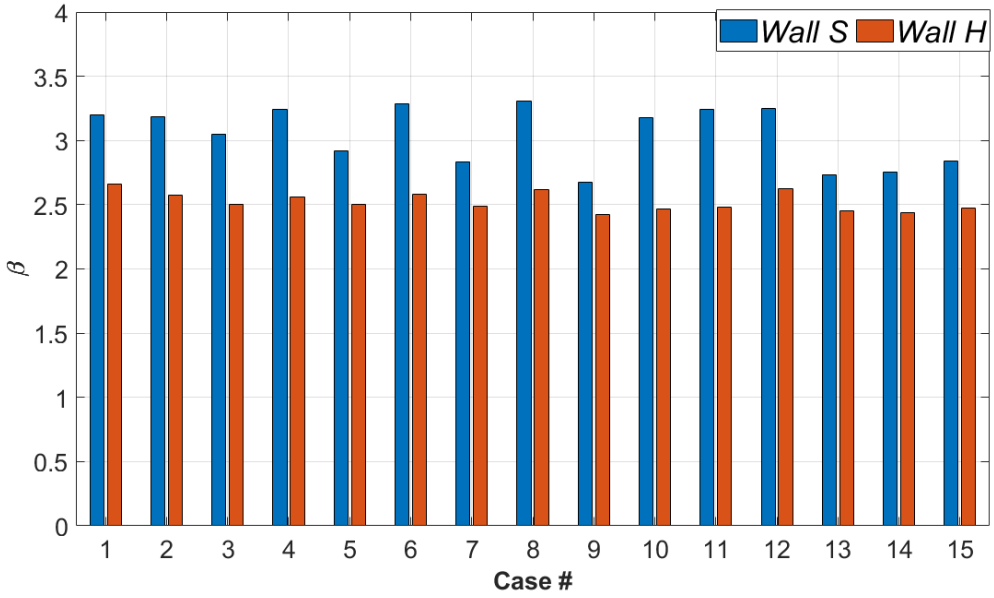

(b)

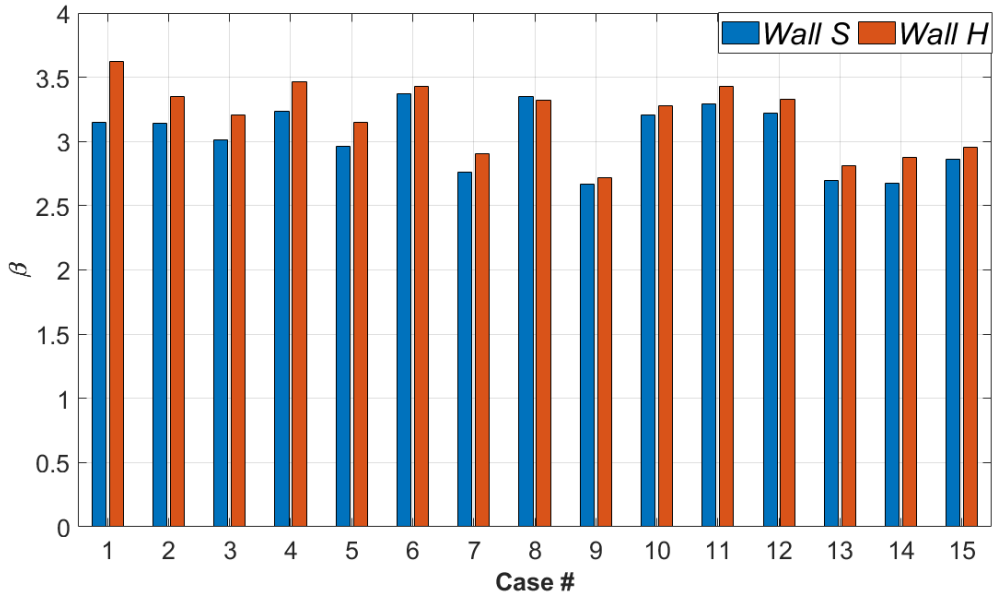

(c)

Figure 4-10 Comparison between the reliability indices (β) for wall S and wall H: (a) ${e_n}/{t} = 0.1$, (b) ${e_n}/{t} = 0.5$, and (c) ${e_n}/{t} = 2.0$

In addition to the aforementioned factors, the reliability indices can be sensitive to the load ratios (e.g., α_{PL}, α_{PS}). Figure 4-11 shows the comparison between the reliability indices (β) for the considered walls when loaded with (${e_n}/{t} = 0.1,2.0$) considering load combination #2 (where the live load is a principal load and snow load is a companion load) and load combination #3 (where snow load is a principal load and live load is a companion load) with different companion load to dead load ratios. Note that the results shown here are with considering the model error and the ratio between the nominal principal load (e.g., live or snow) and the nominal dead load is (1). It is shown that the load combinations with the snow load as principal loads are associated with generally lower reliability indices (β) compared to the ones with the live load as a principal load

for the same load ratio. This can be attributed to the higher uncertainty associated with snow loads. The same trend was also observed and reported in (Moosavi and Korany 2014).

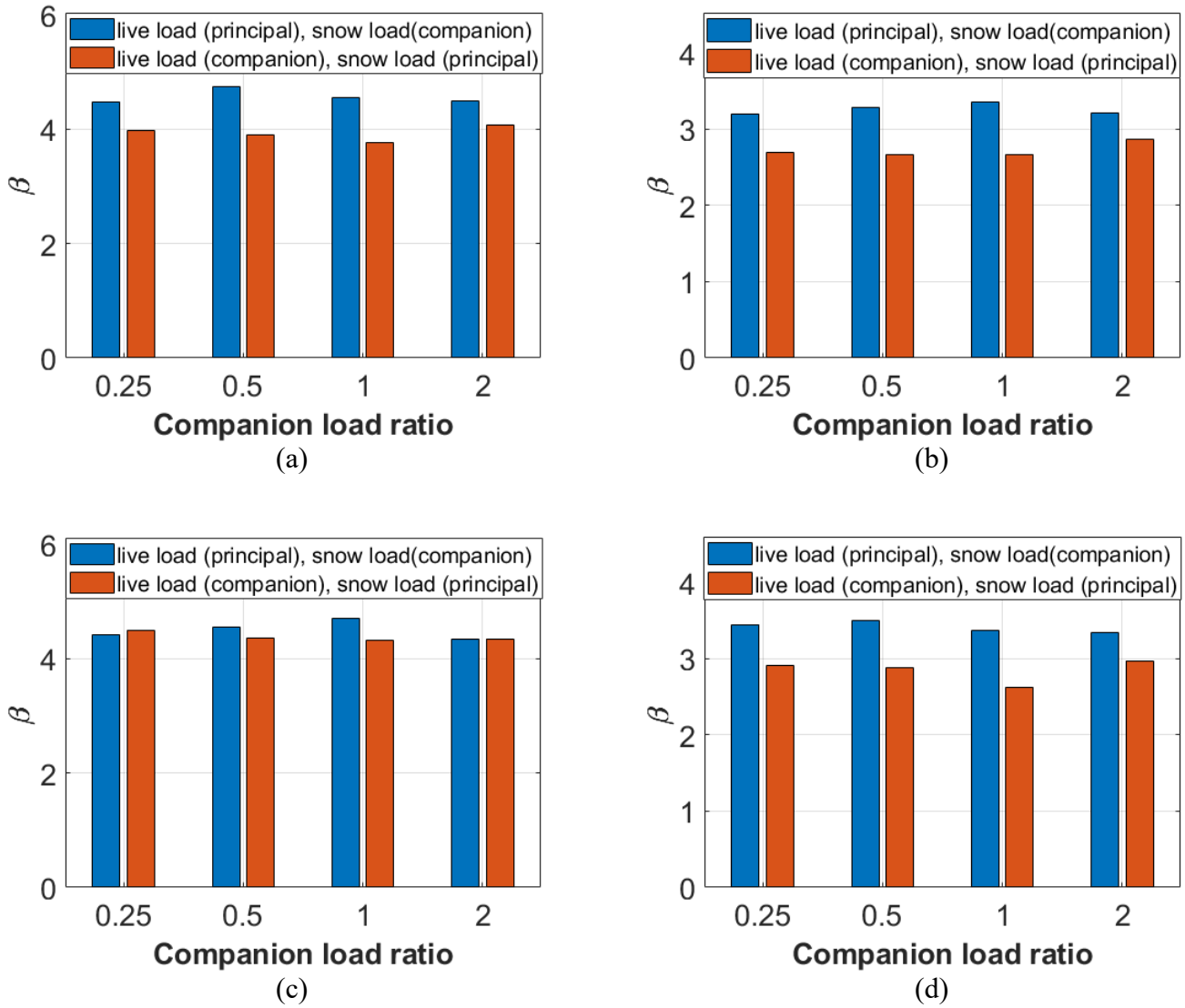

Figure 4-11 Comparison between the reliability indices (β) for load combinations #2 and #3: (a) Wall S ($^{e_n}/_t$=0.1), (b) Wall S ($^{e_n}/_t$=2.0), (c) Wall H ($^{e_n}/_t$=0.1), (d) and Wall H ($^{e_n}/_t$=2.0)

4.6 Reliability Analysis for Local Failure of Walls

4.6.1 Local failure-based limit state function

The limit-state function formulated above serves to describe the global failure of a structural member, which implies the incapability of the masonry wall to resist the loads applied. In contrast, the current design codes (e.g., CSA S304-14) interpret failure as the incapability of the critical cross-section to sustain the load effects (i.e., applied axial force P and moment M on the section), which is referred to as local failure limit-state for a cross-section. Namely, failure occurs when the sectional moment capacity M_C under the axial load P is less than the applied moment M. In that sense, M_C represents the resistance R while M represents the demand S in the limit state function. Note that the applied moment M on the critical cross-section can be obtained through the moment magnifier method to consider the second-order effect approximately in the wall response. However, the applied moment calculated can suffer from inaccuracy in the moment magnifier method. For a fair comparison, the applied moment is determined through nonlinear FE analysis using the same macro FE model developed earlier. Thus, the limit-state function formulated in a safety margin format reads:

$$G = R(f_m, \varepsilon_0, f_t, f_y, E, d, P) - S(f_m, \varepsilon_0, f_t, f_y, E, d, P) \quad (4\text{-}8)$$

This limit-state function serves to describe the local failure limit-state defined in terms of the cross-section. In order to show the difference in the reliability levels using different failure criteria, or relative conservatism in the current design arising from failure criteria, this study also conducts reliability analyses for the aforementioned walls against local failure in a critical cross-section.

The section capacity M_C can be determined from sectional analysis (i.e., moment-curvature analysis), a well-received approach to characterize the sectional behaviour in engineering practice. Figure 4-12 summarizes the procedure to calculate M_C schematically, in which, the masonry cross-section is discretized into masonry and steel layers associated with the same material stress-strain behaviours (e.g., *Concrete02* and *Steel01*) as those used in the FE model of the masonry wall. The stress in each fibre is determined based on the aforementioned material models. Subsequently, the force carried by each fibre can be calculated given the fibre geometry. Afterwards, the equilibrium of the section under the internal and external forces is checked. If the equilibrium is not satisfied, this means that the neutral axis location (c) is not correct. Accordingly, (c) is changed in an iterative manner until equilibrium is satisfied. From here, the curvature (κ) and the corresponding moment resistance (M) can be obtained. Lastly, the moment-curvature curve can be obtained for different combinations of (κ, M). The peak moment on the moment-curvature curve represents the moment capacity M_C. Note that in the figure, ε_u = ultimate strain, ε_s = steel strain, c = neutral axis depth, d = steel bars depth, C_m = masonry compression force, T_m = masonry tension force, T_s = steel tension force, P= axial load and M = moment resistance. M_C is the peak moment on the moment-curvature curve.

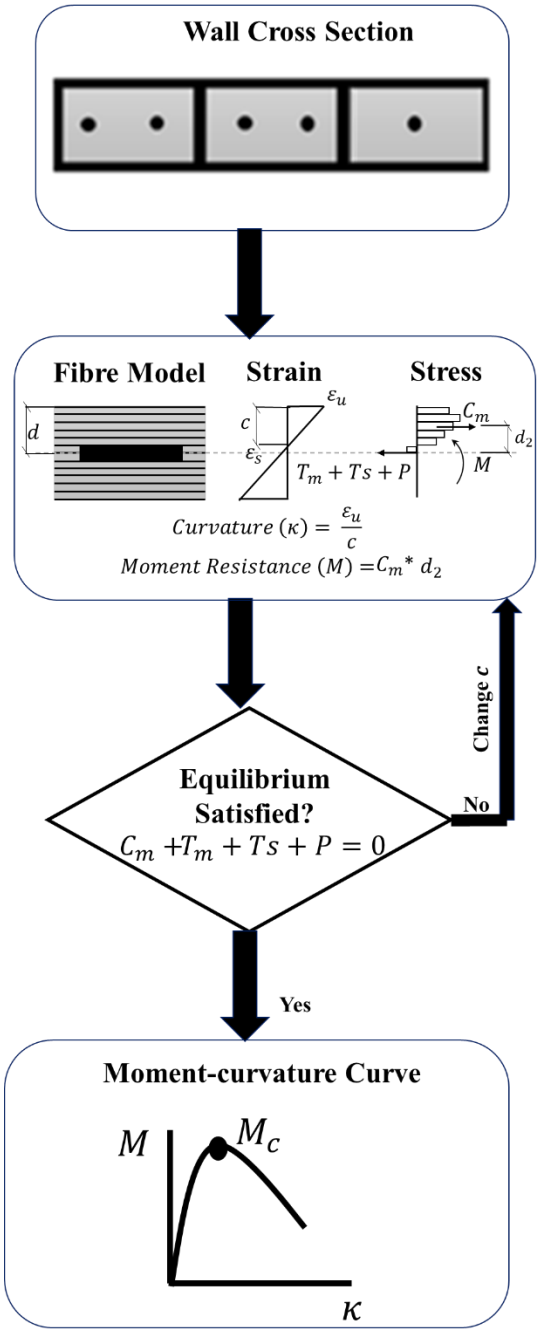

Figure 4-12 Moment-curvature analysis procedure

In addition, another more stringent local failure criterion for material (e.g., concrete compressive crushing) is of interest. This refers to the local failure limit-state defined in terms of material

failure. For comparison purposes, this study also conducts reliability analysis against local failure in a critical cross-section. In this case, M_C is the moment corresponding to the compressive crushing of extreme concrete fibre (i.e., compressive strain = 0.003 (i.e., the crushing strain commonly used in design codes)).

4.6.2 Results and discussion

The effect of the failure criteria on the reliability assessment is investigated in this section by comparing the reliability indices obtained based on global, section and material (i.e., fibre) failure criteria. Figure 4-13 shows the comparison of the reliability indices obtained based on the aforementioned failure criteria (i.e., global failure, section failure and fibre failure) for the two considered walls (i.e., wall S and wall H) at different e_n/t (e.g., 0.1,0.5,2.0) and considering load case #9. It is found that there is a higher probability of material fibre failure (corresponding to a lower reliability index) than section failure. This implies that the material fibre failure is a more stringent criterion and thus more conservative as expected since the sectional failure criterion allows stress redistribution over the cross-section among different material fibres. However, the difference between these two local failure criteria (i.e., section failure and fibre failure) are small for masonry walls that are slender (Wall H) and those with high load eccentricities (e.g., wall S with e_n/t =0.5, 2.0).

Similarly, since stress redistribution (or plastic hinge formulation) is allowed along with the wall height, the probability of global failure is lower (corresponding to higher reliability index) than the probability of local failure (e.g., section failure) for Wall S with high load eccentricities ($\mathrm{e.g.,}\ e_n/t = 0.5, 2.0$), see Figure 4-13(a). However, compared to the global failure criterion,

local failure criteria (e.g., section failure) is not always more conservative. For example, slender Wall H with different load eccentricities (e.g., $^{e_n}/_t = 0.1, 0.5, 2.0$), see Figure 4-13(b), and Wall S with lower load eccentricities (e.g., $^{e_n}/_t = 0.1$), the probability of global failure is higher (corresponding to a lower reliability index). This is because the section failure criterion fails to account for stability failure, while the global failure criterion does. As mentioned previously, highly slender walls (e.g., Wall H) and walls loaded with lower eccentricities (e.g., Wall S with $^{e_n}/_t = 0.1$) are most vulnerable to stability failure.

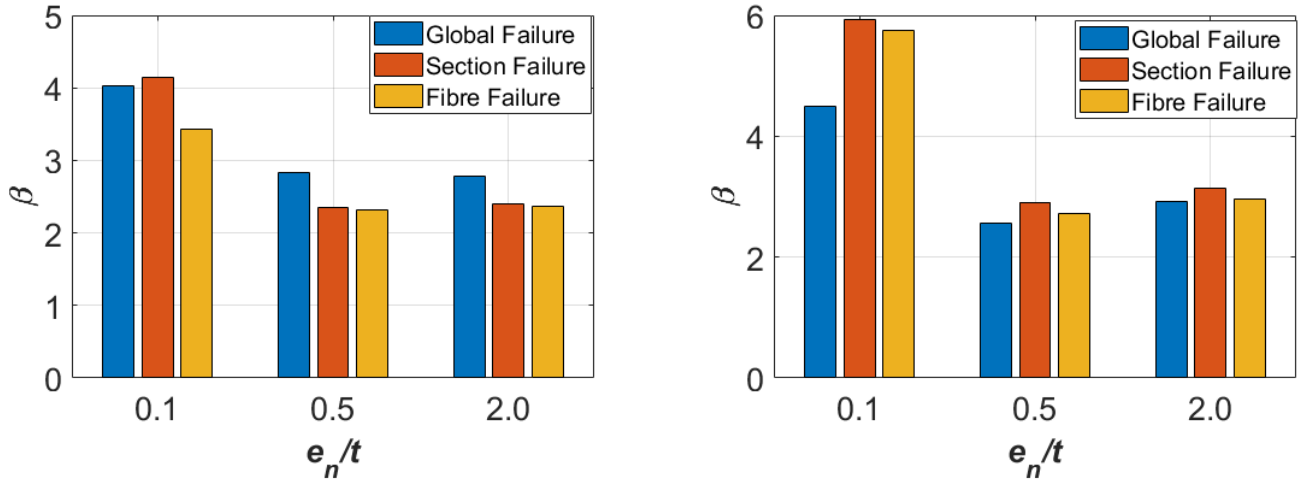

Figure 4-13 Comparison between the reliability indices (β) for different failure criteria for load case #9: (a) Wall S, and(b) Wall H

4.7 Wind load combinations

4.7.1 Global failure-based limit state function for wind load combinations

Previously, the limit-state function that describes the global failure of a structural member (i.e., masonry wall) under a combination of vertical loads (e.g., dead, live and snow) was defined. In addition to that, the limit-state function that describes the global failure for masonry walls subjected to vertical and wind loads (P,W) is discussed in this section.

Similar to the case with only vertical loads, the two walls are assumed to be designed in accordance with CSA S304-14. Accordingly, the factored resistance should be equal to the factored load effect at the limit. The nominal and random properties of the loads can be back-calculated from the factored ones employing the same procedure illustrated in Section 4.4. Assuming a sequential loading approach (i.e., the vertical loads are applied first followed by the wind load), the failure occurs when the wind load capacity W_C under the axial load P is less than the applied wind load W. In that sense, W_C represents the resistance R while W represents the demand S in the limit state function. Thus, the limit-state function formulated in a safety margin format reads:

$$G = R\left(f_m, \varepsilon_0, f_t, f_y, E, d, P\right) - S(W) \qquad (4-9)$$

The corresponding statistical characteristics of the wind load random variables are provided in Table 4-5. according to Bartlett et al. (2003). In this study, the reliability assessment is conducted considering the load combination #4 ($1.25\ D_n + 1.4\ W_n + 0.5\ L_n$), where D_n, W_n and L_n are the nominal dead and wind and live loads, respectively. The analysis is conducted assuming that $\alpha_{PL} = 1$, the wind loads possess no contribution in the axial force (i.e.,$\alpha_{PW} = 0$), while gravitational loads are assumed to be concentric for simplicity and the out-of-plane moment is induced by the uniformly applied wind load only.

Table 4-5 Statistical characterization for wind load

Load Type		***Mean (μ)***	***Coefficient of variation***	***Distribution***
	50-year maximum load	$1.04\ W_n$	0.08	Gumbel

Wind	Point-in-time load	0.16 W_n	0.72	Weibull
	Transformation to load effects	0.68	0.22	Lognormal

4.7.2 Results and discussion

The reliability assessment results considering combination #4 are discussed in this section. Figure 4-14 shows a comparison for the reliability indices associated with the considered walls (i.e., Wall S and Wall H) at different design eccentricity to thickness ratios (e.g., $^{e_n}/_t = 0.1, 0.5, 2.0$). It should be noted that e_n here refers to the ratio between the design primary moment and the design axial load at the critical section along with the wall height (i.e., mid-height). The reliability indices (β) are shown to be sensitive to the design eccentricity to thickness ratio ($^{e_n}/_t$). is shown that the reliability indices corresponding to ($^{e_n}/_t = 0.1$) are higher compared to the other ratios (e.g., $^{e_n}/_t = 0.5, 2.0$) for both of the considered walls, consistent with the trend observed for walls under vertical loads only. In addition, the reliability assessment is found to be sensitive to the model error. Again, similar observations were made for the cases with only vertical loads. Furthermore, it can be seen that both walls are associated with similar reliability indices when the model error is considered except for ($^{e_n}/_t = 2.0$) as wall H is associated with higher reliability than wall S for this eccentricity to thickness ratio.

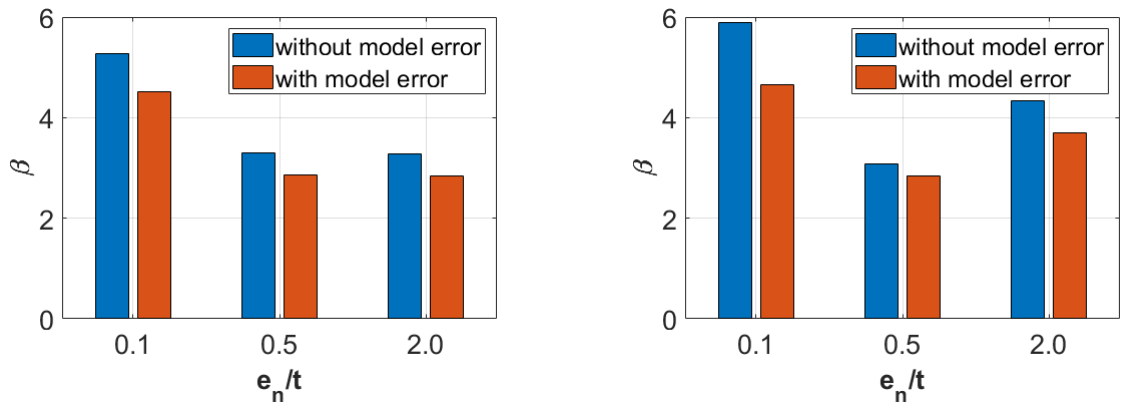

(a) (b)

Figure 4-14 Comparison between the reliability indices (β) for load combination #4: (a) Wall S, and (b) Wall H

4.8 Conclusions

In this study, FE-based reliability analysis for reinforced masonry walls loaded out-of-plane is presented. The reliability assessment is conducted considering two representative walls with different slenderness ratios (e.g., *h/t*=16,42) employing global and two local failure criteria (i.e., section failure and fibre failure). In addition, the effect of the model error on the reliability assessment is investigated. Based on the findings of the conducted analysis, the following conclusions can be drawn:

- The reliability indices (β) were proven to be very sensitive to the modelling error. Accordingly, incorporating the modelling error in the reliability analysis is essential.
- Other factors were found to affect the reliability assessment, such as the load eccentricity to thickness ratio and the slenderness ratio. Specifically, the walls loaded with relatively low load eccentricities (e.g., $^{e_n}/_t = 0.1$) were found to be associated with higher reliability indices compared to those loaded with higher eccentricities (e.g., $^{e_n}/_t = 0.5$). In addition, for the walls loaded with $^{e_n}/_t = 0.5$, highly slender walls were associated

with lower reliability indices compared to other walls with lower slenderness ratios. The same pattern was noticed for walls loaded in vertical eccentric compression or lateral wind loads.

- The reliability assessment is affected by the adopted failure criteria. For instance, adopting the fibre failure criteria generally produced more conservative results for the wall with (h/t=16) compared to the global failure criteria. On the contrary, the local failure criteria resulted were less conservative for the highly slender wall (i.e., h/t=42) compared to the global failure criteria.

4.9 References

ACI-SEASC Task Committee on Slender Walls. (1982). Test report on slender walls. Los Angeles, California.

Au, S. K., Ching, J., & Beck, J. L. (2007). Application of subset simulation methods to reliability benchmark problems. Structural Safety, 29(3), 183-193. doi:10.1016/j.strusafe.2006.07.008

Bartlett, F., Hong, H., & Zhou, W. (2003). "Load Factor Calibration for the Proposed 2005 Edition of the National Building Code of Canada: Statistics of Loads & Load Effects." Canadian Journal of Civil Engineering, 30(2), 429-439.

Barbato, M., Zona, A., & Conte, J. P. (2014). Probabilistic nonlinear response analysis of steel-concrete composite beams. Journal of Structural Engineering, 140(1), 4013034. doi:10.1061/(ASCE)ST.1943-541X.0000803

Bilotta, M. and Cruz, Y. (2021). Evaluation of Second-order Effects in Slender Reinforced Masonry Walls. Proc., 14th Canadian Masonry Symposium, Montreal, QC, Canada.

Bhattacharyya, B. (2021). Uncertainty quantification and reliability analysis by an adaptive sparse bayesian inference based PCE model Springer Science and Business Media LLC. doi:10.1007/s00366-021-01291-0

CSA S304 (2014) Design of Masonry Structures. Canadian Standards Association, Mississauga, Canada.

CSA S408 (2011) Guidelines for the development of limit states design. Canadian Standards Association, Ontario, Canada

Das, S., Tesfamariam, S., Chen, Y., Qian, Z., Tan, P., & Zhou, F. (2020). Reliability-based optimization of nonlinear energy sink with negative stiffness and sliding friction. Journal of Sound and Vibration, 485, 115560. doi:10.1016/j.jsv.2020.115560

Dubourg, V., Sudret, B., & Deheeger, F. (2013). Metamodel-based importance sampling for structural reliability analysis. Probabilistic Engineering Mechanics, 33, 47-57. doi:10.1016/j.probengmech.2013.02.002

Drysdale, R. G. and Hamid, A. A. (2005). Masonry Structures Behaviour and Design, Canada Masonry Design Centre, Mississauga, ON, Canada

Ellingwood B, Galambos TV, MacGregor JG, Cornell CA (1980). Development of a probability based load criterion for American national standard A58, National Bureau of Standards Special Publication 577, U.S. Government Printing Office, Washington, DC.

Ellingwood, B.M. & Tallin, A.A. (1985). Limit States Criteria for Masonry Construction, Journal of Structural Engineering, 111: 108

Frangopol, D. M., Ide, Y., Spacone, E., & Iwaki, I. (1996). A new look at reliability of reinforced concrete columns. Structural Safety, 18(2), 123-150. doi:10.1016/0167-4730(96)00015-X

Ghanem, R. G., & Spanos, P. D. (1991). Stochastic finite elements: A spectral approach. New York: Springer-Verlag.

Grubišić, M., Ivošević, J., & Grubišić, A. (2019). Reliability analysis of reinforced concrete frame by finite element method with implicit limit state functions. Buildings (Basel), *9*(5), 119. doi:10.3390/buildings9050119

Hatzinikolas, M., Longworth, J., and Warwaruk, J. 1978a. Concrete Masonry Walls. University of Alberta - Structural Engineering Report No. 70. Department of Civil and Environmental Engineering, University of Alberta. Edmonton, AB.

Holický, M., Retief, J. V., & Sýkora, M. (2016). Assessment of model uncertainties for structural resistance. Probabilistic Engineering Mechanics, 45, 188-197. doi:10.1016/j.probengmech.2015.09.008

Isfeld, A. C., Müller, A. L., Hagel, M., & Shrive, N. G. (2019). Analysis of safety of slender concrete masonry walls in relation to CSA S304-14. Canadian Journal of Civil Engineering, 46(5), 424-438. doi:10.1139/cjce-2018-0210

Jiang, Y., Peng, S., Beer, M., Wang, L., & Zhang, J. (2020). Reliability evaluation of reinforced concrete columns designed by eurocode for wind-dominated combination considering random loads eccentricity. Advances in Structural Engineering, 23(1), 146-159. doi:10.1177/1369433219866089

Leifsson, L., Du, X., & Koziel, S. (2020). Efficient yield estimation of multiband patch antennas by polynomial chaos ‐ based kriging. International Journal of Numerical Modelling, 33(6), n/a. doi:10.1002/jnm.2722

Li, X., Gong, C., Gu, L., Gao, W., Jing, Z., & Su, H. (2018). A sequential surrogate method for reliability analysis based on radial basis function. Structural Safety, 73, 42-53. doi:10.1016/j.strusafe.2018.02.005

Lourenço PB. (1996) Computational strategies for masonry structures [PhD thesis]. Delft University of Technology.

Marelli, S., & Sudret, B. (2018). An active-learning algorithm that combines sparse polynomial chaos expansions and bootstrap for structural reliability analysis. Structural Safety, 75, 67-74. doi:10.1016/j.strusafe.2018.06.003

Metwally, Z. and Li, Y. (2021). Finite Element-based Probabilistic Behavior Analysis of Slender Reinforcement Masonry Walls Under Out-of-plane Loading. Proc., 14th Canadian Masonry Symposium, Montreal, QC, Canada.

Milner, J., David M, Spacone, E., & Frangopol, D. M. (2001). New light on performance of short and slender reinforced concrete columns under random loads. Engineering Structures, 23(2), 147-157. doi:10.1016/S0141-0296(00)00036-5

Mirza S, Hatzinikolas M, MacGregor J. (1979). Statistical descriptions of the strength of concrete. Journal of Structural Engineering,105(ST6):1021–37.

Mirza, S. A. (1996). Reliability-based design of reinforced concrete columns. Structural Safety, 18(2), 179-194. doi:10.1016/0167-4730(96)00010-0

Mohsin, E. 2005. Support Stiffness Effect on Tall Load Bearing Masonry Walls. Ph.D. thesis, Department of Civil and Environmental Engineering, University of Alberta, Edmonton, AB.

MOOSAVI, H., & KORANY, Y. (2014). Assessment of the structural reliability of loadbearing concrete masonry designed to the Canadian standard S304.1. Canadian Journal of Civil Engineering, 41(12), 1046-1053. doi:10.1139/cjce-2013-0498

Moosavi H. (2017). *S*tructural reliability of non-slender loadbearing concrete masonry members under concentric and eccentric loads. PhD thesis, Department of Civil and Environmental Engineering, University of Alberta, Edmonton, AB.

Pettit, C. (2020). Effect of Rotational Base Stiffness on the Behaviour of Loadbearing Masonry Walls. M.Sc. thesis, Department of Civil and Environmental Engineering, University of Alberta, Edmonton, AB

Priestley, M. J. N., and Elder, D. M. (1983). Stress–strain curves for unconfined and confined concrete masonry. ACI J., 80-3, 192–201

Wang, R., Elwi, A. E., and Hatzinikolas, M. A. (1997). Numerical Study of Tall Masonry Cavity Walls Subjected to Eccentric Loads. Journal of Structural Engineering, Vol. 123, No. 10, pp.1287-1294

Wong, P. S., Veccjio, F. J., and Trommels, H. (2013). VecTor2 & FormWorks User's Manual. Department of Civil Engineering, University of Toronto, second edition.

Schöbi, R., Sudret, B., & Marelli, S. (2017). Rare event estimation using polynomial-chaos kriging. ASCE-ASME Journal of Risk and Uncertainty in Engineering Systems. Part A, Civil Engineering, 3(2) doi:10.1061/AJRUA6.0000870

Schobi, R., Sudret, B., & Wiart, J. (2015). Polynomial-chaos-based kriging. International Journal for Uncertainty Quantification, 5(2), 171-193. doi:10.1615/Int.J.UncertaintyQuantification.2015012467

Shi, Y., Lu, Z., He, R., Zhou, Y., & Chen, S. (2020). A novel learning function based on kriging for reliability analysis. Reliability Engineering &amp, System Safety, 198, 106857. doi:10.1016/j.ress.2020.106857

Stewart MG, Lawrence SJ. (2007). Model error, structure reliability and partial safety factors for structural masonry in compression. Masonry International, 20(3):107–16.

Su, G., Peng, L., & Hu, L. (2017). A gaussian process-based dynamic surrogate model for complex engineering structural reliability analysis. Structural Safety, 68, 97-109. doi:10.1016/j.strusafe.2017.06.003

Suwalski, P.D. (1986). Capacity of eccentrically loaded slender concrete block walls. M.Sc. thesis, Department of Civil Engineering, McMaster University, Hamilton, Ont.

Tee, K. F., Khan, L. R., & Li, H. (2014). Application of subset simulation in reliability estimation of underground pipelines. Reliability Engineering &amp, System Safety, 130, 125-131. doi:10.1016/j.ress.2014.05.006

Turkstra, C. & Ojinaga, J. (1980). Towards a Canadian Limit States Masonry Design Code. In Proceedings of the 2nd Canadian Masonry Symposium, Carleton University, Ottawa, Ontario, Canada.

Yokel, F.Y., Mathey, R.G., and Dikkers, R.D. (1970). Compressive strength of slender concrete masonry walls. Building Science Series 33, U.S. National Bureau of Standards, Washington, D.C.

Yu, Z., Sun, Z., Cao, R., Wang, J., & Yan, Y. (2020). RCA-PCK: A new structural reliability analysis method based on PC-kriging and radial centralized adaptive sampling strategy. Proceedings of the Institution of Mechanical Engineers. Part C, Journal of Mechanical Engineering Science, , 95440622095771. doi:10.1177/0954406220957711

Zhai, X., and Stewart, M. G. (2010). Structural reliability analysis of reinforced grouted concrete block masonry walls in compression. Engineering Structures, 32(1), 106–114.

Zhai, X., Zhong, Z., & Stewart, M. G. (2012). Model error and structural reliability for reinforced concrete block masonry walls in shear. Advances in Structural Engineering, 15(3), 389-398. doi:10.1260/1369-4332.15.3.389

Zuev, K. M., Wu, S., & Beck, J. L. (2015). General network reliability problem and its efficient solution by subset simulation. Probabilistic Engineering Mechanics, 40, 25-35. doi:https://doi.org/10.1016/j.probengmech.2015.02.002

CHAPTER 5: Model Error Assessment of Out-of-plane Load Capacity Models for Reinforced Concrete Masonry Walls in CSA S304-14 and TMS 402-16

This paper investigated the model error associated with out-of-plane capacity models for reinforced concrete masonry walls in the well-known North American provisions, namely, CSA S304-14 and TMS 402-16. Finite element (FE) models together with experimental data are utilized to quantify the model error and develop corrected models using non-parametric probabilistic regression models. The developed regression model is used to (1) investigate the sensitivity of the model error associated with design codes to the variations of different design parameters and (2) provide the corrected model for the considered codes, which can be used in different subsequent analyses (e.g., reliability analysis). It is found that CSA S304-14 is overly biased in different cases, especially for highly slender walls loaded. Whereas TMS 402-16 is found to be generally more consistent and associated with less bias, except for highly slender walls loaded with high reinforcement ratios and relatively high load eccentricities. In addition, the reliability assessment results computed based on the original design code-based models (i.e., without correction) are found to be severely biased and unconservative compared to the ones computed based on the corrected models.

5.1 Introduction

Theoretical models, which are typically established with simplifications and assumptions, are associated with a corresponding model error (Mathews and Vial 2017). This can be most pronounced for capacity models in design codes in the field of civil engineering

In the context of masonry structures, current masonry design standards in North America, such as CSA S304-14 (CSA 2014) TMS 402-16 (TMS 2016), have been examined by other

researchers aiming to investigate the conservatism of the design provisions arising from the inaccuracy in the design code models. For instance, Isfeld et al. (2019) investigated the conservatism of CSA S304-14 in determining the out-of-plane capacity of unreinforced and reinforced masonry walls using a broad set of available experimental data. The findings of the mentioned study indicated the need for re-examination of CSA S304-14 provisions for slender walls because of the undue conservatism. This is consistent with other findings in the literature. For example, Mohsin (2005) recommended re-investigating CSA S304-04, especially the effect of support stiffness for masonry walls, because neglecting the restraining effect of realistic boundary conditions can lead to significant under-prediction of the out-of-plane capacity for highly slender walls. Dawe and Liu (2003) also showed that CSA S304-94 significantly underestimated the effective flexural rigidity (EI_{eff}), leading to an overly conservative design. Similar findings were reported in Pettit et al. (2021) and Bilotta and Cruz (2021) for CSA S304-14 and TMS 402-16. To be specific, Pettit et al. (2021) concluded that TMS 402-16 tends to underestimate effective flexural rigidity (EI_{eff}), especially for cases when the applied moment exceeds the cracking moment. Bilotta and Cruz (2021) evaluated the moment magnifier method (MM) adopted by the considered design provisions (i.e., CSA S304-14 and TMS 402-16) to account for the second-order effects. This study showed that the CSA S304-14 is overly conservative compared to other analytical and numerical models. On the contrary, TMS 402-16 is significantly unconservative for walls with low compressive strengths (f_m) and high reinforcement ratios (ρ_s).

As such, it is essential to quantify the model error associated with out-of-plane capacity models in the design codes mentioned above (e.g., CSA S304-14, TMS 402-16) to facilitate a more

rigorous and reliable assessment of the design standards using reliability analysis. Ideally, the model error can be quantified using sufficient experimental tests of masonry walls by comparing the experimentally predicted capacity to the corresponding design code model prediction (Zhou and Huang 2012). However, only limited experimental data in the public literature is available, particularly when a systematic error exists in the capacity prediction models in the design provisions. In order to correct the systematic error, namely, the correction of the model error with certain design parameters and quantify the model error probabilistically with limited experimental data, a high-fidelity model can be used. For instance, Jiang et al. (2013) used a high-fidelity FE model to correct a low-fidelity model and assess the remaining error in the corrected model for a car crashing problem in mechanical engineering. Similarly, Li et al. (2019) quantified the error of an analytical model for dented pipelines using a high-fidelity FE model. In these works, high-fidelity models are used to generate reference data without considering model error due to the high accuracy of FE models.

A similar approach can be taken to correct the masonry design code models and quantity of the remaining model error. Various FE models have been developed for masonry walls subjected to out-of-plane loading, such as those using the micro FE modelling approach and the macro FE modelling approach. The micro FE modelling approach explicitly accounts for the heterogeneous nature of masonry, which allows capturing complex failure mechanisms but is computationally expensive. Alternatively, the macro FE modelling approach provides a simpler and more efficient solution when the out-of-plane capacity of masonry walls is of interest (Lourenco 1996). For example, the fibre-section-based beam approach, which allows using the stress-strain characteristics of masonry as employed in the current design codes, is widely used for masonry

walls (Ganduscio and Romano 1997). Among these models, although more accurate than design code models, no one is error-free due to the embedded complexity in masonry walls with heterogeneous materials. In order to use FE models with higher fidelity (e.g., efficient beam models) to quantify the error in design code models, the error in FE models needs to be taken into account. To this end, a probabilistic FE-based capacity model is first developed using experimental data available and used to generate reference data after considering model error. The generated reference data can be used to learn the relationship between the model error and different design parameters using regression models (e.g., Gaussian process regression).

To summarize, this paper aims to evaluate the model error associated with the OOP load capacity models in the current North American standards (CSA S304-14; TMS 402-16) using a combination of experimental and numerical simulations. The relationship between the model error and different designed parameters (e.g., load eccentricity, slenderness ratio, masonry compressive strength and reinforcement ratio) is modelled using a non-parametric Gaussian process regression model. Hence, the sensitivity of the model error associated with design code-based models to the variations of the design parameters is investigated. In addition, the corrected models of the code-based design models are provided. Finally, the original (i.e., without model correction) and the corrected models for the design codes are used to assess the reliability of different representative masonry walls to investigate the effect of the accuracy of the prediction model on the reliability assessment.

5.2 Comparison of Model Predictions with Experimental database

5.2.1 Design code-based capacity models

The current masonry design provisions in North America (CSA S304-14; TMS 402-16) adopt a similar design procedure for masonry walls against out-of-plane loading. To account for second-order effects due to geometric nonlinearity, both North American masonry codes recommend the use of the moment magnifier method (MM), in which the maximum moment demand without considering second-order effect, i.e., the applied primary moment (M_p), is magnified by a factor (ψ) and compared with the section capacity characterized by the section P-M interaction diagram (P, M_u). Equivalently, the load capacity of the wall can be determined by the modified P-M interaction diagram (P, M_p). For a given axial load (P), the wall capacity is determined when the combination of the axial load P and the corresponding magnified moment ψM_p is equal to the total magnified moment M_u on the section P-M interaction diagram. The moment magnifier factor is defined in Eq. 5-1.

$$\psi = \frac{C_m}{1 - \frac{P}{P_{cr}}} \quad \text{, in which } P_{cr} = \frac{\pi^2 EI_{eff}}{(kh)^2} \qquad (5-1)$$

Here, C_m is the moment diagram factor, P is the axial load acting on the wall, P_{cr} is Euler buckling load of the wall, EI_{eff} is the effective flexural rigidity, k is the effective length coefficient depending on the boundary conditions (e.g., k = 1.0 for simply supported), and h is the clear unsupported wall length.

In spite of the great similarity of the two code-based capacity models for reinforced masonry walls against OOP loading, there exist slight differences in the derivation of both the cross-

section P-M interaction diagram and the moment magnifier factor. Figure 5-1 summarizes schematically the procedure to determine OOP capacity characterized by (P, M_p), which mainly consists of two steps: (1) the derivation of the section P-M interaction diagram and (2) the moment capacity reduction using moment magnifier method.

In the derivation of section P-M interaction diagram, the normal stress distribution over the cross-section is determined based on a linear strain distribution and the compressive stress block assumption together with several characteristic material strength properties (e.g., the compressive strength f'_m for masonry and the yield strength f_y for steel bars). The linear strain distribution can be fully defined for an assumed neutral axis location (c) and the prescribed maximum usable compressive strain (ε_u) for masonry, which is taken as 0.003 and 0.0025 for CSA S304-14 and TMS 402-16, respectively. The compressive stress distribution is represented approximately by an equivalent stress block with a depth of (βc) and a uniform stress magnitude of ($\alpha f'_m$). The factor (β) is taken as 0.80 for both design codes, while the factor α is taken as 0.85 for CSA S304-14 and 0.80 for TMS 402-16, respectively. Together with the geometric properties of the cross-section (e.g., wall width b, wall thickness t, reinforcement bars location d and reinforcement bars area A_s), the compressive force resultant (C) and tensile force resultant (T) acting on the cross-section can be determined, and thus unknown c can be determined iteratively so that the applied axial load (P) can be in axial force equilibrium with T and C. To this end, the moment resistance (M_r) corresponding to the applied axial load P can be obtained through moment equilibrium of the cross-section. When the aforementioned procedure is repeated for different values of P, the section P-M interaction diagram can be constructed. Afterwards, the global properties of the wall (e.g., slenderness ratio, boundary condition and

loading) are considered to quantify the second-order effects and determine the OOP capacity using the previously introduced moment magnifier method (MM).

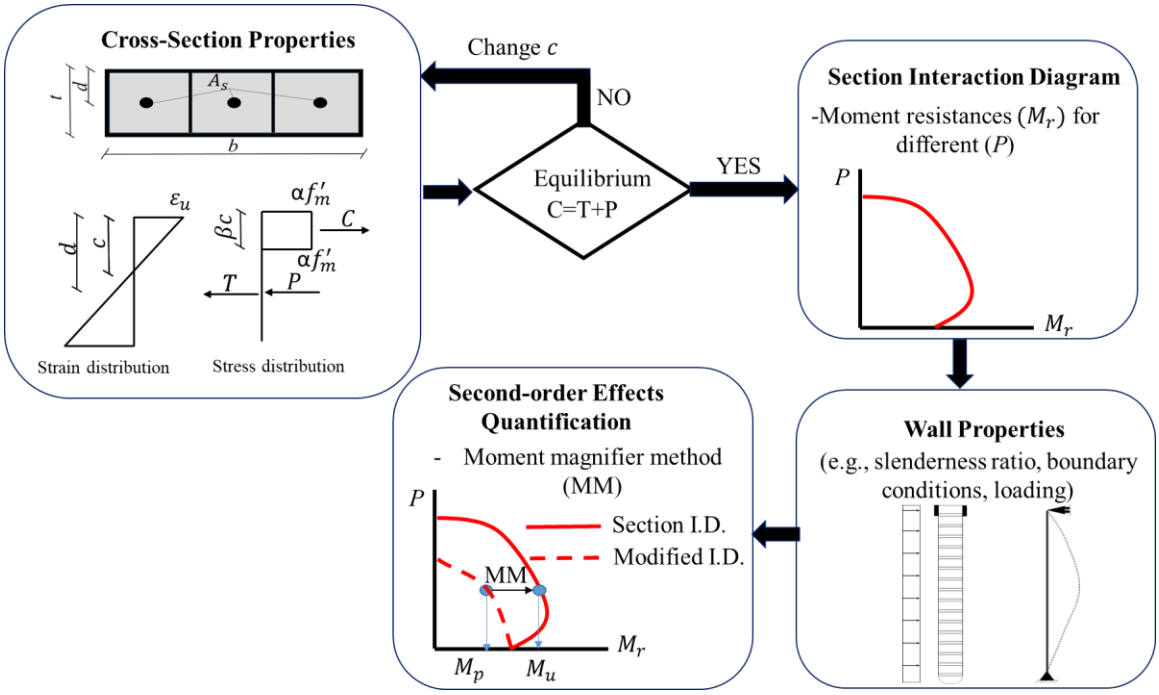

Figure 5-1 Schematic procedure used to determine the OOP capacity of reinforced concrete masonry walls according to CSA S304-14 and TMS 402-16

Although the two considered codes adopt the moment magnifier method to account for second-order effects, their approach in determining the effective flexural rigidity (EI_{eff}), which depends on the cracked characteristics of the walls (e.g., the cracked moment of inertia I_{cr}) is different. which depends on the cracked characteristics of the walls, including the cracked moment of inertia (I_{cr}). Specifically, CSA S304-14 neglects the effect of the axial load when calculating I_{cr}. In that sense, I_{cr} depends on the cross-section properties only. This is not the case for TMS 402-16 as it considers the effect of the applied axial load when calculating I_{cr}. On the other hand, TMS 402-16 conservatively neglects the variation of the stiffness by utilizing the cracked

moment inertia I_{cr} along the wall height when the applied moment (M_p) exceeds the cracking moment (M_{cr}), which can produce very conservative estimations for the (EI_{eff}) (Pettit et al. 2021). The cracked moment of inertia (I_{cr}) and the effective flexural rigidity (EI_{eff}) for CSA S304-14 and TMS 402-16 are calculated as follows:

$$I_{cr}(CSA\ S304) = \frac{bc^3}{3} + nA_s(d-c)^2 \qquad (5-2)$$

$$EI_{eff}(CSA\ S304) = E_m I_{cr} \leq E_m \left[0.25I_o - (0.25I_o - I_{cr})\left(\frac{e-e_k}{2e_k}\right)\right] \leq 0.25E_m I_o \qquad (5-3)$$

$$I_{cr}(TMS\ 402) = \frac{bc^3}{3} + n\left(A_s + \frac{P}{f_y}\right)(d-c)^2 \qquad (5-4)$$

$$EI_{eff}(TMS\ 402) = \begin{cases} 0.75E_m I_o & M_p < M_{cr} \\ E_m I_{cr} & M_p \geq M_{cr} \end{cases} \qquad (5-5)$$

In the formulas above, E_m is the masonry modulus of elasticity, n is the ratio between the modulus of elasticity for masonry and reinforcement steel. e is the eccentricity which is defined as the ratio between M_p and P, e_k is the kern eccentricity which is defined between the ratio between the section modulus S_e and the effective mortared area A_e, A_s is the area of the steel reinforcement, I_o is the gross moment of inertia and M_{cr} is the cracking moment.

To examine the error associated with the aforementioned OOP capacity models for masonry walls as specified in CSA S304-14 and TMS 402-16, an experimental database including 69 reinforced masonry walls subjected to OOP loading (i.e., eccentric axial compression and lateral loading) is compiled from five testing programs in the literature (Yokel et al. 1970, Hatzinkolas et al. 1978, ACI-SEASC 1982, Suwalski 1986, Mohsin 2005). The experimental peak load

capacities are compared against the corresponding predictions using the design code-based models after excluding any design bias (e.g., load or resistance factors), as shown in Figure 5-2. Note that the capacities are measured by the maximum axial load for eccentrically axially loaded walls and the maximum lateral load pressure (normalized by the wall area with a scale factor of 10 for plotting) for laterally loaded walls, respectively. The comparison shows that both design code-based models are associated with noticeable underestimation. The models are generally conservative for design purposes but not acceptable for the reliability assessment of masonry walls.

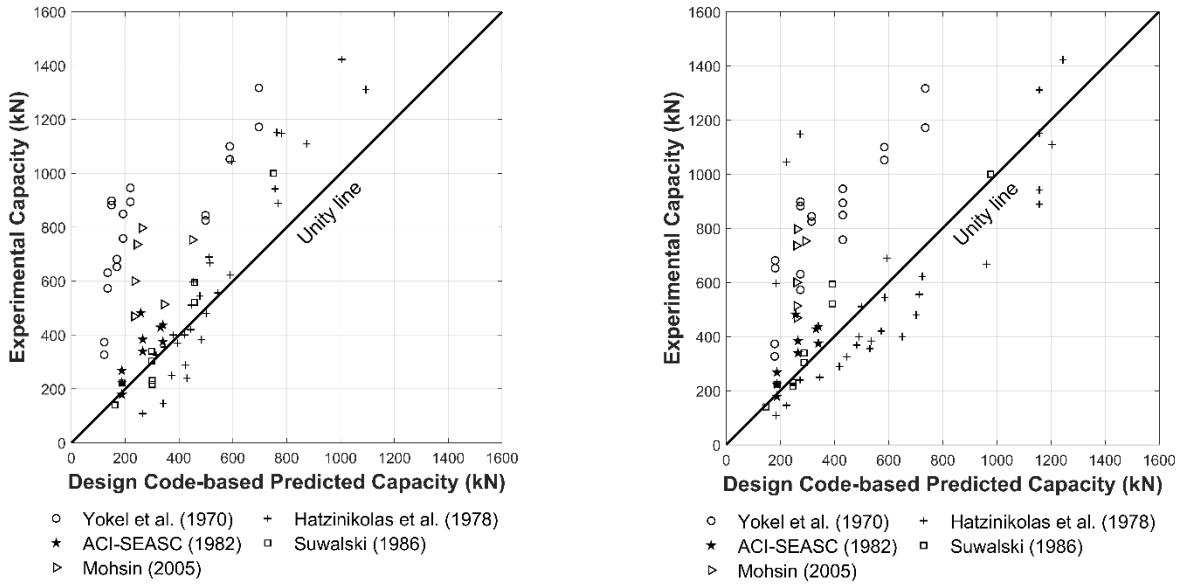

Figure 5-2 Comparison of the experimental and design code-predicted capacities for reinforced concrete masonry walls considered: (a) CSA S304-14, and (b) TMS 402-16

Further investigation shows that the error associated with the considered design codes (i.e., CSA S304-14 and TMS 402-16) is not random (i.e., not free of systematic error) because the errors for both codes are strongly correlated to design parameters, for example, the slenderness ratio (*h/t*)

and the load eccentricity to thickness ratio (*e/t*) of masonry walls. Specifically, both codes are shown to be more conservative for walls with an increasing slenderness ratio (*h/t*) and a decreasing load eccentricity to thickness ratio (*e/t*), as shown in Figure 5-3 and Figure 5-4, respectively. Accordingly, the model errors associated with the code-based models cannot be modelled using the traditional professional factor approach, where the random error is assumed to be independent of the wall and loading properties. Instead, the model should be corrected such that the trend of the model error is independent of the wall and loading properties and thus consistent for all design scenarios.

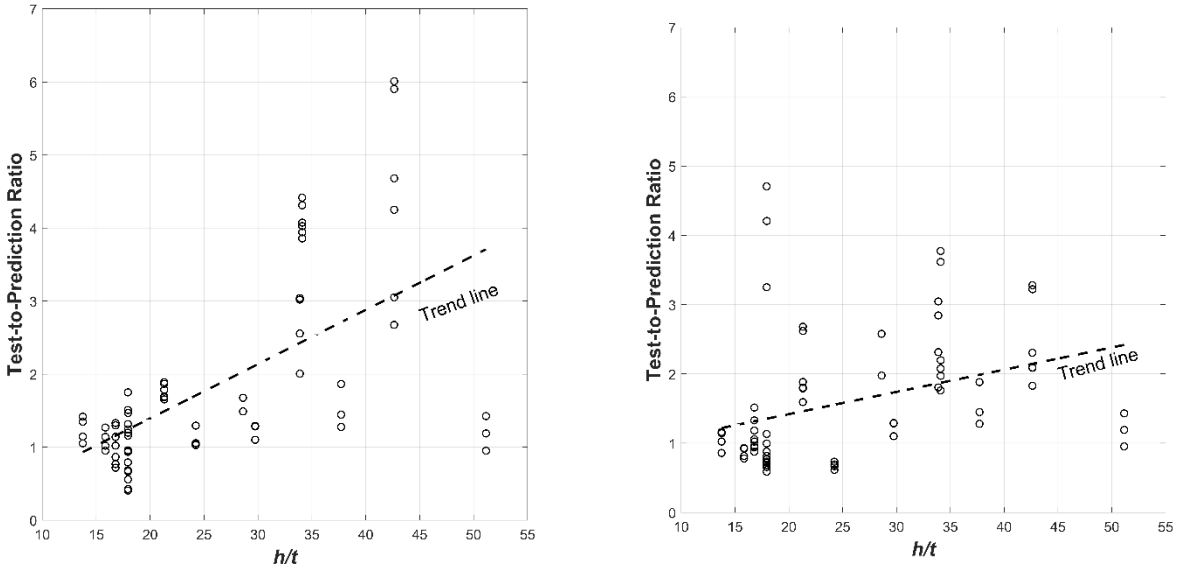

Figure 5-3 The test-to-prediction ratio for OOP capacities of masonry walls tested in the literature with respect to the slenderness ratio *h*/*t*: (a) CSA S304-14, and (b) TMS 402-16

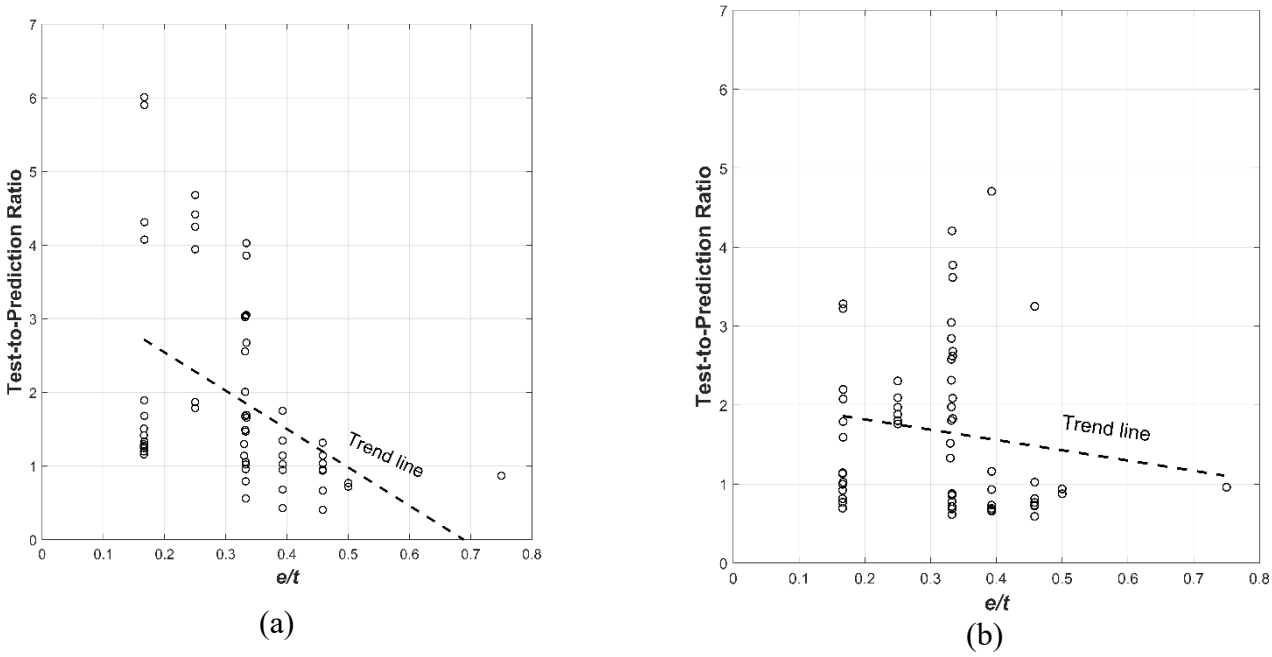

Figure 5-4 The ratio between the Experimental and code-based predicted capacities with respect to the load eccentricity to thickness ratio (a) CSA S304-14, (b) TMS 402-16

5.2.2 Finite element-based capacity model

The mechanics-based FE models are considered to be a more accurate alternative for predicting load capacities of masonry walls compared to the design code-based models. Accordingly, the macro FE modelling approach using fibre-based beam elements in *OpenSees* is adopted herein to predict the OOP capacities of those tested walls considered above. In FE models, geometric nonlinearity is taken into account rigorously. The configuration and the schematic view of the FE model used for simply supported walls loaded in eccentric compression are shown in Figure 5-5. In the model, the eccentric loading is applied through a rigid beam with a length equal to the load eccentricity (e). The walls are modelled using displacement-based fibre beam elements, each with 5 Gaussian-Legendre integration points. Each integration point is assigned with a generalized fibre section consisting of masonry and steel fibres. The behaviour of each fibre is modelled by a uniaxial material model that represents the uniaxial stress-strain behaviour of

masonry or steel. In the material model adopted for masonry (i.e., *Concrete02* as shown in Figure 5-5), f_m and ε_0 represent the tested masonry compressive strength and the corresponding strain for the wall considered. In contrast, the masonry tensile strength f_t, the masonry residual compressive strength f_{mu} and the corresponding strain ε_u, as well as the ultimate tensile strain ε_{tu}, are determined based on literature findings when tested values are missing. Specifically, f_t is taken 0.5 MPa according to Drysdale and Hamid (2005); f_{mu} and ε_u are determine based on the models proposed in (Pritsley and Elder 1983) for homogenous masonry, whereas ε_{tu} is taken as 0.004 (Wang et al. 1997). On the other hand, *Steel01* is used to model steel fibres and the parameters f_y, E and b which represent the yield strength of steel reinforcement, the Young's modulus and the strain hardening ratio, respectively, are determined according to the experimental tests.

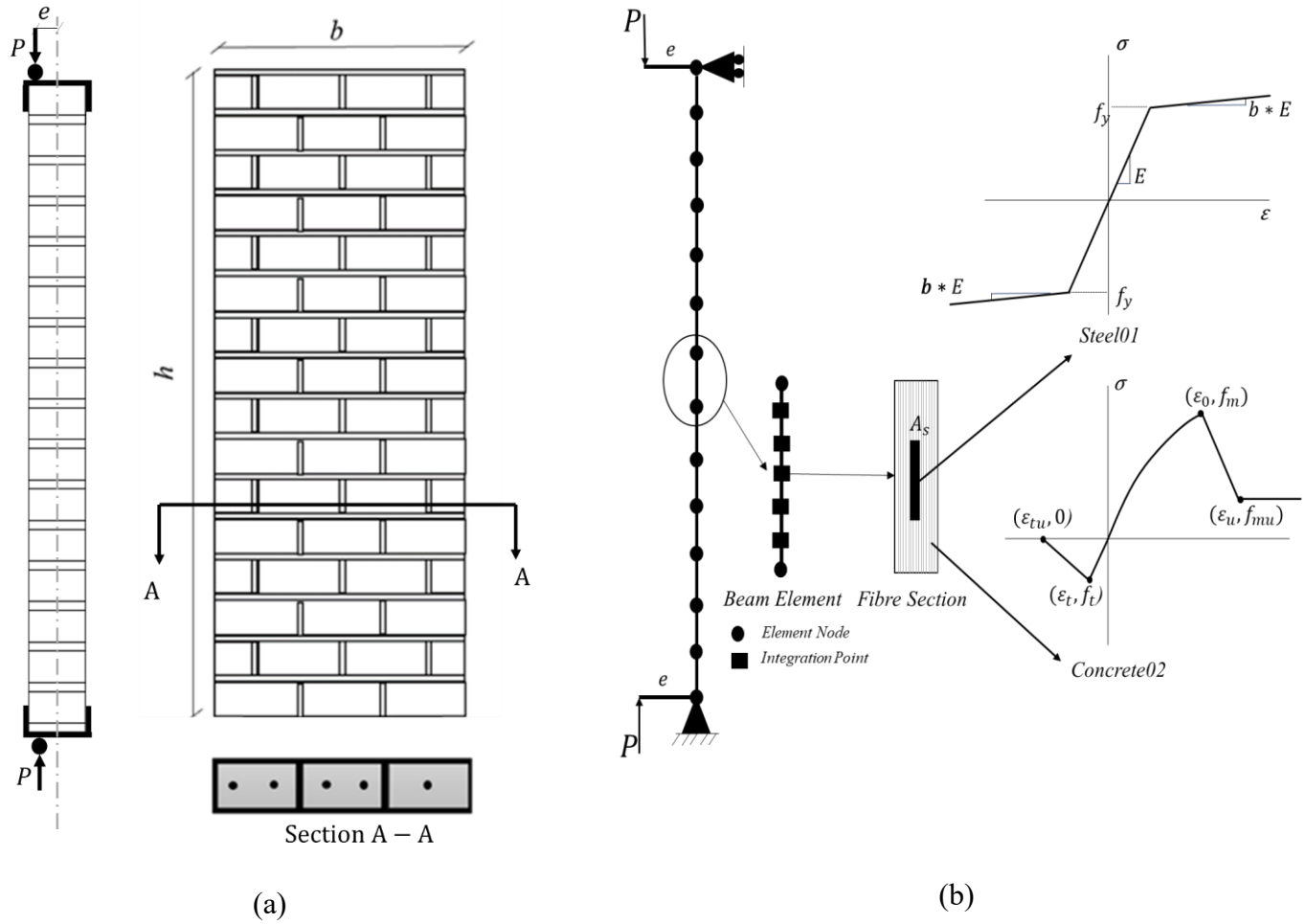

Figure 5-5 Simply supported masonry walls subjected to eccentric loads *P* with an eccentricity *e* (a) wall configuration, and (b) schematic view of the FE model

The accuracy of the introduced FE model for load capacity prediction is examined using the same experimental database previously used to examine the accuracy of the design code-base models. The comparison between the experimental and FE-predicted capacities, as shown in Figure 5-6, indicates that the FE model predicts the experimental capacities with a reasonable level of accuracy without severe bias.

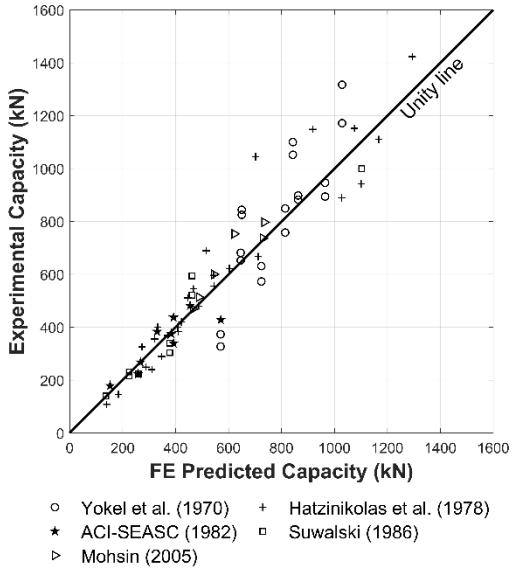

Figure 5-6 Comparison of the experimental and FE-predicted capacities for reinforced concrete masonry walls tested in the literature

The correlation between the FE-prediction error (indicated by the test-to-prediction ratio) and the design parameters (e.g., slenderness ratio h/t, eccentricity to thickness ratio e/t) is shown in Figure 5-7. It is shown that FE-prediction error is not sensitive to the variation of the aforementioned design parameters, especially when compared to the design code-based models. This can be evidenced by the trend line of the FE-prediction, which is in contrast with the trend lines of design code-based predictions (i.e., CSA S304-14 and TMS 402-16). In that sense, the FE-prediction error is considered to be independent of the design parameters. To this end, the modelling error (ME) associated with the FE model can be quantified using the test-to-prediction ratio, which can be modelled by a random variable ME independent of the design variables. It is found that ME follows a normal distribution with a mean of $\mu_{ME} = 1.02$ and coefficient of variation $COV_{ME} = 0.17$ (see Figure 5-8).

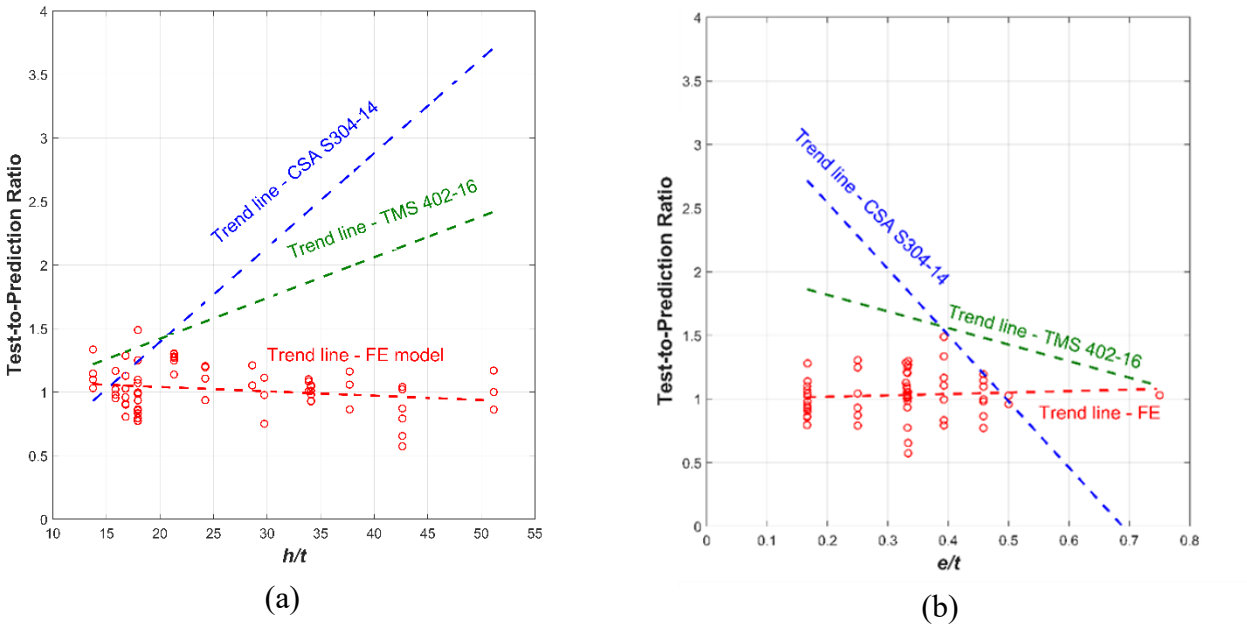

Figure 5-7 The test-to-prediction between the experimental and FE-based predicted capacities with respect to (a) slenderness ratio *h*/*t*, and (b) eccentricity to thickness ratio *e*/*t*

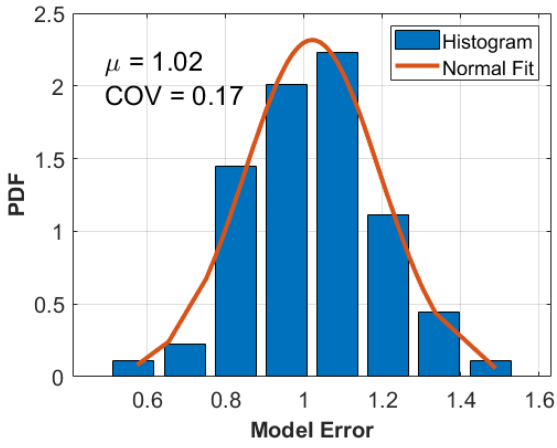

Figure 5-8 Histogram and fitted probability density function (PDF) for the model error distribution

5.3 Problem Statement and Methodology

As illustrated previously, the prediction error in the design code-based models for the load capacity of reinforced concrete masonry walls is strongly correlated to the design parameters

(e.g., slenderness ratio, eccentricity to thickness ratio), while the FE models are not. In that sense, the systematic error in the design code-based models (e.g., CSA S304-14 and TMS 402-16) can be potentially corrected using the data generated based on mechanics-based FE models with higher fidelity. In order to use FE models with higher fidelity (e.g., efficient beam models) to quantify the error in design code models, the error in FE models is taken into account by considering the associated ME. To this end, a probabilistic FE-based capacity model is first developed and can be used to generate reference data. The reference data can be employed to investigate the systematic error trend associated with the design code-based models.

The reference data can be generated by the probabilistic FE-based capacity prediction model, i.e., by applying a random multiplier (ME) to the load capacities obtained from the FE model. In that sense, the corrected load capacities are considered to represent the numerical experiments. To this end, 4000 data points are randomly generated by considering a wide range of values for each key design parameter (see Table 5-1), which was found to affect the error trend associated with the design code-based models. The four key design parameters include the masonry compressive strength f_m, and the steel reinforcement ratio ρ_s, in addition to the two as illustrated earlier, i.e., the slenderness ratio h/t, the load eccentricity to thickness ratio e/t (Isfeld et al. 2019, Bilotta and Cruz 2021). It should be noted that all the walls simulated are assumed to have a constant block thickness of 190 mm, conforming to the typical values in Canada, and pinned-roller conditions.

Table 5-1 Numerical experimental design of reinforced concrete masonry walls with the four key design parameters and their range considered

Design parameter	*Lower bound*	*Upper bound*
e/t	0.1	2.5
h/t	15	45
f_m	10 MPa	20 MPa
ρ_s	0.0013	0.019

The test-to-prediction ratio (ξ) between the numerical experiments and design code-based models for the OOP load capacities of the 4000 walls simulated can be examined to show its dependence on design parameters (e.g., Figure 5-9 for the eccentricity to thickness ratio *e/t*). A similar trend associated with test-to-prediction ratios (ξ) is captured by the numerical experiments as Figure 5-4 for the physical experiments. Thus, the reference data can be used to learn the systematic error trend as a function of the four key design parameters considered.

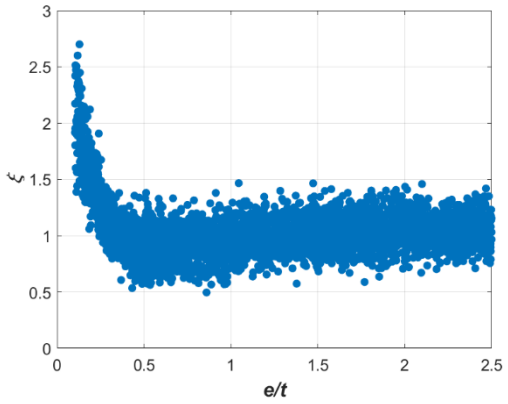

(a)

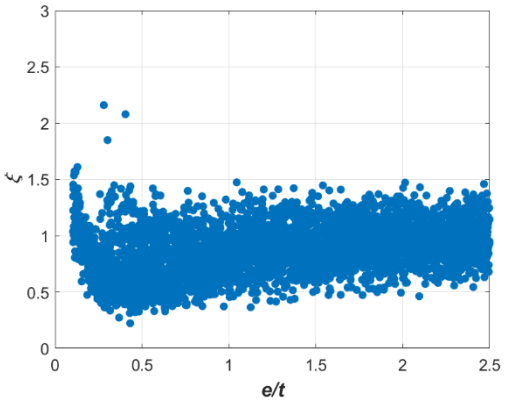

(b)

Figure 5-9 The dependency on *e/t* of the test-to-prediction ratio (ξ) between the numerical experiments and design code-based models: (a) CSA S304-14, and (b) TMS 402-16

To this end, the non-parametric Gaussian process regression (GPR) technique is adopted in this study. The theoretical background behind GPR is briefly summarized here (Sammut and Webb 2017, Su et al. 2017, Jiang et al. 2013, Li et al. 2019).

GPR is a non-parametric method that can be used to build the input/output relationship without assuming a specific function form from the observed data using a Bayesian probabilistic approach. In that sense, the model output prediction $\xi(\boldsymbol{x})$ for an input point, e.g., $\boldsymbol{x} = (h/t, e/t,\ f_m, \rho_s)$, is modelled by a Gaussian process, which is entirely defined by the mean function $m(\boldsymbol{x})$ and the covariance function $c(\boldsymbol{x}, \boldsymbol{x}')$, i.e., $\xi(\boldsymbol{x}) \sim GPR\left(m(\boldsymbol{x}), c(\boldsymbol{x}, \boldsymbol{x}')\right)$. In the Bayesian framework, the data observed in the training dataset can be used to update the prior statistics. The prior for the mean function $m(x)$ can take different forms (e.g., zero, linear, quadratic) to represent the prior information on the trend of the relation between input and output and is typically zero function, $m(x) = 0$ as considered here due to lack of prior knowledge. The best covariance function $c(\boldsymbol{x}, \boldsymbol{x}')$ from several candidates (e.g., exponential, squared exponential, rational quadratic and ARD rational quadratic), as well as the corresponding hyperparameters, are optimized by using the Statistics and Machine Learning Toolbox in MATLAB (Matlab 2019b) in this study.

Accordingly, random variables $\xi(\boldsymbol{x}_1), \xi(\boldsymbol{x}_2), \ldots \xi(\boldsymbol{x}_n)$ at points $\boldsymbol{x}_1, \boldsymbol{x}_2, \ldots, \boldsymbol{x}_n$ follow a jointly normal distribution as follows

$$\begin{bmatrix} \xi(\boldsymbol{x}_1) \\ \vdots \\ \xi(\boldsymbol{x}_n) \end{bmatrix} \sim \boldsymbol{N}\left(\boldsymbol{0},\quad \boldsymbol{C}_{X,X} = \begin{bmatrix} c(\boldsymbol{x}_1, \boldsymbol{x}_1) & \cdots & c(\boldsymbol{x}_1, \boldsymbol{x}_n) \\ \vdots & \ddots & \vdots \\ c(\boldsymbol{x}_n, \boldsymbol{x}_1) & \cdots & c(\boldsymbol{x}_n, \boldsymbol{x}_n) \end{bmatrix}\right) \qquad (5-6)$$

where $\boldsymbol{C_{X,X}}$ is a covariance matrix with $C_{ij} = c(\boldsymbol{x}_i, \boldsymbol{x}_j)$. In order to account for noisy output observations, an independent and normally distributed noise term $\varepsilon_i \sim N(0, \sigma^2_{noise})$, where σ^2_{noise} is the noise variance, can be incorporated. Accordingly, the output observation (y_i) corresponding to the input point ($\boldsymbol{x_i}$) reads:

$$y_i = \xi(\boldsymbol{x}_i) + \varepsilon_i \qquad (5-7)$$

Subsequently, the outputs $\boldsymbol{Y} = (y_1, y_2, \dots, y_n)^T$ at $\boldsymbol{X} = (\boldsymbol{x}_1, \boldsymbol{x}_2, \dots, \boldsymbol{x}_n)$ in the training dataset (reference data) follows a joint Gaussian (normal) distribution, i.e., $\boldsymbol{Y}|\boldsymbol{X} \sim N\big(\boldsymbol{0}, \boldsymbol{C_{X,X}} + \sigma^2_{noise}\boldsymbol{I}\big)$, in which $\boldsymbol{I}$ is an identity matrix of dimension $n \times n$.

Similarly, for an unobserved point $\boldsymbol{x}$, the probability distribution of the corresponding observation y can be determined by marginalizing the joint distribution for $\boldsymbol{Y}$ *and* y, i.e., $Y, y|X, y \sim N(0, \boldsymbol{C}_*)$,

where $\boldsymbol{C}_*$ is the covariance matrix as follows:

$$\boldsymbol{C}_* = \begin{bmatrix} \boldsymbol{C}_{X,X} + \sigma^2_{noise}\boldsymbol{I} & \boldsymbol{C}_{X,x} \\ \boldsymbol{C}^T_{X,x} & c(\boldsymbol{x}, \boldsymbol{x}) + \sigma^2_{noise} \end{bmatrix} \qquad (5-8)$$

in which $\boldsymbol{C}_{X,x} = \big(c(\boldsymbol{x}_1, \boldsymbol{x}), c(\boldsymbol{x}_2, \boldsymbol{x}), \dots, c(\boldsymbol{x}_n, \boldsymbol{x})\big)^T$. Accordingly, the conditional predictive distribution for y follows a normal distribution, $y \mid x, \mathbf{X}, \mathbf{Y} \sim N(\mu_*(\boldsymbol{x}), \sigma^2_*(\boldsymbol{x}))$,

where μ_* and σ^2_* are the mean and variance function of the posterior process for an unobserved point $\boldsymbol{x}$,

$$\mu_*(\boldsymbol{x}) = \boldsymbol{C}^T_{X,x_*}\big(\boldsymbol{C}_{X,X} + \sigma^2_{noise}\boldsymbol{I}\big)^{-1}\boldsymbol{Y} \qquad (5-8)$$

$$\sigma_*^2(\boldsymbol{x}) = c(x_*, x_*) - c_{X,x_*}^T (C + \sigma_{noise}^2 I)^{-1} c_{X,x_*} + \sigma_{noise}^2 \qquad (5-9)$$

The posterior mean prediction provides the model for the test-to-prediction ratio: $\xi_{GPR}(\boldsymbol{x}) = \mu_*(\boldsymbol{x})$.

5.4 GPR-based Model Correction and Error Quantification

5.4.1 GPR model results

The comparison between the reference modelling error (ξ_{REF}), which is defined as the test-to-prediction ratios for the code-based models, and the corresponding GPR-based predictions (ξ_{GPR}) is provided in Figure 5-10. As observed, the GPR-based predictions (ξ_{GPR}) are in good alignment with the reference modelling error data (ξ_{REF}) as they almost coincide with the unity line.

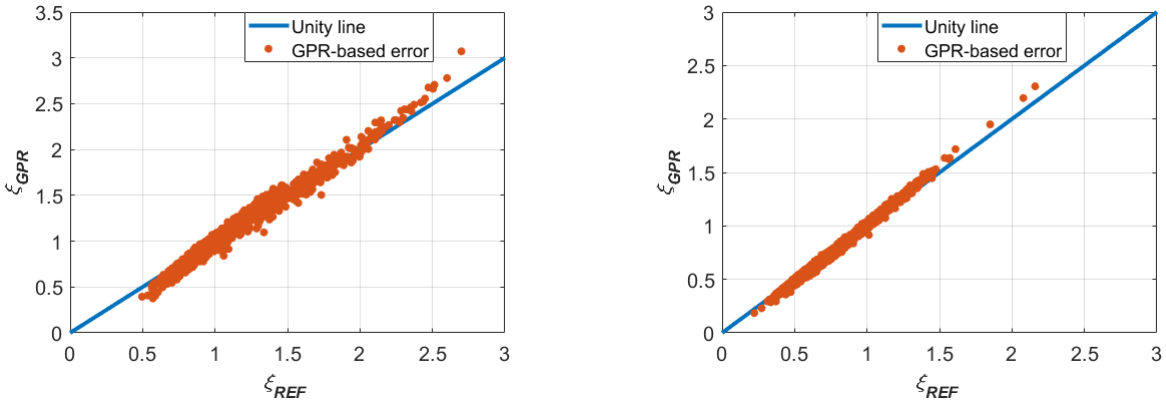

Figure 5-10 Reference ζ versus predicted ζ for (a): CSA S304-14, and (b): TMS 402-16

To this end, the GPR model can be used in two different applications. The first is to investigate the sensitivity of the model error associated with design codes to the variations of the design parameters. Whereas the second one is to provide the corrected model for the considered codes, which can be used in different subsequent analyses (e.g., reliability analysis).

5.4.2 Systematic error in design code-based models

The test-to-prediction ratio models $\xi_{GPR}^{CSA}(\boldsymbol{x})$ *and* $\xi_{GPR}^{TMS}(\boldsymbol{x})$ for the two design codes allow providing more insight into their systematic error as a function of the four key design parameters considered. Among the four key design parameters, the masonry compressive strength (f_m) is found to be the least influential, as shown in Figure 5-11. It can be shown that systematic error correctors ($\xi_{GPR}^{CSA}(\boldsymbol{x})$ *and* $\xi_{GPR}^{TMS}(\boldsymbol{x})$) associated with both design codes (i.e., CSA S304-14 and TMS 402-16) are not sensitive to the variations of f_m.

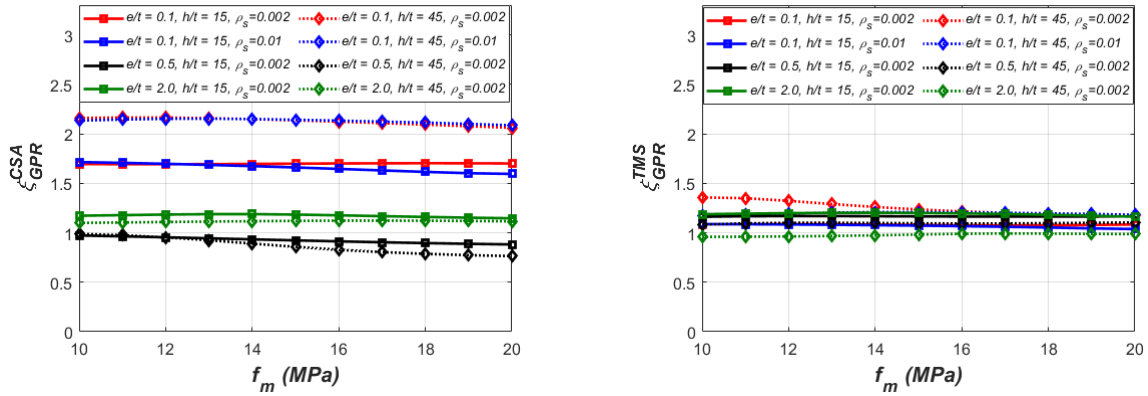

Figure 5-11 GPR-based systematic error corrector versus f_m considering various combinations of (*e/t*, *h/t* and ρ_s): (a) CSA S304-14, and (b) TMS 402-16

Similarly, it is also found that the systematic error associated with CSA S304-14 only slightly depends on the steel reinforcement ratio (ρ_s), see Figure 5-12 (a) for the case with f_m fixed at a value of 15 MPa. The same is observed for TMS 402-16 except for highly slender walls loaded with relatively high load eccentricities (e.g., walls with h/t = 45, e/t = 0.5, 2.0), see Figure 5-12 (b). Specifically, one can notice that systematic error ($\xi_{GPR}^{TMS}(\boldsymbol{x})$) decreases significantly with increasing ρ_s for such walls, leading to more unconservative designs than other walls by TMS 402-16.

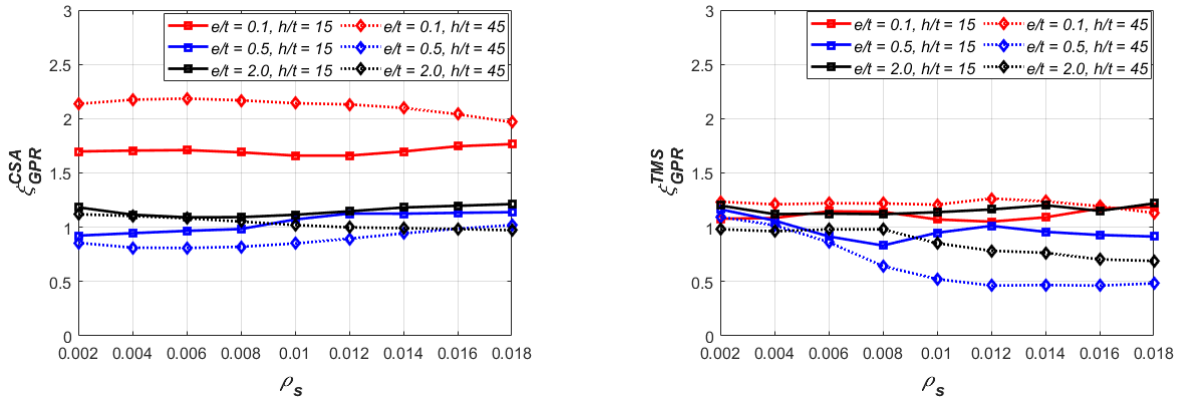

Figure 5-12 GPR-based systematic error corrector versus ρ_s considering various combinations of (*e/t*, *h/t*) with f_m = 15 MPa: (a) CSA S304-14, and (b) TMS 402-16

Figure 5-13 and Figure 5-14 show how GPR-based systematic error correctors for CSA S304-14 and TMS 402-16 vary with respect to the load eccentricity to thickness ratio (*e/t*) and the slenderness ratio (*h/t*). it is observed that the systematic error associated with CSA S304-14 is significantly influenced by the eccentricity to thickness ratio (*e/t*). It can be seen that CSA S304-14 is much more conservative for walls with low eccentricity to thickness ratios, particularly when the slenderness ratio is large, see Figure 5-14 (a). On the contrary, CSA S304-14 is shown to be unconservative (i.e., ξ <1) for walls loaded with other eccentricity ratios (e.g., $0.5 \leq e/t \leq 1.0$). In contrast, the systematic error associated with TMS 402-16 is less dependent on the load eccentricity to thickness ratio (*e/t*) and the slenderness ratio (*h/t*) when compared to CSA S304-14. Overall, TMS 402-16 has a less systematic error, i.e., the bias is more consistent for different walls, except the highly slender walls loaded with high reinforcement ratios and relatively high load eccentricities.

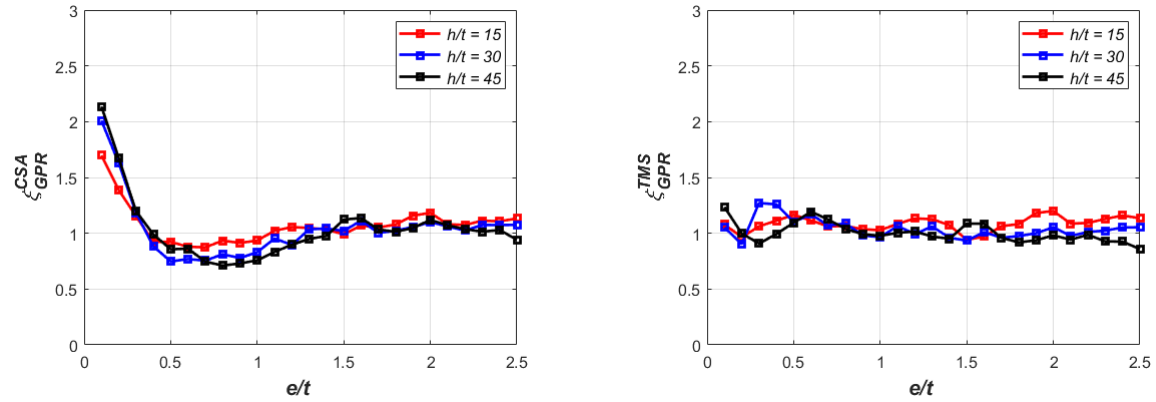

Figure 5-13 GPR-based systematic error corrector versus *e/t* considering different values of *h/t* with f_m = 15 MPa and ρ_s = 0.002: (a) CSA S304-14, and (b) TMS 402-16

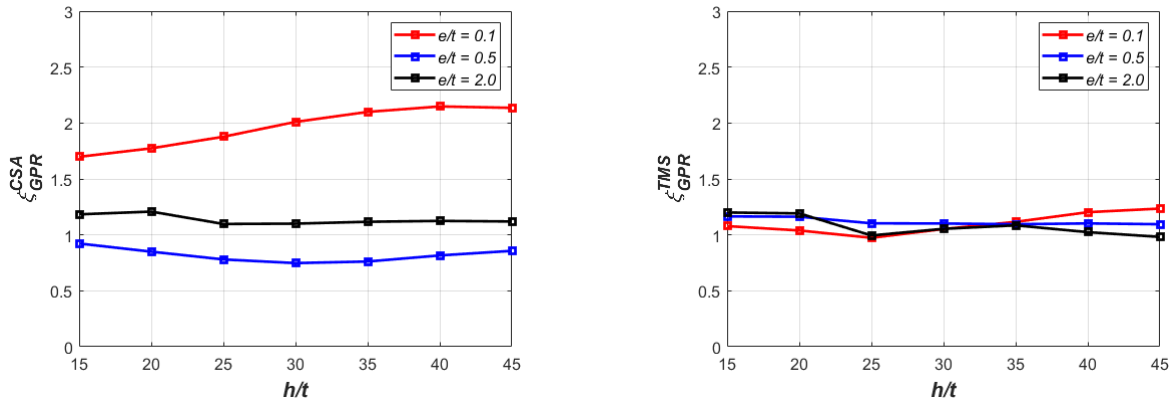

Figure 5-14 GPR-based systematic error corrector versus *h/t* considering different values of *e/t* with f_m = 15 MPa and ρ_s = 0.002: (a) CSA S304-14, and (b) TMS 402-16

5.4.3 Corrected model

The developed GPR model provides systematic error corrector (ζ) associated with the design code models (i.e., CSA S304-14 and TMS 402-16) for a given wall with certain design parameters (e.g., *e/t, h/t,* f_m *and* ρ_s). Based on the systematic error corrector (ζ) provided, the

design code models can be corrected by multiplying (ζ) to the load capacities obtained from the code-based models. With this done, the model error of the corrected model should be independent of the design parameters (e.g., *e/t*) (i.e., the corrected model has no systematic error). The scatter plots between the test-to-prediction ratio (ξ) of the corrected models for CSA S304-14 and TMS 402-16 and the eccentricity to thickness ratio (*e/t*) throughout the 4000 FE simulations (i.e., training samples) are shown in Figure 5-15. One can notice that the model error of the corrected model is not affected by the variations of (*e/t*) (i.e., independent of the design parameter). However, this is not the case for the original code models (i.e., without corrections) as they were more conservative (i.e., associated with higher values of (ζ)) for lower *e/t* values (i.e., *e/t* =0.1).

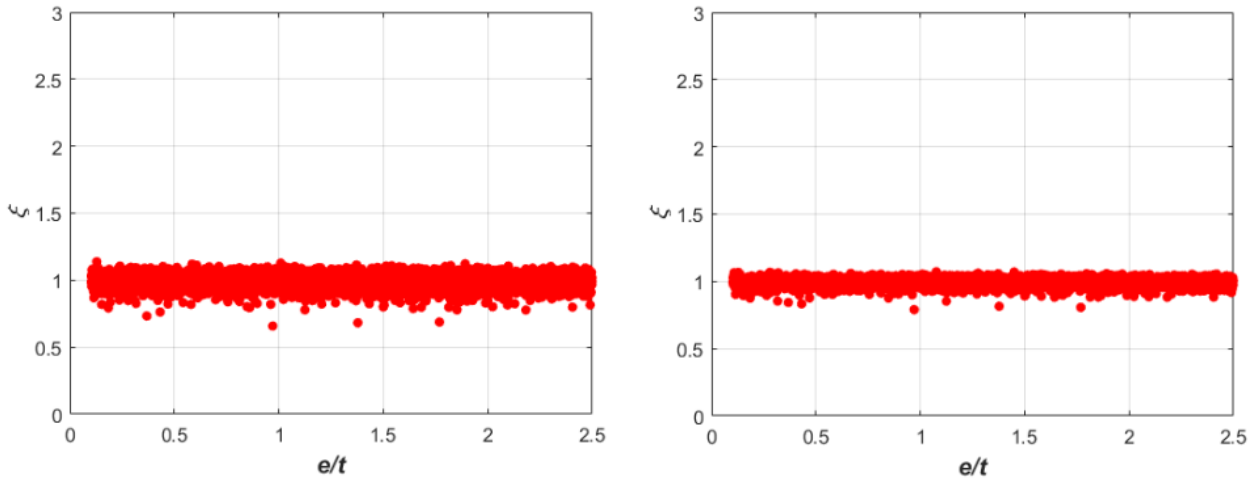

(a) (b)

Figure 5-15 The test-to-prediction ratio (ξ) for the corrected model versus the eccentricity to thickness ratio *e/t* (a) CSA S304-14, (b) TMS 402-16

5.5 Application to Reliability Assessment

To investigate the effect of the accuracy of the adopted behavioural model on the reliability

assessment, the reliability analysis of two representative walls (i.e., wall S and wall H) is conducted based on the original and the corrected models of CSA S304-14, as a representative of the design codes-based models. The slenderness ratios are 16 and 42 for wall S and wall H, respectively. In addition, both walls have a characteristic compressive strength f'_m, nominal yield strength of the reinforcement bars f_{yn}, reinforcement ratio ρ_s of 10 MPa, 400 MPa, 0.0019, respectively.

For the original CSA S304-14, the reliability analysis is conducted without considering its associated model error (i.e., assuming it is accurate enough for such an application), while the uncertainty in the capacity predictions of the corrected model for CSA S304-14 is considered by a coefficient of variation of 0.17, which is determined based on 2000 independent FE simulations. The resistance random variables listed in Table 5-2, including the mean, coefficient of variation (COV), and probability distribution types, are considered for the reliability assessment conducted herein. Note that the randomness in f_t and ε_o is not considered as these parameters are not included in the capacity prediction model of CSA S304-14.

Table 5-2 Statistical characterization of random variables considered for the original and corrected design code-based reliability assessment

Random variable	***Mean (μ)***	***Coefficient of variation***	***Probability distribution***	***Reference***
f_m	1.6 f'_m	0.24	Gumbel	Moosavi and Korany 2014, Moosavi 2017
f_y	1.14 f_{yn}	0.07	Normal	Moosavi 2017
E	200 GPa	0.033	Normal	Mirza, 1998
d	d_n	$4.0\ mm/d_n$	Normal	Moosavi 2017

The probabilistic load capacities obtained based on the considered two models (i.e., the original and corrected models for CSA S304) for wall S and Wall H when loaded with e/t = 0.1, 0.5 is shown in Figure 5-16. It found that the original model for CSA S304-14 (i.e., without correction) can be significantly biased, which conforms to the findings illustrated in section 5.4.2. In addition, the original model for CSA S304-14 is associated with a noticeably lower variance compared to the corrected model, which can lead to misinformative reliability assessment results.

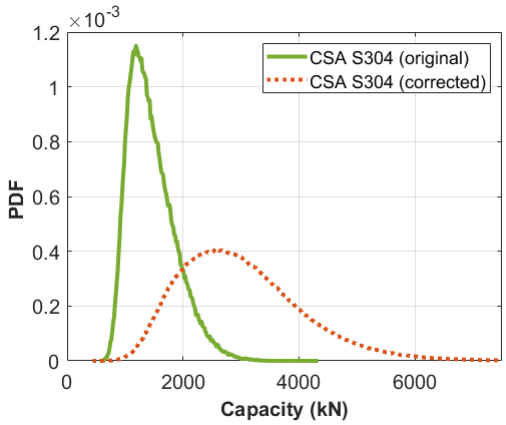

(a)

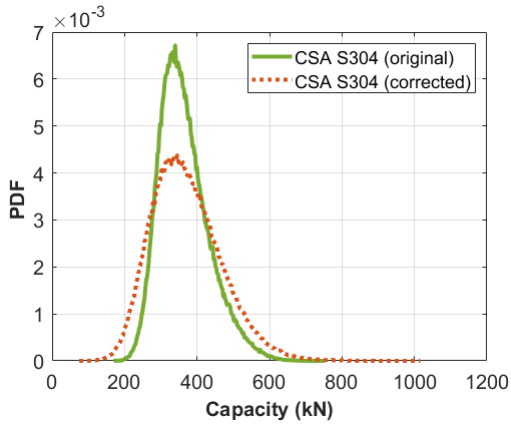

(b)

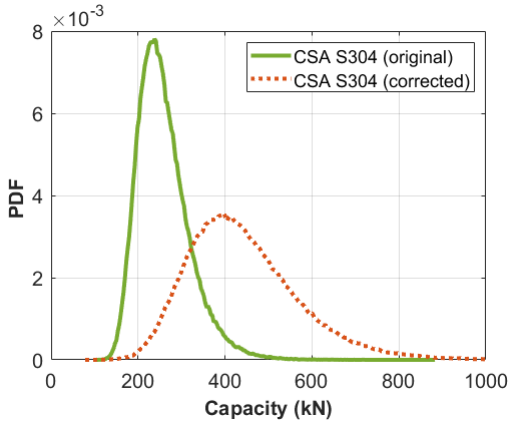

(c)

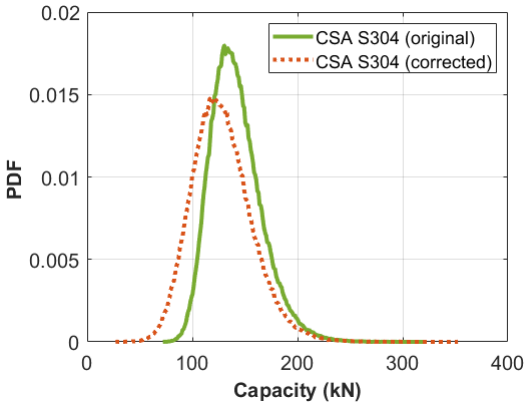

(d)

Figure 5-16 Comparison of the probabilistic load capacity for the original and corrected CSA S304-14 model (a) wall S (*e/t*=0.1), (b) wall S (*e/t*=0.5) (c) wall H (*e/t*=0.1), and (d) wall H (*e/t*=0.5)

The results of the reliability assessment conducted based on the two considered models for the dead load combination (i.e., 1.4 D_n, where D_n is the nominal dead load) are shown in Figure 5-17. The comparison reveals that reliability assessment results can be significantly biased when assuming design code models are accurate (i.e., without model error). In that sense, it is essential to rigorously consider the modelling error of the design codes when they are employed for reliability assessment.

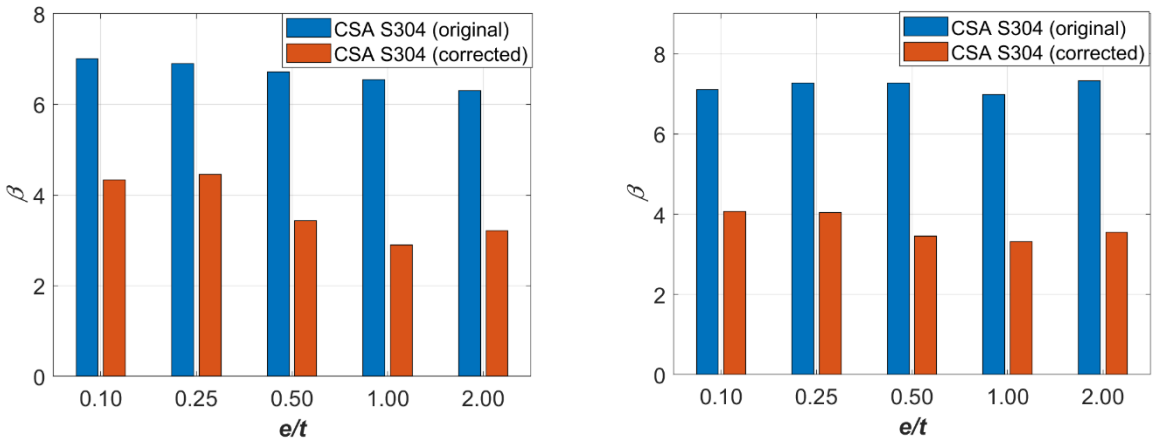

(a) (b)

Figure 5-17 Reliability index (β) versus *(e/t)* based on FE and CSA S304-14 models (a): Wall S, and (b) Wall H

5.6 Summary and Conclusions

The model error associated with the out-of-plane capacity models for reinforced concrete masonry walls in CSA S304-14 and TMS402-16 was investigated and quantified using well-validated finite element (FE) models and experimental data. The design code-based models were

found to be associated with a systematic error (i.e., a dependency between the model error and design parameters). The relationship between the model error and different design parameters (e.g., load eccentricity to thickness ratio, slenderness ratio, masonry compressive strength and steel reinforcement ratio) was studied using a non-parametric Gaussian process regression model. Thereafter, the systematic error associated with the design codes was investigated. It was found that CSA S304-14 is overly conservative for highly slender walls loaded with relatively low load eccentricities. On the other hand, TMS 402-16 was found to be less biased, except for highly slender walls loaded with high reinforcement ratios and relatively high load eccentricities. The code-based models were corrected using the developed regression model. The model error of the corrected model was found to be independent of the design parameters. The original and corrected code-based models for CSA S304-14 were used to conduct reliability analysis of two representative masonry walls with different slenderness ratios. It was found that adopting the design code-based models without correction can lead to biased and unconservative reliability estimates.

5.7 References

ACI-SEASC Task Committee on Slender Walls. (1982). Test report on slender walls. Los Angeles, California:USA.

Bilotta, M. and Cruz, Y. (2021). Evaluation of Second-order Effects in Slender Reinforced Masonry Walls. Proc., 14th Canadian Masonry Symposium, Montreal, QC, Canada.

CSA. 2019. Design of masonry structures. Standard CSA-S304-14 (R2019), Canadian Standards Association, Rexdale, ON.

Dawe, J. L., & Liu, Y. (2003). Analytical modeling of masonry load-bearing walls. Canadian Journal of Civil Engineering, 30(5), 795-806. doi:10.1139/l03-036

Drysdale, R. G. and Hamid, A. A. (2005). Masonry Structures Behaviour and Design, Canada Masonry Design Centre, Mississauga, ON, Canada.

Ganduscio S, Romano F. (1997). FEM and analytical solutions for buckling of nonlinear masonry members. Journal of Structural Engineering,123(1):104–11.

Hatzinikolas, M., Longworth, J., and Warwaruk, J. 1978a. Concrete Masonry Walls. University of Alberta - Structural Engineering Report No. 70. Department of Civil and Environmental Engineering, University of Alberta. Edmonton, AB.

Jiang Z., Chen W., Fu Y., & Yang R. (2013). Reliability-based design optimization with model bias and data uncertainty. SAE International Journal of Materials and Manufacturing, 6(3), 502-516. doi:10.4271/2013-01-1384

Isfeld, A. C., Müller, A. L., Hagel, M., & Shrive, N. G. (2019). Analysis of safety of slender concrete masonry walls in relation to CSA S304-14. Canadian Journal of Civil Engineering, 46(5), 424-438. doi:10.1139/cjce-2018-0210

Li, Y, Li, Y, Hassanien, S, Okoloekwe, C, & Adeeb, S. "Application of Gaussian Process Regression for the Accuracy Assessment of a Three-Dimensional Strain-Based Model." Pressure Vessels and Piping Conference. Volume 3: Design and Analysis. San Antonio, Texas, USA. July 14–19, 2019. V003T03A098. ASME. https://doi.org/10.1115/PVP2019-94039

Lourenço PB. (1996) Computational strategies for masonry structures. Ph.D thesis. Delft University of Technology.

Mathews, G. M., & Vial, J. (2017). Overcoming model simplifications when quantifying predictive uncertainty. Retrieved from https://arxiv.org/abs/1703.07198

Mirza, S. A. (1996). Reliability-based design of reinforced concrete columns. Structural Safety, 18(2), 179-194. doi:10.1016/0167-4730(96)00010-0

Mohsin, E. (2005). *Support stiffness effect on tall load bearing masonry walls.* PhD Thesis, University of Alberta, Edmonton.

MOOSAVI, H., & KORANY, Y. (2014). Assessment of the structural reliability of loadbearing concrete masonry designed to the Canadian standard S304.1. Canadian Journal of Civil Engineering, 41(12), 1046-1053. doi:10.1139/cjce-2013-0498

Moosavi H. (2017). *S*tructural reliability of non-slender loadbearing concrete masonry members under concentric and eccentric loads. PhD thesis, Department of Civil and Environmental Engineering, University of Alberta, Edmonton, AB.

MSJC. (2016). Building Requirements and Specifications for Masonry Structures. Standard TMS 402/602- 16, The Masonry Society, Longmont, CO.

Ni, P., Xia, Y., Li, J., & Hao, H. (2019). Using polynomial chaos expansion for uncertainty and sensitivity analysis of bridge structures. Mechanical Systems and Signal Processing, 119, 293-311. doi:10.1016/j.ymssp.2018.09.029

Ozbakkaloglu, T., & Saatcioglu, M. (2004). Rectangular stress block for high-strength concrete. ACI Structural Journal, 101(4) doi:10.14359/13333

Sammut, C., & Webb, G. I. (2017). Encyclopedia of machine learning and data mining. Boston, MA: Springer.

Pettit, C. E. J., Mohsin, E., Cruz-Noguez, C., & Elwi, A. E. (2021). Experimental testing of slender load-bearing masonry walls with realistic support conditions. Canadian Journal of Civil Engineering, doi:10.1139/cjce-2020-0297

Priestley, M. J. N., and Elder, D. M. 1983. Stress–strain curves for unconfined and confined concrete masonry. ACI J., 80-3, 192–201

Schobi, R., Sudret, B., & Wiart, J. (2015). Polynomial-chaos-based kriging. International Journal for Uncertainty Quantification, 5(2), 171-193. doi:10.1615/Int.J.UncertaintyQuantification.2015012467

Su, G., Peng, L., & Hu, L. (2017). A Gaussian process-based dynamic surrogate model for complex engineering structural reliability analysis. Structural Safety, 68, 97-109. doi:10.1016/j.strusafe.2017.06.003

Suwalski, P.D. (1986). Capacity of eccentrically loaded slender concrete block walls. M.Sc. thesis, Department of Civil Engineering, MCMaster University, Hamilton, Ont.

Wang, R., Elwi, A. E., and Hatzinikolas, M. A. (1997). Numerical Study of Tall Masonry Cavity Walls Subjected to Eccentric Loads. Journal of Structural Engineering, Vol. 123, No. 10, pp.1287-

Yokel, F.Y., Mathey, R.G., and Dikkers, R.D. (1970). Compressive strength of slender concrete masonry walls. Building Science Series 33, U.S. National Bureau of Standards, Washington, D.C.

CHAPTER 6:Summary, Conclusions and Recommendations

6.1 Summary

The behaviour of masonry walls is associated with large scatter due to the inherent uncertainties in the material and geometric properties. These uncertainties are not considered within the scope of the deterministic models (e.g., mechanics-based finite element (FE) models, design code-based models). In addition, developing an accurate model to predict the behaviour of masonry walls with deterministic properties (i.e., without uncertainties) is still considered to be challenging due to the embedded complexity in masonry walls with heterogeneous materials, which gives rise to the importance of considering the uncertainty in the model predictions along with the uncertainties in material and geometric properties. To this end, the probabilistic behaviour of masonry walls subjected to out-of-plane loading was investigated employing mechanics-based macro FE models in conjunction with Monte Carlo simulations (MCS). The outcomes of the probabilistic analysis were used to identify the influential parameters and their effect on different response quantities (e.g., load capacity and ductility) through a variance-based global sensitivity analysis.

The developed mechanics-based FE models were used to assess the reliability of masonry walls with different slenderness ratios and loading scenarios using the efficient subset simulation algorithm in conjunction with polynomial chaos-kriging surrogate models to address the computational cost. The aforementioned uncertainties (e.g., material, geometric and model uncertainties) were incorporated in the reliability analysis. In addition, different global and local failure criteria were considered.

Furthermore, the validated mechanics-based FE models in conjunction with the available experimental data in the literature were used to investigate the model error associated with the

design code-based models for masonry walls (e.g., CSA S304-14 and TMS-402-16). The systematic error of the design code-based models was investigated through probabilistic regression analysis. The regression models were thereafter used to correct the model error associated with the design codes. To further understand the effect of the accuracy of the behaviour model on the reliability of masonry walls, reliability analysis is conducted for the considered masonry walls employing the original (i.e., without model correction) and the corrected models of CSA S304-14 for comparison.

6.2 Conclusions

The main conclusions of this research can be summarized as follows:

- The probabilistic analysis showed that the behaviour of the highly slender wall was found to be associated with larger scatter compared to walls with less slenderness ratios.
- The load capacity variance was mostly attributed to the uncertainty associated with the masonry compressive strength f_m, the yield strength of steel f_y, and steel bar location d. In contrast, the deformation capacity variance was mostly attributed to the uncertainty associated with the masonry compressive strength f_m, and the masonry tensile strength f_t.
- The model uncertainty was found to be non-negligible compared to other geometric and material uncertainties, as incorporating the model error in the probabilistic analysis led to a substantial increase in the variance of load capacity.
- Similarly, the reliability assessment was found to be sensitive to the model uncertainty, which indicated the importance of the rigorous quantification and incorporating of the model error in the context of the uncertainty analysis.

- Other factors were found to affect the reliability assessment for masonry walls, such as the slenderness ratio, load eccentricity. For instance, walls with low slenderness ratios (e.g., 16) loaded with relatively low load eccentricities were found to be associated with higher reliability indices (β) compared to highly slender walls or walls loaded with larger eccentricities.
- The failure criteria were found to affect the reliability assessment significantly. For instance, adopting local failure criteria was generally more conservative for the wall with relatively low slender ratios (e.g., h/t=16) compared to the global failure criteria. On the contrary, the local failure criteria were less conservative for the highly slender wall (e.g., h/t=42) compared to the global failure criteria.
- The design code-based models were found to be associated with a systematic error (i.e., a correlation between the model error and design parameters such as the load eccentricity, slenderness ratio, masonry compressive strength and steel reinforcement ratio).
- The investigation of the model error associated with the design codes-based models revealed that CSA S304-14 is overly conservative for highly slender walls loaded with relatively low load eccentricities, while TMS 402-16 was found to be less biased, except for highly slender walls loaded with high reinforcement ratios and relatively high load eccentricities.
- Adopting the code-based models without the rigorous incorporating of the associated model error in the reliability analysis can lead to significantly biased results.

6.3 Recommendations for Future Work

This section describes the limitations of the present study in addition to the recommendations for future work.

- The probabilistic structural analysis and the variance-based sensitivity analysis were conducted on the macroscopic level, which does not capture the influence of the local properties of masonry (e.g., unit-mortar interface, reinforcement bond-slip). To get further insight into the contribution of the local properties of masonry, the analysis can be conducted on the microscopic level.
- The provided probabilistic structural analysis approach can be expanded to investigate other response quantities (e.g., cracking load, elastic stiffness). In addition, the analysis can be applied to walls with different loading conditions (e.g., in-plane loading).
- The provided outcomes of the reliability analysis are not sufficient for code calibration. Expanding the analysis to cover all the design combinations is recommended.
- The model error associated with the developed FE models is quantified using the limited experimental data available in the literature. However, the available experimental data is insufficient to address the model error for design code-based models, which can be associated with systematic trends. Accordingly, more experimental tests for masonry structures are needed.

References

Abbiati, G., Marelli, S., Tsokanas, N., Sudret, B., & Stojadinović, B. (2021). A global sensitivity analysis framework for hybrid simulation. Mechanical Systems and Signal Processing, 146, 106997. doi:https://doi.org/10.1016/j.ymssp.2020.106997

Abdulla, K. F., Cunningham, L. S., & Gillie, M. (2017). Simulating masonry wall behaviour using a simplified micro-model approach. Engineering Structures, *151*, 349-365. doi:10.1016/j.engstruct.2017.08.021

ACI-SEASC Task Committee on Slender Walls. (1982). Test report on slender walls. Los Angeles, California.

Ali,S., Page A.W. and Kleeman P.W. (1986). Non-Linear Finite Element Model for Concrete Masonry with Particular Reference to Concentrated Loads. 4th Canadian Masonry Symposium-1986, New Brunswick, Canada.

Aridru, G.G. (1997). Effective flexural rigidity of plain and reinforced concrete masonry walls. Ph.D. thesis, Department of Civil Engineering, University of New Brunswick, Fredericton, N.B.

Athmani A., Khemis A., Hacene-Chaouche A., Tee K.F., Ferreira T.M., Vicente R. (2019). Buckling uncertainty analysis for steel pipelines buried in elastic soil using FOSM and MCS methods. International Journal of Steel Structures, 19 (2) 381–397.

Au, S. K., Ching, J., & Beck, J. L. (2007). Application of subset simulation methods to reliability benchmark problems. Structural Safety, 29(3), 183-193. doi:10.1016/j.strusafe.2006.07.008

Barbato, M., Gu, Q., & Conte, J. P. (2010). Probabilistic push-over analysis of structural and soil-structure systems. Journal of Structural Engineering, *136*(11), 1330-1341. doi:10.1061/(ASCE)ST.1943-541X.0000231

Barbato, M., Zona, A., & Conte, J. P. (2014). Probabilistic nonlinear response analysis of steel-concrete composite beams. Journal of Structural Engineering, *140*(1), 4013034. doi:10.1061/(ASCE)ST.1943-541X.0000803

Barbato, M., Zona, A., & Conte, J. P. (2014). Probabilistic nonlinear response analysis of steel-concrete composite beams. Journal of Structural Engineering, 140(1), 4013034. doi:10.1061/(ASCE)ST.1943-541X.0000803

Bartlett, F., Hong, H., & Zhou, W. (2003). Load Factor Calibration for the Proposed 2005 Edition of the National Building Code of Canada: Statistics of Loads & Load Effects. Canadian Journal of Civil Engineering, 30(2), 429-439.

Bastug, E., Menafoglio, A., & Okhulkova, T. (2013). Polynomial chaos expansion for an efficient uncertainty and sensitivity analysis of complex numerical models. European safety and reliability, Amsterdam, Netherlands.

Bhattacharyya, B. (2021). Uncertainty quantification and reliability analysis by an adaptive sparse bayesian inference based PCE model Springer Science and Business Media LLC. doi:10.1007/s00366-021-01291-0

Bilotta, M. and Cruz, Y. (2021). Evaliation of Second-order Effects in Slender Reinforced Masonry Walls. Proc., 14th Canadian Masonry Symposium, Montreal, QC, Canada.

Bui, T. T., Limam, A., Sarhosis, V., & Hjiaj, M. (2017). Discrete element modelling of the in-plane and out-of-plane behaviour of dry-joint masonry wall constructions. Engineering Structures, *136*, 277-294. doi:10.1016/j.engstruct.2017.01.020

Buonopane, S. G. (2008). Strength and reliability of steel frames with random properties. Journal of Structural Engineering*, 134*(2), 337-344. doi:10.1061/(ASCE)0733-9445(2008)134:2(337)

Chen, W. F., & Atsuta, T. (1973). Strength of eccentrically loaded walls. *International Journal of Solids and Structures, 9*(10), 1283-1300. doi:10.1016/0020-7683(73)90115-7

Chrysler J, Bannett M.R., Peterson R, Dalrymple A., Pierson D., Samblanet P.J. (2021). A Preview of Expected Changes to TMS 402/602, with a Look at the 6-year Revisions Cycle. 14th Canadian Masonry Symposium, Montreal, QC, Canada.

CSA S304 (2014) Design of Masonry Structures. Canadian Standards Association, Mississauga, Canada.

CSA S408 (2011) Guidelines for the development of limit states design. Canadian Standards Association, Ontario, Canada

D'Altri AM, Sarhosis V, Milani G, Rots J, Cattari S, Lagomarsino S, Sacco E, Tralli A, Castellazzi C, & de Miranda S. "A review of numerical models for masonry structures." Numerical modeling of masonry and historical structures. Woodhead Publishing; 2019. p. 3–53.

D’Altri AM, Sarhosis V, Milani G, Rots J, Cattari S, Lagomarsino S, Sacco E, Tralli A, Castellazzi C, & de Miranda S. A review of numerical models for masonry structures. Numerical modeling of masonry and historical structures. Woodhead Publishing; 2019. p. 3–53.

D'Altri, A. M., de Miranda, S., Castellazzi, G., & Sarhosis, V. (2018). A 3D detailed micro-model for the in-plane and out-of-plane numerical analysis of masonry panels. Computers & Structures*, 206*, 18-30. doi:10.1016/j.compstruc.2018.06.007

Das, S., Tesfamariam, S., Chen, Y., Qian, Z., Tan, P., & Zhou, F. (2020). Reliability-based optimization of nonlinear energy sink with negative stiffness and sliding friction. Journal of Sound and Vibration, 485, 115560. doi:10.1016/j.jsv.2020.115560

Dawe, J. L., & Liu, Y. (2003). Analytical modeling of masonry load-bearing walls. Canadian Journal of Civil Engineering*, 30*(5), 795-806. doi:10.1139/l03-036

Dimov, I., & Georgieva, R. (2010). Monte carlo algorithms for evaluating sobol’ sensitivity indices. Mathematics and Computers in Simulation, 81(3), 506-514. doi:10.1016/j.matcom.2009.09.005

Drysdale, R. G. and Hamid, A. A. (2005). *Masonry Structures Behaviour and Design*, Canada Masonry Design Centre, Mississauga, ON, Canada

Dubourg, V., Sudret, B., & Deheeger, F. (2013). Metamodel-based importance sampling for structural reliability analysis. Probabilistic Engineering Mechanics, 33, 47-57. doi:10.1016/j.probengmech.2013.02.002

Ellingwood B, Galambos TV, MacGregor JG, Cornell CA (1980). Development of a probability based load criterion for American national standard A58, National Bureau of Standards Special Publication 577, U.S. Government Printing Office, Washington, DC.

Ellingwood, B.M. & Tallin, A.A. (1985). Limit States Criteria for Masonry Construction, Journal of Structural Engineering, 111: 108

Erdogmus E, Dutrisac H, Thompson J, Bennett B.(2021). Comparison of Selected CSA S304-14 AND TMS 402-16 Reinforced Masonry Design Provisions and Material Properties. 14th Canadian Masonry Symposium, Montreal, QC, Canada.

Frangopol, D. M., Ide, Y., Spacone, E., & Iwaki, I. (1996). A new look at reliability of reinforced concrete columns. Structural Safety, 18(2), 123-150. doi:10.1016/0167-4730(96)00015-X

Ganduscio S, Romano F. (1997). FEM and analytical solutions for buckling of nonlinear masonry members. Journal of Structural Engineering,123(1):104–11.

Gardoni, P., Der Kiureghian, A., & Mosalam, K. M. (2002). Probabilistic capacity models and fragility estimates for reinforced concrete columns based on experimental observations. Journal of Engineering Mechanics, 128(10), 1024-1038. doi:10.1061/(ASCE)0733-9399(2002)128:10(1024)

Ghanem, R. G., & Spanos, P. D. (1991). Stochastic finite elements: A spectral approach. New York: Springer-Verlag.

Grubišić, M., Ivošević, J., & Grubišić, A. (2019). Reliability analysis of reinforced concrete frame by finite element method with implicit limit state functions. Buildings (Basel), *9*(5), 119. doi:10.3390/buildings9050119

Grubišić, M., Ivošević, J., & Grubišić, A. (2019). Reliability analysis of reinforced concrete frame by finite element method with implicit limit state functions. Buildings (Basel), *9*(5), 119. doi:10.3390/buildings9050119

Hariri-Ardebili, M. A., Mahdavi, G., Abdollahi, A., & Amini, A. (2021). An RF-PCE Hybrid Surrogate Model for Sensitivity Analysis of Dams. Water, 13(3), 302.

Hatzinikolas, M., Longworth, J., and Warwaruk, J. (1978). Concrete Masonry Walls. University of Alberta - Structural Engineering Report No. 70. Department of Civil and Environmental Engineering, University of Alberta. Edmonton, AB.

Holický, M., Retief, J. V., & Sýkora, M. (2016). Assessment of model uncertainties for structural resistance. Probabilistic Engineering Mechanics, 45, 188-197.

Holický, M., Retief, J. V., & Sýkora, M. (2016). Assessment of model uncertainties for structural resistance. Probabilistic Engineering Mechanics, 45, 188-197.

Hu, C., & Youn, B. (2011). Adaptive-sparse polynomial chaos expansion for reliability analysis and design of complex engineering systems. Structural and Multidisciplinary Optimization, 43(3), 419-442. doi:10.1007/s00158-010-0568-9

Isfeld, A. C., Müller, A. L., Hagel, M., & Shrive, N. G. (2019). Analysis of safety of slender concrete masonry walls in relation to CSA S304-14. Canadian Journal of Civil Engineering, 46(5), 424-438. doi:10.1139/cjce-2018-0210

Isfeld, A. C., Stewart, M. G., & Masia, M. J. (2021). Stochastic finite element model assessing length effect for unreinforced masonry walls subjected to one-way vertical bending under out-of-plane loading. Engineering Structures, 236, 112115. doi:https://doi.org/10.1016/j.engstruct.2021.112115

Jiang Z., Chen W., Fu Y., & Yang R. (2013). Reliability-based design optimization with model bias and data uncertainty. SAE International Journal of Materials and Manufacturing, 6(3), 502-516. doi:10.4271/2013-01-1384

Jiang, Y., Peng, S., Beer, M., Wang, L., & Zhang, J. (2020). Reliability evaluation of reinforced concrete columns designed by eurocode for wind-dominated combination considering random loads eccentricity. Advances in Structural Engineering, 23(1), 146-159. doi:10.1177/1369433219866089

Koutromanos, I., Stavridis, A., Shing, P. B., & Willam, K. (2011). Numerical modeling of masonry-infilled RC frames subjected to seismic loads. Computers & Structures, 89(11), 1026-1037. doi:https://doi.org/10.1016/j.compstruc.2011.01.006

Kuang JS, Yuen Y. Simulations of masonry-infilled reinforced concrete frame failure. Proc Inst Civ Eng – Eng Comput Mech 2013;166(4):179.

Leifsson, L., Du, X., & Koziel, S. (2020). Efficient yield estimation of multiband patch antennas by polynomial chaos ‐ based kriging. International Journal of Numerical Modelling, 33(6), n/a. doi:10.1002/jnm.2722

Li, J., Masia, M. J., Stewart, M. G., & Lawrence, S. J. (2014). Spatial variability and stochastic strength prediction of unreinforced masonry walls in vertical bending. *Engineering Structures, 59*, 787-797. doi:10.1016/j.engstruct.2013.11.031

Li, J., Stewart, M. G., Masia, M. J., & Lawrence, S. J. (2016). Spatial correlation of material properties and structural strength of masonry in horizontal bending. *Journal of Structural Engineering, 142*(11), 4016112. doi:10.1061/(ASCE)ST.1943-541X.0001488

Li, X., Gong, C., Gu, L., Gao, W., Jing, Z., & Su, H. (2018). A sequential surrogate method for reliability analysis based on radial basis function. Structural Safety, 73, 42-53. doi:10.1016/j.strusafe.2018.02.005

Li, Y, Li, Y, Hassanien, S, Okoloekwe, C, & Adeeb, S. "Application of Gaussian Process Regression for the Accuracy Assessment of a Three-Dimensional Strain-Based Model." Pressure Vessels and Piping Conference. Volume 3: Design and Analysis. San Antonio, Texas, USA. July 14–19, 2019. V003T03A098. ASME. https://doi.org/10.1115/PVP2019-94039

Liu, Y., and Dawe, J.L. (2001). Experimental determination of masonry beam–column behaviour. Canadian Journal of Civil Engineering, 28(5): 794–803.

Lopez, J. Oiler, S., Onate, E. and Lubliner J. (1999) A homogeneous Constitutive Model for Masonry. International Journal for Numerical Methods in Engineering, Vol. 46, pp. 1651-1671,1999.

Lourenco PB & Rots JG. (1997). A multi-surface interface model for the analysis of masonry structures. Journal of Engineering Mechanics 1997: 123(7): 660–668

Lourenco PB, Rots JG, Blaauwendraad J. (1995). Two approaches for the analysis of masonry structures: micro and macro-modeling. Heron, 1950;40(4):313–40.

Lourenço PB. (1996) Computational strategies for masonry structures. Ph.D thesis. Delft University of Technology.

Lu, M. 2003. Stability of Unreinforced Masonry Members Under Simultaneous Vertical & Out-of-Plane Lateral Loads. Ph.D., University of Minnesota, Minnesota.

Marelli, S., & Sudret, B. (2018). An active-learning algorithm that combines sparse polynomial chaos expansions and bootstrap for structural reliability analysis. Structural Safety, 75, 67-74. doi:10.1016/j.strusafe.2018.06.003

Martini, K. 1997. Finite Element Studies in the Out-of-Plane Failure of Unreinforced Masonry. In Proc., 7th Int. Conf. on Computing in Civil & Building Engineering, Vol. 1, pp. 179-184.

Mathews, G. M., & Vial, J. (2017). Overcoming model simplifications when quantifying predictive uncertainty. arXiv preprint arXiv:1703.07198.

Mckenna, F., Scott, M. H., & Fenves, G. L. (2010). Nonlinear finite-element analysis software architecture using object composition doi:10.1061/ASCÊCP.1943-5487.0000002

Melander, J. M., & Lauersdorf, L. R. (1993). Masonry: design and construction, problems and repair. ASTM.

Melchers, R. E. (1989). Importance sampling in structural systems. Structural Safety, 6(1), 3-10. doi:10.1016/0167-4730(89)90003-9

Metropolis, N., & Ulam, S. (1949). The monte carlo method. Journal of the American Statistical Association, 44(247), 335-341. doi:10.1080/01621459.1949.10483310

Metwally, Z. and Li, Y. (2021). Finite Element-based Probabilistic Behavior Analysis of Slender Reinforcement Masonry Walls Under Out-of-plane Loading. Proc., 14th Canadian Masonry Symposium, Montreal, QC, Canada.

Milner, J., David M, Spacone, E., & Frangopol, D. M. (2001). New light on performance of short and slender reinforced concrete columns under random loads. Engineering Structures, 23(2), 147-157. doi:10.1016/S0141-0296(00)00036-5

Milner, J., David M, Spacone, E., & Frangopol, D. M. (2001). New light on performance of short and slender reinforced concrete columns under random loads. Engineering Structures, 23(2), 147-157. doi:10.1016/S0141-0296(00)00036-5

Minga, E., Macorini, L., Izzuddin, B. A., & Calio', I. (2019). Chapter 8 - macromodeling. In B. Ghiassi, & G. Milani (Eds.), Numerical modeling of masonry and historical structures (pp. 263-294) Woodhead Publishing. doi:https://doi.org/10.1016/B978-0-08-102439-3.00008-7

Mirza S, Hatzinikolas M, MacGregor J. (1979). Statistical descriptions of the strength of concrete. Journal of Structural Engineering,105(ST6):1021–37.

Mirza, S. A. (1996). Reliability-based design of reinforced concrete columns. Structural Safety, 18(2), 179-194. doi:10.1016/0167-4730(96)00010-0

Mirza, S. A. (1998). Monte carlo simulation of dispersions in composite steel-concrete conumn strength interaction. Engineering Structures*, 20*(1), 97-104. doi:10.1016/S0141-0296(97)00049-7

Mohsin, E. (2005). Support stiffness effect on tall load bearing masonry walls. PhD Thesis, University of Alberta, Edmonton.

Mojsilović, N., & Stewart, M. G. (2015). Probability and structural reliability assessment of mortar joint thickness in load-bearing masonry walls. Structural Safety, 52, 209-218. doi:https://doi.org/10.1016/j.strusafe.2014.02.005

Moosavi H. (2017). *S*tructural reliability of non-slender loadbearing concrete masonry members under concentric and eccentric loads. PhD thesis, Department of Civil and Environmental Engineering, University of Alberta, Edmonton, AB.

MOOSAVI, H., & KORANY, Y. (2014). Assessment of the structural reliability of loadbearing concrete masonry designed to the Canadian standard S304.1. Canadian Journal of Civil Engineering, 41(12), 1046-1053. doi:10.1139/cjce-2013-0498

MSJC. (2016). Building Requirements and Specifications for Masonry Structures. Standard TMS 402/602- 16, The Masonry Society, Longmont, CO.

Mukherjee, D., Rao, B. N., & Meher Prasad, A. (2011). Global sensitivity analysis of unreinforced masonry structure using high dimensional model representation. Engineering Structures, 33(4), 1316-1325. doi:https://doi.org/10.1016/j.engstruct.2011.01.008

Ni, P., Xia, Y., Li, J., & Hao, H. (2019). Using polynomial chaos expansion for uncertainty and sensitivity analysis of bridge structures. Mechanical Systems and Signal Processing, 119, 293-311. doi:10.1016/j.ymssp.2018.09.029

Ozbakkaloglu, T., & Saatcioglu, M. (2004). Rectangular stress block for high-strength concrete. ACI Structural Journal, 101(4) doi:10.14359/13333

Page, A.W. (1978). Finite Element Model for Masonry. Journal of Structural Division, ASCE, Vol. 104, No. ST, August 1978, pp. 1267-1285.

Pettit, C. (2020). Effect of Rotational Base Stiffness on the Behaviour of Loadbearing Masonry Walls. M.Sc. thesis, Department of Civil and Environmental Engineering, University of Alberta, Edmonton, AB.

Pettit, C. E. J., Mohsin, E., Cruz-Noguez, C., & Elwi, A. E. (2021). Experimental testing of slender load-bearing masonry walls with realistic support conditions. Canadian Journal of Civil Engineering, doi:10.1139/cjce-2020-0297

Pluijm, van der, R. (1999). Out-of-plane bending of masonry : behaviour and strength. Eindhoven: Technische Universiteit Eindhoven. https://doi.org/10.6100/IR528212

Priestley, M. J. N., and Elder, D. M. (1983). Stress–strain curves for unconfined and confined concrete masonry. ACI J., 80-3, 192–201

Sammut, C., & Webb, G. I. (2017). Encyclopedia of machine learning and data mining. Boston, MA: Springer.

Sarhosis, V., & Lemos, J. V. (2018). A detailed micro-modelling approach for the structural analysis of masonry assemblages. *Computers & Structures, 206*, 66-81. doi:10.1016/j.compstruc.2018.06.003

Sayed-Ahmed, E.Y. and Shrive, N.G. (1996) "Nonlinear Finite Element Model of Hollow Masonry" Journal of Structural Engineering,Vol.l22, No.6 June 1996, pp. 683-1587.

Schöbi, R., Sudret, B., & Marelli, S. (2017). Rare event estimation using polynomial-chaos kriging. ASCE-ASME Journal of Risk and Uncertainty in Engineering Systems. Part A, Civil Engineering, 3(2) doi:10.1061/AJRUA6.0000870

Schobi, R., Sudret, B., & Wiart, J. (2015). Polynomial-chaos-based kriging. International Journal for Uncertainty Quantification, 5(2), 171-193. doi:10.1615/Int.J.UncertaintyQuantification.2015012467

Shi, Y., Lu, Z., He, R., Zhou, Y., & Chen, S. (2020). A novel learning function based on kriging for reliability analysis. Reliability Engineering &amp, System Safety, 198, 106857. doi:10.1016/j.ress.2020.106857

Shing PB, Cao L. (1997) Analysis of partially grouted masonry shear walls. Gaitherburg (MD): US Department of Commerce. National Institute of Standards and Technology. NISTIR GCR 97-710.

Sobol′, I. M. (2001). Global sensitivity indices for nonlinear mathematical models and their monte carlo estimates. *Mathematics and Computers in Simulation, 55*(1-3), 271-280. doi:10.1016/s0378-4754(00)00270-6

Stewart MG, Lawrence SJ. (2007). Model error, structure reliability and partial safety factors for structural masonry in compression. Masonry International, 20(3):107–16.

Su, G., Peng, L., & Hu, L. (2017). A Gaussian process-based dynamic surrogate model for complex engineering structural reliability analysis. Structural Safety, 68, 97-109. doi:10.1016/j.strusafe.2017.06.003

Su, L., Wan, H., Li, Y. Y., & Ling, X. (2018). Soil-pile-quay wall system with liquefaction-induced lateral spreading: Experimental investigation, numerical simulation, and global sensitivity analysis. American Society of Civil Engineers (ASCE). doi:10.1061/(asce)gt.1943-5606.0001977

Sudret, B. (2008). Global sensitivity analysis using polynomial chaos expansions. Reliability Engineering & System Safety, 93(7), 964-979. doi:10.1016/j.ress.2007.04.002

Sundararajan, C. (1995). Probabilistic structural mechanics handbook. Houston, Texas: Springer Science+ Business Media Dordrecht.

Sustersic H, Stubbs D, Peterson R, Bannett R., Pettit C., Flisak B., Erdogmus E., Thompson J., Bennett B., Cruz C. (2021). Parametric Studies on Reinforced Masonry Walls Resisting Out-of-plane Loads: A Comparison of CSA S304-14 and TMS 402-16. 14th Canadian Masonry Symposium, Montreal, QC, Canada.

Suwalski, P.D. (1986). Capacity of eccentrically loaded slender concrete block walls. M.Sc. thesis, Department of Civil Engineering, MCMaster University, Hamilton, Ont.

Tee, K. F., Khan, L. R., & Li, H. (2014). Application of subset simulation in reliability estimation of underground pipelines. Reliability Engineering &amp, System Safety, 130, 125-131. doi:10.1016/j.ress.2014.05.006

Tubaldi E, Macorini L, Izzuddin BA. (2020). Identification of critical mechanical parameters for advanced analysis of masonry arch bridges. Structure and Infrastructure Engineering, 16(2):328–45.

Turkstra, C. & Ojinaga, J. (1980). Towards a Canadian Limit States Masonry Design Code. In Proceedings of the 2nd Canadian Masonry Symposium, Carleton University, Ottawa, Ontario, Canada.

Wang, R., Elwi, A. E., and Hatzinikolas, M. A. (1997). Numerical Study of Tall Masonry Cavity Walls Subjected to Eccentric Loads. Journal of Structural Engineering, Vol. 123, No. 10, pp.1287-1294

Wong, P. S., Veccjio, F. J., and Trommels, H. (2013). VecTor2 & FormWorks User's Manual. Department of Civil Engineering, University of Toronto, second edition.

Yokel, F.Y., Mathey, R.G., and Dikkers, R.D. (1970). Compressive strength of slender concrete masonry walls. Building Science Series 33, U.S. National Bureau of Standards, Washington, D.C.

Yu, Z., Sun, Z., Cao, R., Wang, J., & Yan, Y. (2020). RCA-PCK: A new structural reliability analysis method based on PC-kriging and radial centralized adaptive sampling strategy. Proceedings of the Institution of Mechanical Engineers. Part C, Journal of Mechanical Engineering Science, , 95440622095771. doi:10.1177/0954406220957711

Zhai, X., and Stewart, M. G. (2010). Structural reliability analysis of reinforced grouted concrete block masonry walls in compression. Engineering Structures, 32(1), 106–114.

Zhai, X., Zhong, Z., & Stewart, M. G. (2012). Model error and structural reliability for reinforced concrete block masonry walls in shear. Advances in Structural Engineering, 15(3), 389-398. doi:10.1260/1369-4332.15.3.389

Zhu, F., Zhou, Q., Wang, F., & Yang, X. (2017). Spatial variability and sensitivity analysis on the compressive strength of hollow concrete block masonry wallettes. Construction & Building Materials*, 140*, 129-138. doi:10.1016/j.conbuildmat.2017.02.099

Zuev, K. M., Wu, S., & Beck, J. L. (2015). General network reliability problem and its efficient solution by subset simulation. Probabilistic Engineering Mechanics, 40, 25-35. doi:https://doi.org/10.1016/j.probengmech.2015.02.002